NASA Technical Memorandum 109051

A Conceptual Design Study for a Two-Dimensional, Electronically Scanned Thinned Array Radiometer

Philip Mutton
Christopher C. Chromik
Patrick A. Cosgrove
Iain Dixon
Richard B. Statham
Frederic H. Stillwagen
Alfred E. Von Theumer
Lockheed Engineering and Sciences Company
Hampton, Virginia

George G. Ganoe
Washito A. Sasamoto
Langley Research Center

Paul A. Garn
Science and Technology Corporation
Hampton, Virginia

November 1993

National Aeronautics and
Space Administration

Langley Research Center
Hampton, Virginia 23681-0001

ERRATA

NASA Technical Memorandum 109051

A Conceptual Design Study for a Two-Dimensional,
Electronically Scanned Thinned Array Radiometer

Phil Mutton, Christopher C. Chromik, Iain Dixon,
Richard B. Statham, Frederic H. Stillwagen, Alfred E. Von Theumer,
Washito A. Sasamoto, and Paul A. Garn

November 1993

Two authors were inadvertently omitted from the cover and included under the Acknowledgments section.

A corrected cover, Acknowledgments page, and Report Documentation Page are attached.

Issued January 1994

TABLE OF CONTENTS

TABLE OF CONTENTS (continued)

TABLE OF CONTENTS (continued)

APPENDICES

1. INTRODUCTION

Soil moisture measurements are required by hydrologists and climatologists to develop a greater understanding of the global hydrologic cycle, and the relationships between surface moisture and climate. Satellite measurements are the only practical approach for providing the required systematic coverage, due to the large spatial and temporal variability of soil moisture on a global basis. The Electronically Scanned Thinned Array Radiometer (ESTAR) is an instrument concept proposed for the measurement of soil moisture from a satellite platform (ref. 1). The ESTAR is an imaging microwave radiometer operating at 1.41 GHz, and utilizing the aperture synthesis method of imaging. This measurement technique derives its heritage from the radio astronomy field, and is adapted for remote sensing of the Earth. The complement of instruments on the ESTAR satellite also includes the capability to measure sea surface temperature. This provides the capability to determine sea surface salinity which provides ocean circulation information required in global heat transport analyses and modeling. There are several options for making the sea surface temperature measurement including the use of various wavelengths in the microwave and infrared (IR) regions. For this study the L-band radiometer was complemented with an infrared instrument. The general configuration of the L-band antenna array and the spacecraft can be seen in figure 1.0-1. Figure 1.0-2 shows the satellite configuration and the field of view of the L-band radiometer.

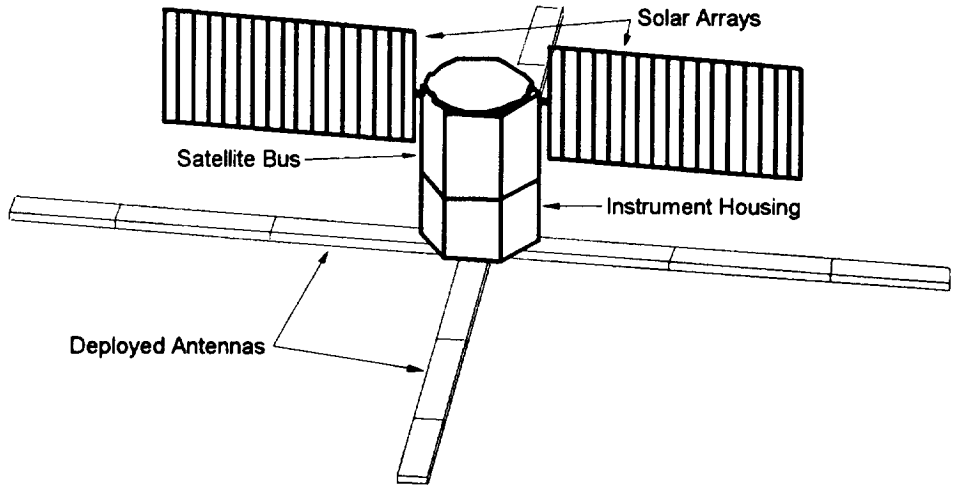

Figure 1.0-1. 2D-Estar Satellite Configuration

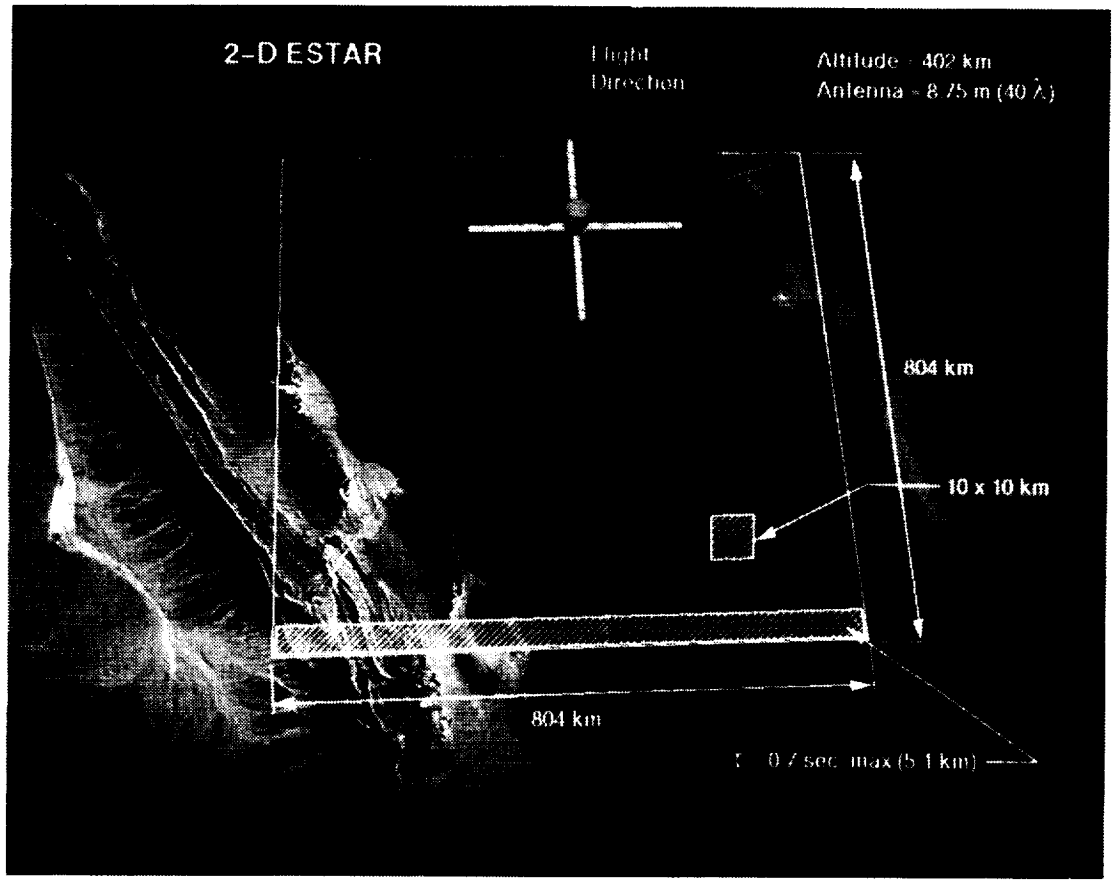

Figure 1.0-2. 2D-Estar Satellite Configuration and Field of View

2. BACKGROUND

A radiometer, operating at 1.41 GHz, requires a relatively large antenna aperture to provide adequate spatial resolution for the soil moisture measurement. Array thinning, in conjunction with aperture synthesis, is a technique that is used to reduce instrument mass and launch packaging volume as compared to a filled array, real aperture approach. However, these benefits must be traded against a reduction in receiver performance, and an increase in signal processing complexity.

In aperture synthesis a large antenna aperture is effectively achieved through cross correlation of received signals from pairs of individual antenna elements making up an array. Satellite instruments proposed to date have been designed as hybrid systems with real aperture viewing along track and aperture synthesis in the cross track direction. However, in its general form this technique involves synthesizing an image in two dimensions (ref. 2), and when feasible offers maximum savings in mass and volume. Therefore, the objective of this study was to design a spacecraft and mission implementing the Two-Dimensional ESTAR (2-D ESTAR) concept.

Prior NASA efforts to develop the aperture synthesis concept for measuring soil moisture include an ongoing aircraft measurement program conducted by the Goddard Space Flight Center (GSFC) and the University of Massachusetts, a spaceborne system design study, and selected theoretical studies. The instrument in the aircraft program is a hybrid system that has been used to study fundamental system design issues, and to develop image inversion algorithms. One of the concepts from the design study for the spaceborne instrument and spacecraft (ref. 3), which was completed in 1990, is shown in figure 2.0-1. The satellite instruments operated at three microwave frequencies (L-band, S-band, and C-band) with significant array thinning in each case. Subsequent to this study GSFC conducted a preliminary feasibility assessment for a small low cost 2-D system. This assessment did not include a detailed spacecraft design or mission analysis, but the results showed that such a system with a low mission cost might be possible, and that a thorough feasibility study was worthwhile.

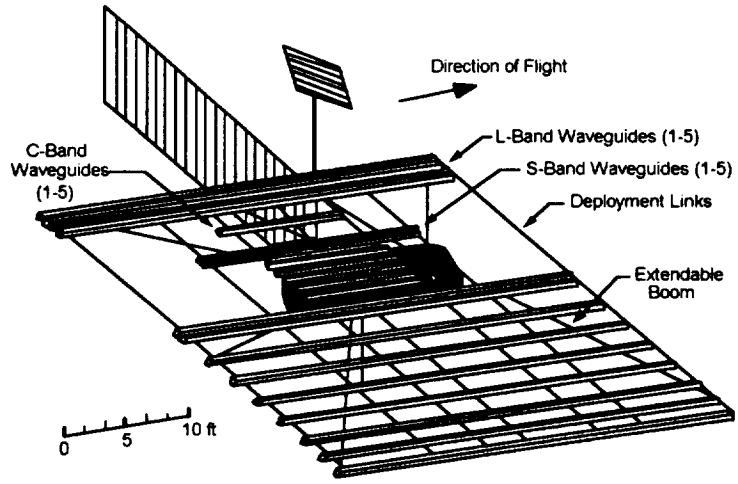

Figure 2.0-1. Earlier One-Dimensional ESTAR Concept

3. STUDY APPROACH

A collaborative approach was followed with GSFC responsible for defining the measurement requirements and the instrument functional design. LaRC was responsible for the physical definition of the instruments, the spacecraft design, the mission analysis, and the launch vehicle requirements.

The fundamental study goal was to produce a spacecraft conceptual design, for the estimation of size, weight, power, and cost, and to identify the smallest launch vehicle capable of reaching the required orbit. Conceptual designs for an L-Band synthetic aperture radiometer, and its complementary sensors (a visible and IR radiometer, and a video camera) were developed. A structural and mechanical concept for an antenna that met both the on-orbit performance requirements and the launch requirements was defined. Preliminary structural and thermal analyses were conducted to evaluate the antenna characteristics under launch loads and in the on-orbit thermal environment. A detailed layout was defined for the L-Band electronic components and cabling. The spacecraft bus concept was based on specific designs currently offered in the aerospace industry. Some systems were configured uniquely for this particular application using currently offered components. Orbit analyses were conducted to determine the fuel requirements for orbit maintenance and the launch vehicle performance requirements. No performance analyses were conducted on the L-band instrument, and no calibration concept was included in the design. Further instrument definition is required.

From the spacecraft mass estimate it was determined that the performance of the Pegasus launch vehicle was not adequate to achieve the required orbit. Consequently the Taurus was baselined as the launch vehicle, and the Taurus mission was developed as a feasible baseline concept. A further assessment was then conducted to define a mission that could use a Pegasus class launch vehicle, and to determine the extent to which the mission requirements and the L-Band instrument capability would need to be relaxed to make such a mission feasible.

3.1. Mission Requirements and Guidelines

The 2-D ESTAR mission requirements and guidelines for the L-band microwave radiometer are given in table 3.1-1.

Mission Requirements	
Operating Frequency	1.41 GHz
Microwave Wavelength	21.26 cm
Coverage	90%, 3 day repeat
Orbit Inclination	Sun Synchronous, 11:00 am nodal crossing
Spatial Resolution	10 km (soil moisture), 50 km (salinity)
Sensitivity	1 K (soil moisture), 0.25 K (salinity)
Accuracy	1 K (soil moisture), 1 K (salinity)
Mission Lifetime	3 years
Mission Guidelines	
Orbit Altitude	402 km
Swath Width	+/- 45 degrees
Antenna Length	Approx. 40 wavelengths (8.75 m)
Antenna Configuration	Cross (+), 73 x 73 active elements

Table 3.1-1. Mission Requirements and Guidelines for the L-band Radiometer

4. LAUNCH VEHICLES

Several launch vehicles were considered for the 2D-ESTAR mission. The Pegasus and Taurus offered by Orbital Sciences Corporation (refs. 4 and 5) were evaluated. A general compatibility assessment was made of the Conestoga family of vehicles offered by EER Systems (ref. 6). The Connestoga data was not obtained until late in the study, and hence, no detailed feasibility analysis was undertaken for these alternatives. The minimum performance curves for the Pegasus and Taurus are shown in figure 4.0-1.

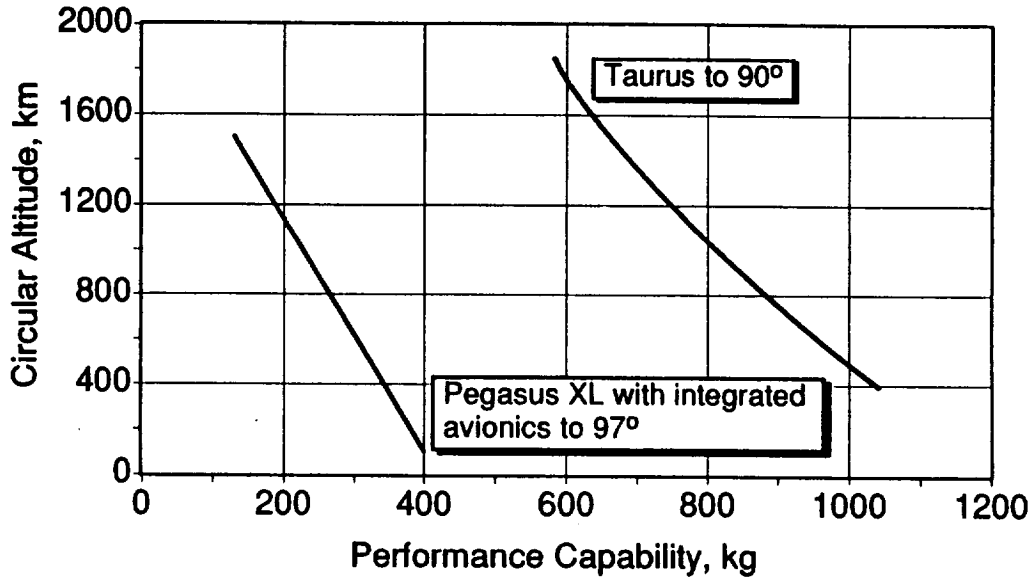

Figure 4.0-1. Launch Vehicle Performance Curves

4.1. Pegasus

Pegasus is a three-stage, solid-propellant, inertially-guided, all-composite, winged space booster (figure 4.1-1). As of December 1992, two demonstration flights had taken place. The Pegasus XL used in this study is a higher capability version of the current vehicle. The XL will be baselined for launches after 1993. The Pegasus is launched from an aircraft and is subjected to significant lateral loads during ascent. A launch loads analysis was completed as part of the structural design exercise, and the loads are described along with the analysis results in section 7.1.

4.1.1. Volume

Given a typical spacecraft bus and a standard Pegasus shroud, there is insufficient volume to accommodate the ESTAR L-band radiometer. There are two options that increase the length of the payload volume. The first is to extend the length of the Pegasus shroud.

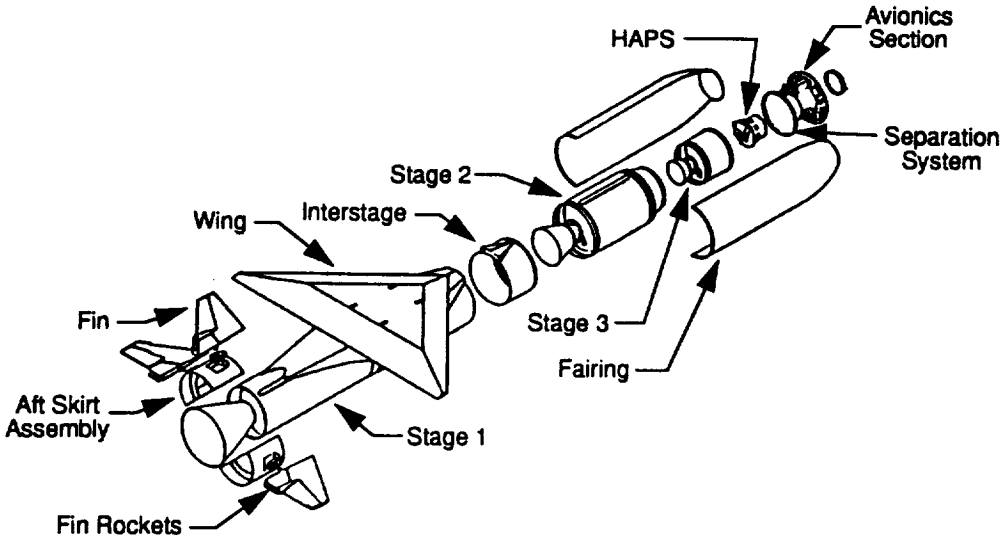

Figure 4.1-1. Exploded View of the Pegasus Launch Vehicle

The cylindrical section of the shroud can be lengthened in 15.2 cm increments up to 61.0 cm.. However, due to the size of the instrument, this option alone does not provide enough volume. The second option involves integrating the Pegasus third stage avionics into the spacecraft bus thereby eliminating redundant structure and hardware. This is possible by utilizing OSC's integrated bus concept (figure 4.1-2) which results in additional cylindrical length for the payload.

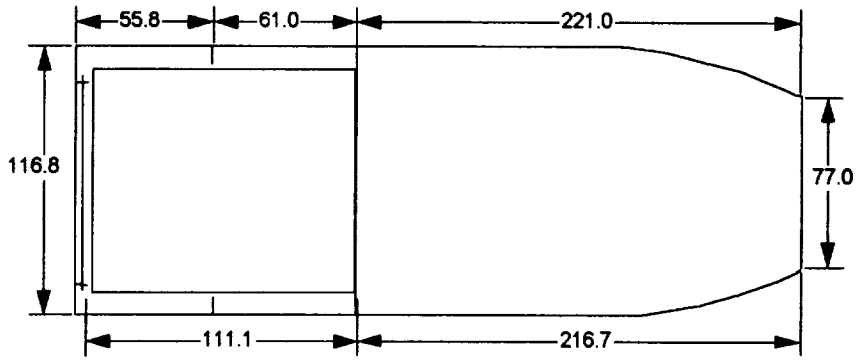

Figure 4.1-2. Pegasus Fairing

The payload volume requirement was driven primarily by the L-Band antenna. Its overall size (8.75 x 8.75 m) and cross sectional area (30 x 9 cm) were determined by the instrument requirements described in section 5.1. A number of deployment mechanisms were considered. The initial goal was to launch the instrument on a Pegasus, and the stowed configuration was therefore constrained to remain within a 117 cm diameter dynamic envelope. This limited the number of folds to three for each of the antenna arms. Additionally, the taper of the Pegasus envelope dictated that one fold be shorter than the others. The resulting 168 cm long stowed antenna combined with a typical spacecraft bus could not be accommodated within a standard Pegasus shroud. The overall length of the dynamic envelope within the shroud may be increased by extending the shroud by 61 cm, and using the OSC integrated bus concept that increases the effective length of the envelope an additional 56 cm. The resulting length inside the shroud is 338 cm, which is more than enough to accommodate the bus and instruments.

4.1.2. Mass

The nominal capability of a Pegasus XL to a 402 km sun synchronous orbit is 286 kg. Utilizing the integrated avionics concept described above has the added benefit of increasing the vehicle's performance by 54 kg. Thus the capability to this orbit with integrated avionics is 340 kg as can be seen in figure 4.0-1.. However, the spacecraft must carry an additional 36 kg of Pegasus provided equipment; hence the net benefit is actually 18 kg. Injection into a parking orbit at 194 km and utilization of the spacecraft's orbit adjust system to transfer to 402 km yielded an additional 19 kg gain for an optimized maximum mass to orbit of 359 kg. The estimated total payload mass (spacecraft plus instruments) with a fully capable radiometer is 535 kg. Alternative approaches were therefore considered.

4.1.3. Performance Reduction Option

In an effort to achieve a 402 km orbit with the Pegasus vehicle, several options were considered including the use of an orbit with a 60 degree inclination. This increased the launch capability to 413 kg for the desired altitude. The total mass of the integrated spacecraft was still 158 kg over the predicted capability of the launch vehicle. It was concluded that the instrument, as configured, could not be manifested on a Pegasus class spacecraft. An alternate configuration was also addressed and is described in section 8.

4.2. Taurus

Taurus is essentially a wingless Pegasus atop a Castor 120 base stage (figure 4.2-1). OSC currently has a contract with DARPA for two vehicles, and options for 41 more. The first flight is scheduled for late 1993.

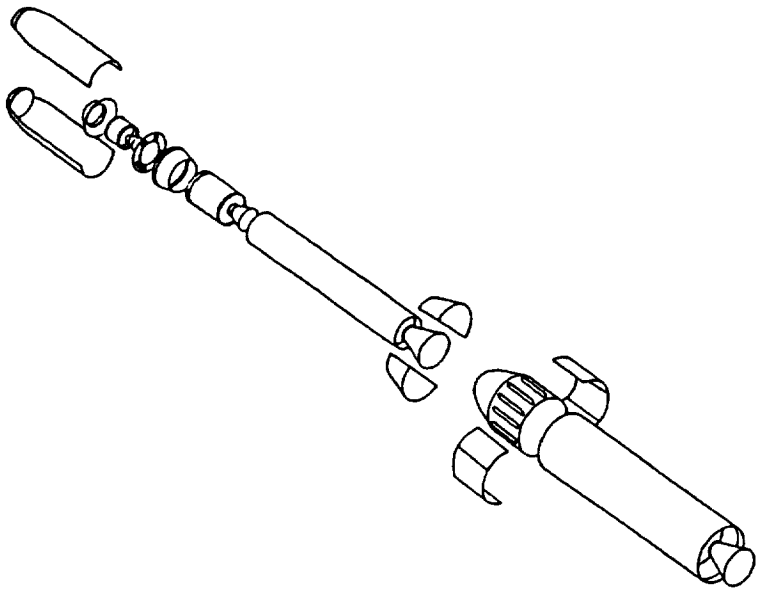

Figure 4.2.1. Exploded View of the Taurus Launch Vehicle

4.2.1. Volume

The Taurus offers a 137 x 330 cm dynamic envelope (figure 4.2-2), which is large enough to accommodate the instrument configuration described earlier. The length of a standard Taurus shroud eliminates the need to use the integrated bus concept which in turn allows the consideration of other spacecraft buses.

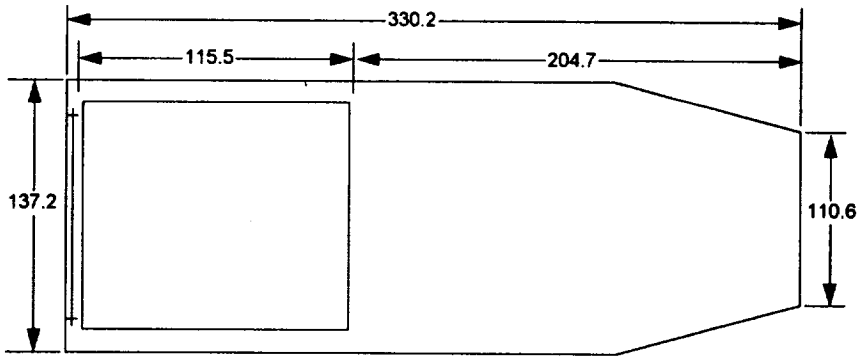

Figure 4.2-2. Taurus Fairing

4.2.2. Mass

The Taurus vehicle is capable of inserting a 1044 kg payload into a 90 degree orbit at 402 km (see figure 4.0-1). Despite a slight performance degradation for a sun synchronous inclination, the mass and volume margins afforded by the vehicle eliminate the requirement for integrated avionics. This allows the use of virtually any Pegasus or Taurus class bus. Using the bus described in section 6.0 the gross payload mass is 535 kg resulting in a large positive mass margin of 509 kg.

4.3. Conestoga

EER Systems' Conestoga uses Delta derived Castor IV engines in multiple configurations offering a range of performances (figure 4.3-1). At the time of writing the first launch is scheduled for third quarter of 1993. Orders for this vehicle include 3 firm with 2 options.

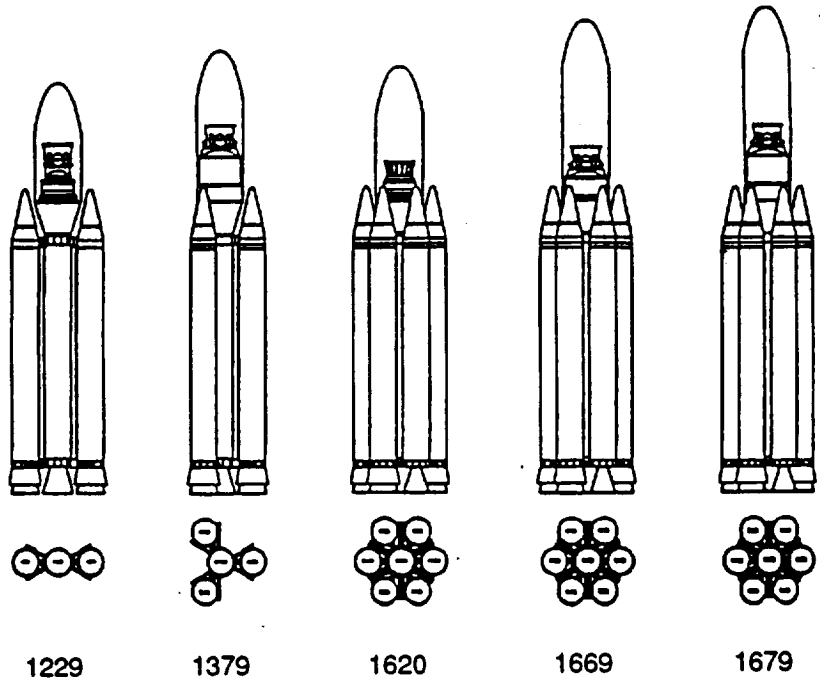

Figure 4.2-3. Conestoga Launch Vehicle Configurations

4.3.1. Capability

The Conestoga capability is dependent on the configuration. Potentially useful configurations for ESTAR include the 1379, 1620, and 1669, which deliver 544, 805, and 1020 kg to 402 km at 90 degrees respectively. Performance to a sun synchronous orbit is

slightly less. Conestoga's 1.8 x 6.55 m shroud provides adequate payload volume. With the performance and volume available it is unlikely that integration of launch vehicle avionics into the spacecraft will be necessary, and a variety of spacecraft buses may be considered. One area of concern is the high lateral launch loads of approximately 2.5 to 3.5 g. These are similar to the structural loading concerns for a Pegasus launch (section 4.1).

5. INSTRUMENTS

The primary instrument on the ESTAR spacecraft is an L-band microwave radiometer that is described in detail in the following sections. This instrument is used to obtain soil moisture measurements over land, and ocean salinity measurements over water. The L-band radiometer can achieve the science goals for soil moisture as a single instrument. To achieve the ocean salinity measurement, the sea surface temperature (SST) must be obtained simultaneously with the L-band data. Two possible concepts are: the use of another microwave radiometer operating in the C-band region, and the use of a thermal infrared (TIR) radiometer in the 10 μ spectral region.

An all microwave system, the L-band radiometer used with a C-band radiometer, is highly desirable. It has all weather capability, day and night capability, and can be used to measure both sea surface temperature and sea state. The drawback is that it is relatively large and has the greatest mass penalty. Using a TIR radiometer in place of the C-band instrument reduces the payload mass and size significantly but surrenders the capability to measure the sea state and reduces the ability to penetrate cloud cover.

To obtain reliable measurements of soil moisture, factors such as land form and vegetation must be identified. Compensating factors may then be applied to optimize the calibration of the instrument. Hence, it is desirable to obtain a high resolution image of the scene where the soil moisture data is taken. For measurements of coastal salinity, images providing identification and correlation with geographical features are of benefit in the interpretation of the science data. The IR radiometer could perform the role of a mapper with reasonable resolution. However, a small video camera can provide higher resolution and add to the science utility of the spacecraft, but it significantly increases the downlink data rate and the spacecraft data storage requirements. Several combinations of scientific output and instrument capabilities are summarized in table 5.0-1.

A number of instrument combinations and their advantages and disadvantages for the ESTAR mission are shown in table 5.0-2. Limitations on the mass, volume, and data handling capability of a small satellite were the main constraints in the selection of the instruments for this study. To provide the required soil moisture and salinity measurements within these constraints, the L-band radiometer, a TIR radiometer, and a black and white video camera were selected.

Science	Requirements	Remarks
Soil Moisture	L-Band	Vegetation index or cues desirable
Ocean Salinity	L-Band + Sea Surface Temp	SST by two microwave radiometers (L/C band ratio) SST by TIR - One band in 10μ window (4μ potential TBD) - $\Delta T < 1$-3 K
Sea Surface Temperature by TIR	Water Vapor Correction	2 band: 11 μ, and 8.1 μ or 3-5 μ (H_2O absorbtion edges)
Sea Surface State	C-Band	TV and IR not much help
Collocation	Imager Good resolution Cues	L-Band, IR and TV are all imagers 10 km minimum--higher desirable but not necessary (Data rate increase) Science Cues: - computer vs. human searches - color TV (bands, B/W only, DP rate) - 1 vs. 2 band IR
Vegetation	Presence & L-band effects	Presence by TV or IR bands L-band effects by C-Band only
IR & TV Haze immunity	"Long" spectral bands (lambda >> droplet size)	TV--NIR @ 0.9μ, TIR@10μ

Table 5.0-1. Science Capability versus Instrument Combinations

Instruments	Bands	Science	Advantages	Disadvantages
L-Band + C-Band	1.41 GHz 5 GHz	SM + SST	All weather/day-night Sea state, etc.	Size
L-Band IR (1)	1.41 GHz 10 μ	SM SST	Min. for SM & SST Size and mass	Clouds, water vapor, sea state, min. collocate
L-Band + TV	1.41 GHz	SM Collocate	Color, Resolution	No SST capability
L-Band + IR (2)	1.41 GHz 10μ + 8μ	SM SST	Size and mass Water vapor correct	Clouds, sea state
L-Band + VIRR (2)	1.41 GHz 10μ + vis	SM SST B/W collocate	Size and mass VIRR heritage Data rate	Clouds, sea state water vapor correction TV haze
L-Band + IR (2 band) + TV (B/W)	1.41 GHz 10μ + 8μ 0.6-1.0μ	SM SST Collocate	Collocation cues Water vapor correct, TV haze Spatial cues	Clouds, data rate, sea state
L-Band + IR (2 band) + TV (color)	1.41 GHz 10μ + 8μ 3 bands	SM SST+ WV Cues & haze	Collocation Water vapor correct Veg. & spatial cues	Clouds, sea state System size and mass High res = high data rate TV day only (night TBD)

Table 5.0-2. Instrument Combinations with Advantages and Disadvantages

5.1. L-band Radiometer

The L-band frequency of 1.41 GHz was selected to optimize the sensitivity of the soil moisture measurement. The minimum performance requirements for the radiometer measurements were defined at the beginning of the study and are listed in table 5.1-1.

	Soil Moisture	Ocean Salinity
Frequency	1.41 GHz	1.41 GHz
Spatial Resolution	10 km	50 km
Sensitivity	1 K	0.25 K
Accuracy	1 K	1 K

Table 5.1-1. L-Band Radiometer Requirements

The correlation of frequency to soil moisture measurements (ref. 7) is shown in figure 5.1-1. The selected frequency of 1.41 GHz is close to the peak of this curve, and is within a 1.400 to 1.427 GHz band that is reserved for passive remote sensing applications.

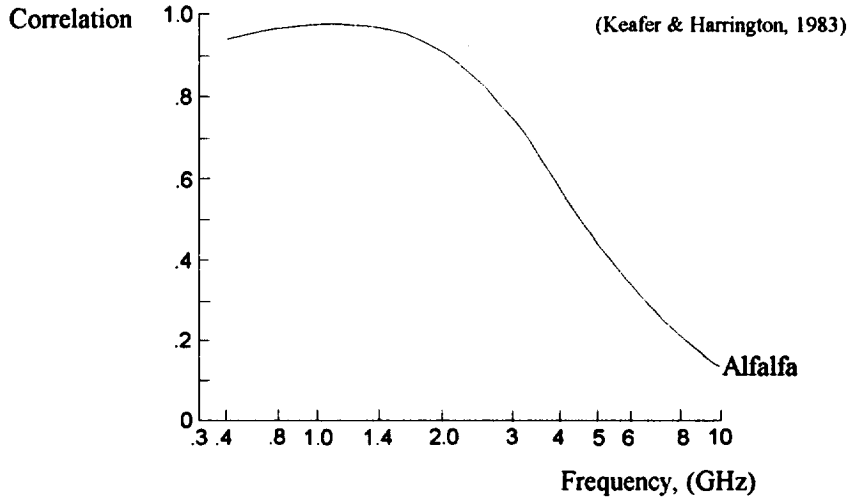

Figure 5.1- 1. Correlation of Frequency with Soil Moisture

In figure 5.1-2, the sensitivity of 1.41 GHz microwave radiation to ocean salinity is shown. Note that the salinity measurement is also a strong function of sea surface temperature, which must be determined from an independent measurement. For this reason another microwave frequency either C or S-band, or an IR radiometer, is necessary for the salinity measurement.

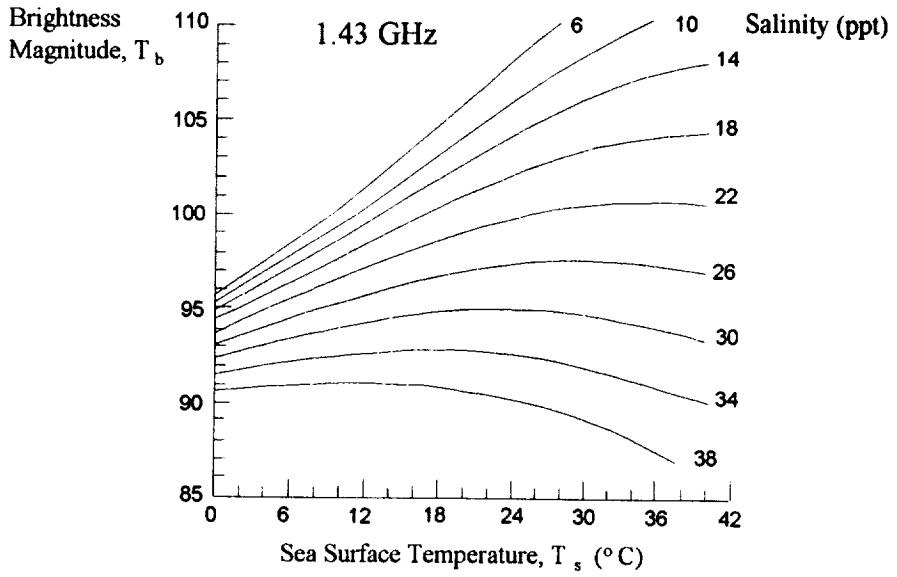

Figure 5.1-2. Brightness Temperature and Salinity versus Sea Surface Temperature

5.1.1. General Description, Electrical and Physical

The sun synchronous 402 km orbit, the 1.41 GHz frequency, and the desired spatial resolution of 10 km require an antenna assembly with a major dimension of 8.75 meters (approximately 40λ) from tip to tip.

The L-Band radiometer is configured as a 73 element-by-73 element cross array of microwave antennas. The antenna elements are microstrip patch antennas mounted on a fiberglass-epoxy honeycomb base. The base is mounted on a rectangular tube structure that is used to contain the electronics, and the cables for both RF and digital signals.

This tube structure is the major structural component of the instrument, and occupies a large part of the available volume in the launch vehicles considered. It is constructed in folding sections that are deployed on orbit. The number and dimensions of the sections are constrained to be stowed within the shroud of the launch vehicle. As can be seen in figure 5.1-3, each arm of the cross is in three sections. This enables the instrument to be folded into a stowed configuration for launch. The configuration of the folded instrument relative to the dynamic envelope of the Pegasus shroud considered initially, is shown in figure 5.1-4. Further discussion of the volume constraints is included in section 7 of this report. Figure 5.1-5 is an illustration of the instrument stowed for launch within the Taurus shroud.

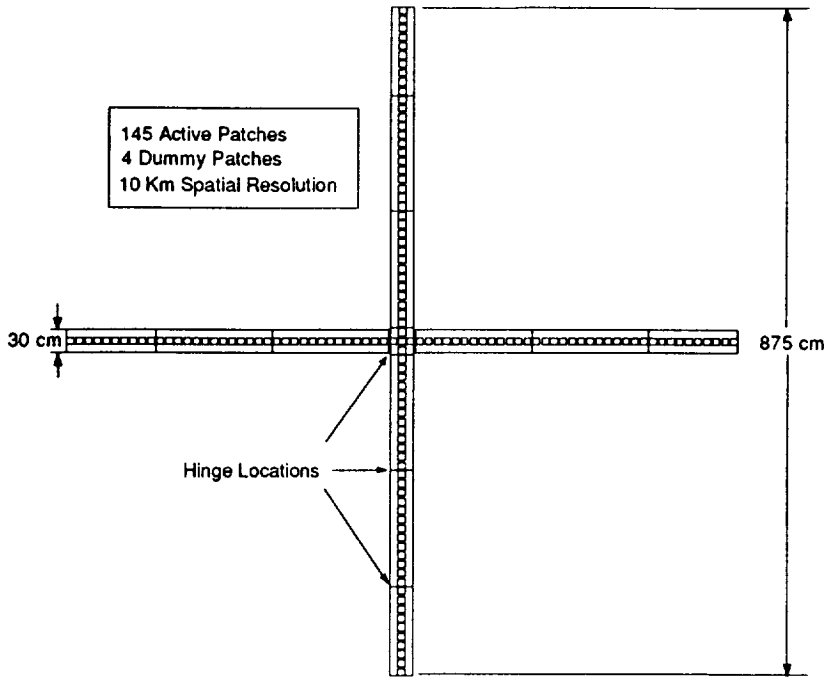

Figure 5.1-3. ESTAR Hinge Locations

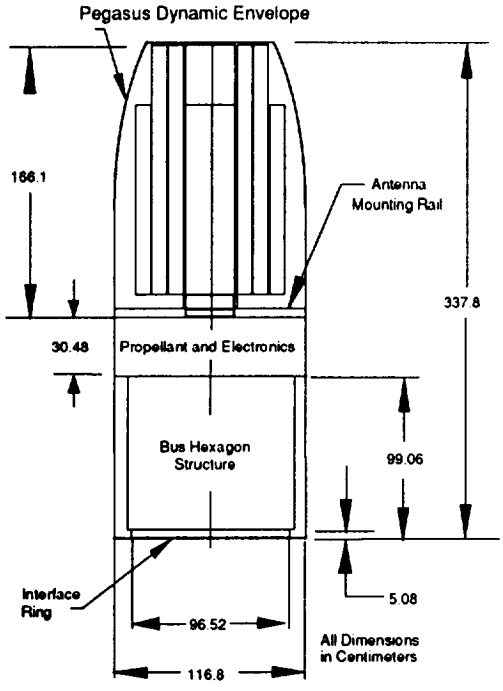

Figure 5.1-4. Three-Fold Antenna Stowed in Pegasus

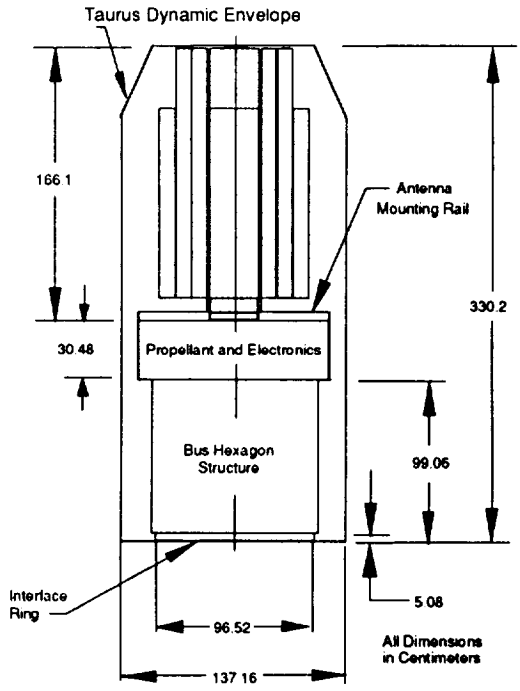

Figure 5.1-5. Three-Fold Antenna Stowed in Taurus

5.1.2. Structural Description

The arms of the antenna support tube are fabricated using a graphite-epoxy composite. The tube cross section is 30 cm wide and seven centimeters deep with a wall thickness of 1.25 mm. This provides sufficient internal volume to house the distributed radiometer electronics. The composite selected has adequate strength and structural rigidity to withstand the launch loads, and to provide a low coefficient of thermal expansion. The material selection and laminate properties are optimized to achieve the minimum wall thickness as described in section 8.1.2. This provides the lowest possible mass consistent with meeting the loading and thermal requirements. The fiberglass-epoxy antenna base is fabricated in segments and attached to the support tube with small expansion gaps between the segments. Thermally induced deformations of the antenna assembly are thus controlled by the characteristics of the main structure. The multi-layer insulation used for thermal protection also protects the graphite-epoxy composite from atomic oxygen.

5.1.2.1. Deployment Mechanisms

Several mechanisms were considered for the antenna deployment. Cables and linkages were determined to be less reliable, and to require more power for operation, than a harmonic drive and stepper motor combination. This combination is the drive assembly selected and is enclosed in a Mycalex housing. The hinges are also made of Mycalex, which has a high dielectric coefficient, and was selected to minimize effects on the antenna viewing pattern.

All the drive assemblies are mounted to the side of the arm structure. The innermost hinges (figure 5.1-6) only rotate through 90 degrees, and for these each drive assembly is entirely behind the ground plane. The other hinges rotate through 180 degrees, and in this concept the drive assembly extends forward of the ground plane (figure 5.1-7). This configuration provides a compact drive without the complexity of coupling gears. No analysis was made to determine whether the extension forward of the ground plane would significantly impact the antenna pattern. However, it is feasible to provide a mechanism without such an extension if future analysis deems it necessary. Incorporated around the hinge area are electrical contact fingers, or flexible braid segments, which provide continuity of the ground plane in the deployed configuration.

5.1.2.2. Launch restraints

Stops are provided for positive positioning in the stowed configuration. These are located at the top (referring to the launch position illustrated in figures 5.1-4 and 5.1-5), and at the free end of the short segment of each arm. Kevlar launch restraints are used to secure the arms during launch. These restraints are based on existing flight qualified designs.

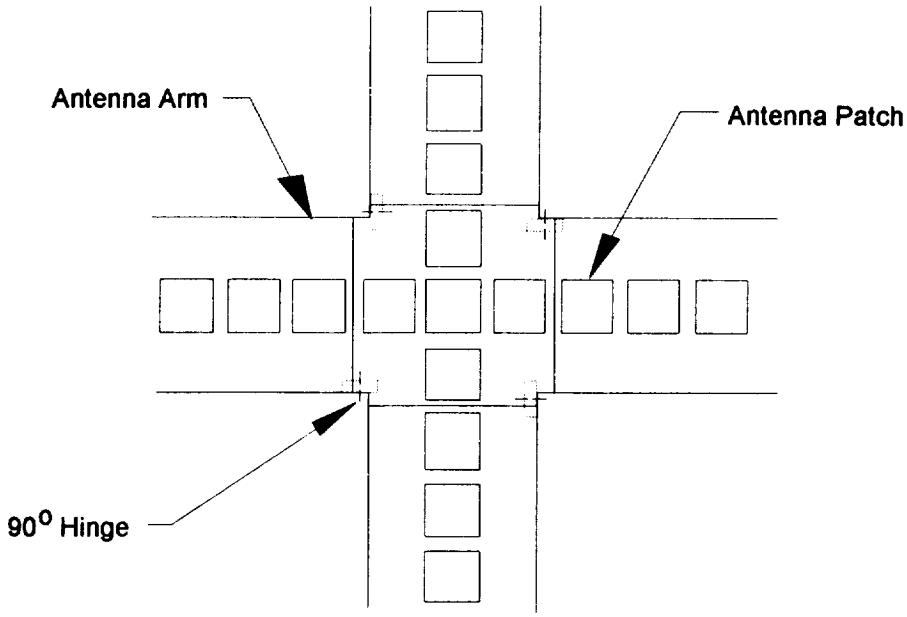

Figure 5.1-6. Center Section of Antenna Array

5.1.3. Antenna

The L-Band Radiometer antenna elements are microstrip patch antennas operating at a frequency of 1.41 GHz. Of the 149 elements, four are dummy units, providing antenna pattern matching for the outermost elements. The central antenna element is common to both the cross track and the along track arrays resulting in a 73 x 73 element array. The overall size of the antenna assembly (8.75m) is determined by the total number of patches (75 x 75), and the center to center spacing of the patches (0.55 x wavelength).

The 145 active antennas are connected to the radio frequency (RF) receiver circuits. The antennas are fabricated on a two-centimeter thick fiberglass-epoxy honeycomb base having a very high dielectric constant. A ground plane is bonded to the back of the antenna base. The antenna bases are then mounted to the graphite-epoxy tube structure arms (figure 5.1-7). Each antenna consists of an outer patch, which is 9.2 cm square, and an internal patch to which the feed is connected. Each antenna feeds its RF output through the ground plane to the inside of the tube where it is directly connected to an RF Front End Module (FEM). This direct connection minimizes the distance between the antenna and the FEM, and provides a well-controlled dimension for precise phase matching of all elements.

5.1.4. Electrical Description

Each microstrip antenna element connects to an FEM. The FEM receives the antenna output, performs down-conversion, produces both in-phase and quadrature (I&Q)

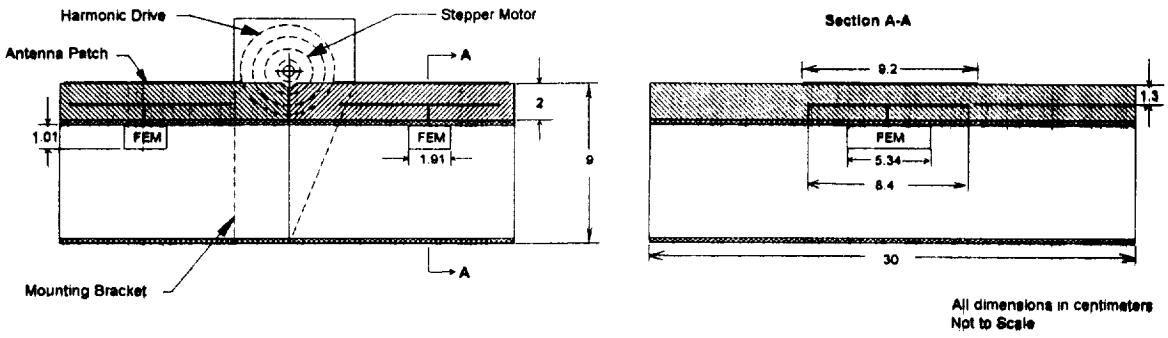

Figure 5.1-7. Cross Section Showing Hinge, Antenna Patches, and FEM.

intermediate frequency (IF) signals, and provides analog-to-digital (A/D) conversion of these two signals (figure 5.1-8). The digitized signals are routed via the data transmitter section to the CPU/Correlator. The I&Q reference oscillator signals are derived from a single Master Oscillator (MO). This MO signal is distributed through seven Master Oscillator Distribution Interfaces (MODIFs) to 33 Injection Locked Phase Locked Loop (ILPLL) circuits. Synchronized up-converted outputs from the ILPLLs provide the I&Q local oscillator (LO) reference signals for the FEMs.

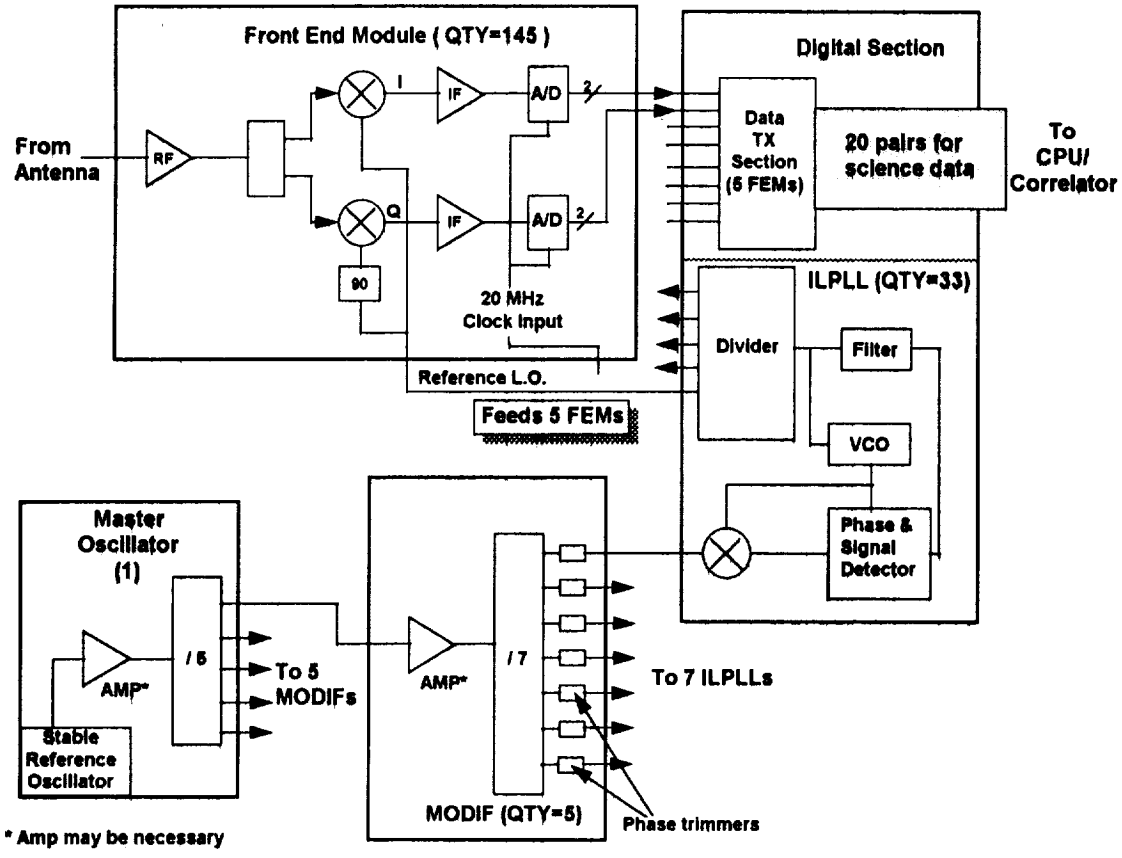

Figure 5.1-8. Schematic of ESTAR RF Electronics

The physical layout of L-band radiometer electronics is shown in figure 5.1-9. Each FEM is located inside the antenna support tube directly behind the corresponding antenna patch.

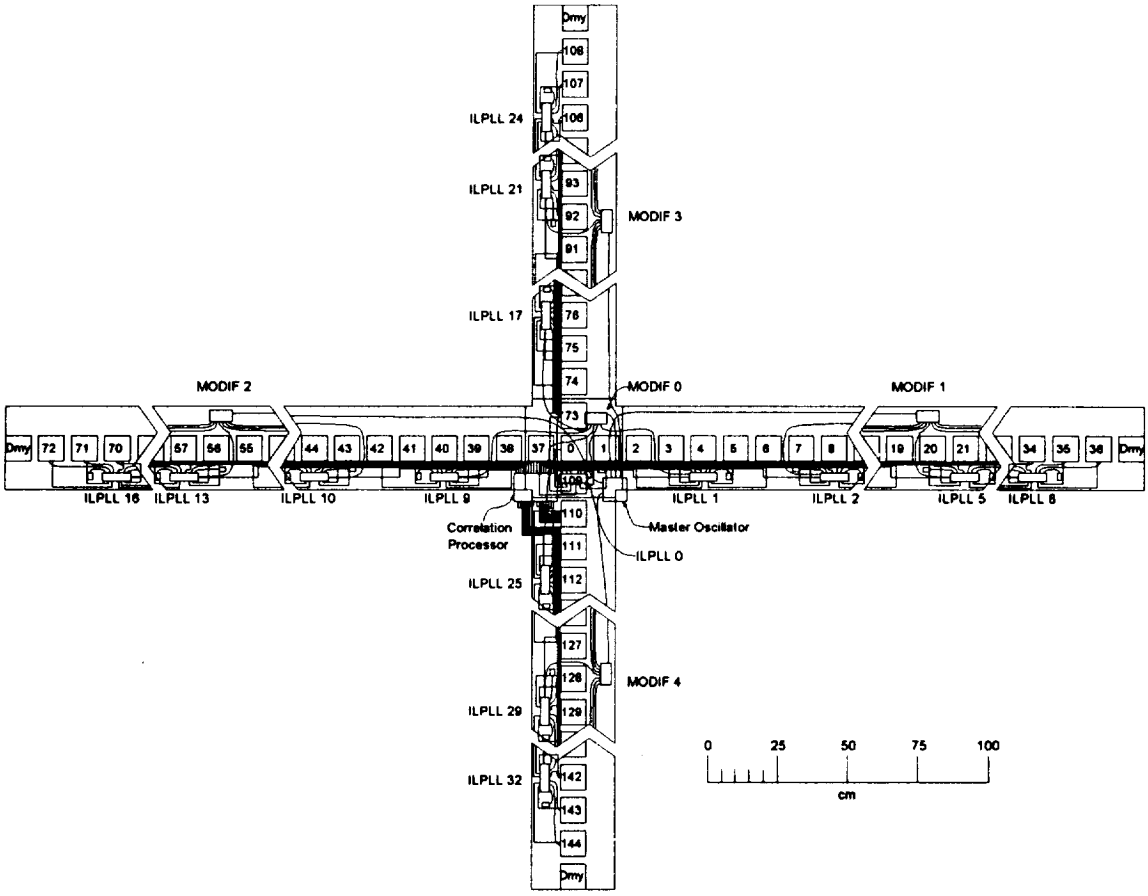

Figure 5.1-9. Layout of Radiometer Electronics

Also located within the tube structure are ILPLL modules, MODIFs, and RF, digital and power cables. The center section (figure 5.1-10) of the antenna structure houses the digital receiver modules, the Master Oscillator, cables and connections to the CPU/ Correlator, and the power supply. Correct correlation of received signal pairs requires knowledge of all instrument induced phase errors at the A/D converter in each channel. The distributed system architecture used in this concept is highly susceptible to time varying phase differences that could produce errors, particularly in the presence of temperature variations induced by the space environment. Therefore, the instrument design must either match all reference (LO) signals and eliminate receiver phase errors in all channels, or a phase stability calibration scheme must be added to the instrument design. The thermal design is an important factor in both approaches.

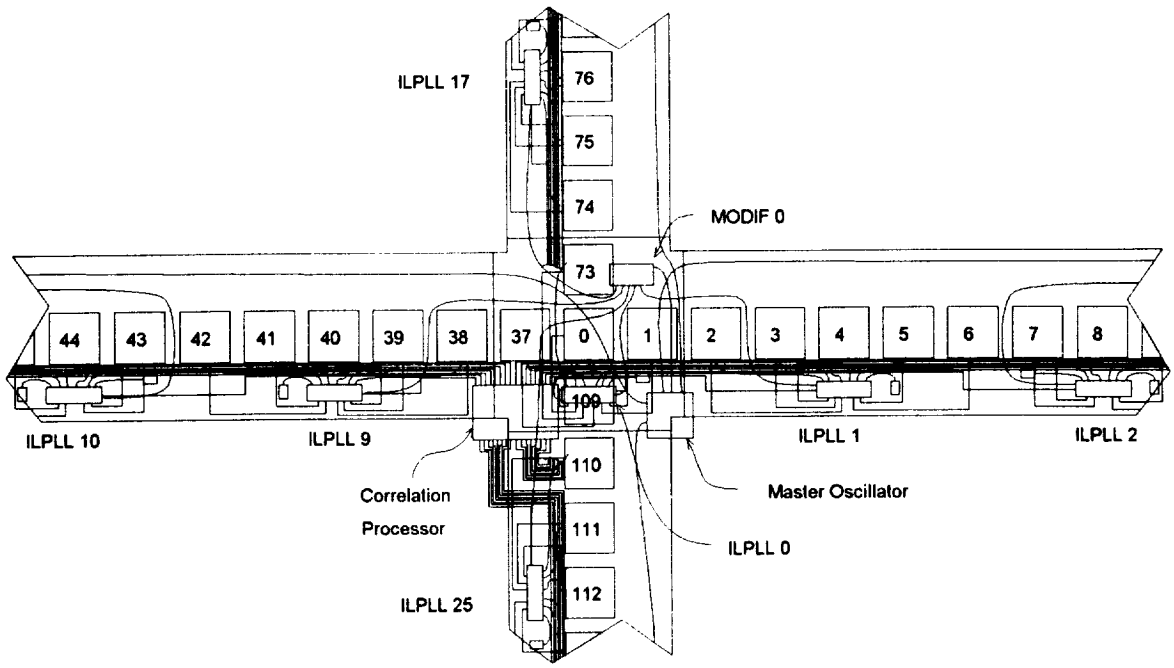

Figure 5.1-10. Layout of RF Electronics in Center Section

5.1.4.1. Front End Module (FEM)

The signal from the antenna is amplified, filtered, and fed to the mixer. The mixer accepts an LO signal from the ILPLL, and provides down-conversion creating both I&Q channels. The resulting baseband I&Q signals, having a bandwidth of approximately 30 MHz, are amplified by IF amplifiers, and then passed through 10 MHz low pass filters to obtain the desired signals for A/D conversion. These signals are subsequently sampled at 20 Msamples/second by high speed 2-bit A/D converters. Phase compensation networks are included in each FEM to establish accurate phase relationships between the I&Q channels, and between all the FEMs in the array. The digital outputs are routed to the transmitter circuits housed in the ILPLL module.

To minimize volume, power and mass of the FEM, both hybrid and monolithic microwave integrated circuit (MMIC) technologies were considered for the design and integration of the FEMs. With limited circuit details available for the FEM, the MMIC technology was selected for this concept on the basis of lower power and volume. Tables 5.1-2 and 5.1-3 show the comparison between MMIC and hybrid technologies with respect to power and mass for the L-band electronics. A trade study to select the optimum technology for the FEM design should be conducted when the design is more mature. The thermal characteristics of the FEM were not modeled in this study although it is recognized that thermal stability is an important factor in the calibration of the radiometer. A comprehensive thermal analysis will be an important part of future design studies.

	MMIC			HYBRID		
	Power (watts)	Mass (kg)	Size (cm) L x W x H	Power (watts)	Mass (kg)	Size (cm) L x W x H
Master Oscillator	2.75	0.245	5.08 x 2.54 x 1.27	0.878	0.042	10.16 x 5.08 x 0.96
ILPLL	22.5	4.90	6.35 x 3.81 x 1.91	38.61	1.69	9.85 x 5.08 x 0.96
Front End Module	72.5	13.34	5.34 x 1.91 x 1.01	130.1	11.17	11.43 x 5.08 x 0.96
MO Distribution I/F	2.5	0.47	2.54 x 3.05 x 0.76	1.14	0.22	7.62 x 5.08 x 0.96

Table 5.1-2. Comparison of MMIC and Hybrid Components

	MMIC	Hybrid
Power (watts)	100.25	214.64
Volume (cm^3)	78.83	189.40
Total Mass (kg)	18.96	13.13

Table 5.1-3. Radiometer Resource Requirements for MMIC and Hybrid Designs

5.1.4.2. Master Oscillator

The MO is a highly stable, temperature compensated, relatively low frequency RF signal source (probably in the order of 100 MHz). The MO output is the reference for all the LO signals in the instrument. It is located in the L-band electronics compartment and feeds phase and amplitude matched signals to the MODIFs.

5.1.4.3. Master Oscillator Distribution Interface (MODIF)

The MODIFs distribute the MO reference signal to all the ILPLLs. The MODIF design consists of an amplifier, and a seven-way signal splitter that has port-to-port phase matching (the phase tolerance is TBD). There are five MODIFs in the radiometer; all are strategically located to minimize cabling. One MODIF is located in each of the four arm structures, and one in the central electronics section. MMIC technology was used in this study for consistency with other modules, but further analysis may show that hybrid technology is better suited for this low quantity application.

5.1.4.4. Injection Lock Phase Lock Loop (ILPLL)

The ILPLL module contains two distinct sections: the ILPLL itself, and a digital transmitter section. The ILPLL receives the reference signal (approximately 100 MHz) from the MODIF, and generates I&Q pairs of phase-locked LO signals at 1.41 GHz. There are five output pairs from each ILPLL. Therefore, each ILPLL can supply I&Q LO signals to five FEMs. As with the FEMs, a preliminary comparison of MMIC versus hybrid technologies was made, and MMIC was chosen because of the potential savings in volume, and power. The digital transmitter section has five input channels, and receives the digital signals from the FEM A/D converters. Each input channel consists of two (I&Q) 2-bit parallel data connections plus a ground connection. The transmitter circuits convert these signals to differential signal levels, and retransmit them to the Data Receive modules.

5.1.4.5. RF Cables

Micro-coaxial RF cable that displays good phase and attenuation stability under varying temperature conditions is utilized to meet the phase sensitivity criteria mentioned previously. Cable lengths are also matched to minimize phase differences. For example, all MODIF-to-ILPLL cables are of equal length and all ILPLL-to-FEM cables are of equal length. The cable routing and module placement is designed to keep any high frequency RF distribution cables from crossing over a fold joint in the structure. This removes the potential of amplitude and phase changes due to the initial bending of the cable when the radiometer array is deployed.

5.1.4.6. Data Transmission

The L-band radiometer data system features an interface to transfer data from the FEMs to the CPU/ Correlators, and from the CPU/ Correlators to the spacecraft Command and Data Handling (C&DH) system. The FEMs provide two-bit parallel digital outputs at standard logic levels, and have a sample rate of 20 Msamples per second. To transmit these signals to the CPU/Correlators with adequate EMC performance, two methods of data transmission were considered: 1. Fiber optic transmission, and 2. Differential data transmission. The ILPLL modules were selected as the locations to house the transmitters, and the Data Receive modules were located close to the CPU/Correlators.

A fiber optic multiplex scheme was investigated, but did not provide a significant reduction in the estimated mass or power consumption, and was therefore not pursued. However, the fiber optic option is worthy of future study to take into consideration the improved EMC performance afforded by this technology.

The differential interface provides good noise immunity over the long signal path from the antenna arms to the central electronics compartment. Very thin, very flexible multi-conductor cables (similar to flexible printed circuit boards) are used from the FEMs to the

ILPLLs, and from the ILPLLs to the Data Receiver modules. All the FEM-to-ILPLL cables are matched in length to minimize delay differences. Each ILPLL accepts up to five FEM channels (four bits of data per channel: two each for the I &Q signals), and converts these to differential levels for transmission to the Data Receive modules located in the center section of the antenna structure. The Data Receive modules (one per arm) include differential receivers, digital data latches, and synchronization timing logic, thus providing the interface to the CPU/ Correlators. The phase delays in the data transmission, and in the sample and hold circuits at the CPU/Correlators are precisely matched to maintain the integrity of the correlated output products. An adjustment capability is provided to achieve adequate matching.

5.1.4.7. Computer Processing Unit (CPU)/Correlator

A general definition of the CPU/Correlator electronics was created to permit estimation of the data rate, mass and power requirements for the spacecraft subsystems. The specifications for an advanced digital correlator integrated circuit were obtained from the preliminary product specification (ref. 8) of a CMOS digital correlator proposed by the NASA Space Engineering Research Center for VLSI Systems Design at the University of Idaho. This design, shown in figure 5.1-11, is a VLSI correlator chip that has excellent size and power characteristics. Each VLSI chip is capable of 1600 correlations (40 x 40 inputs), and has a power dissipation of 800 mw. However, the device is a paper design that has not been built. Therefore, as a solution to the large scale correlation requirement, it requires further development.

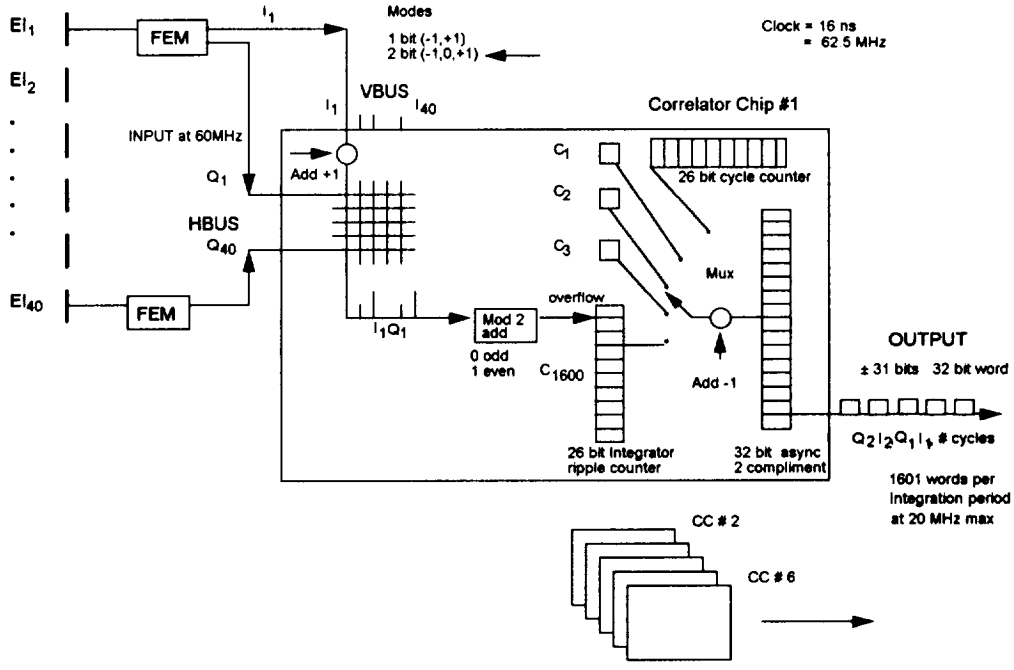

Figure 5.1-11. Correlator Schematic

The total number of correlations used in this study is 20,880 for the 73 x 73 element design. There is considerable redundancy in the correlation data due to duplicate spacing of antenna elements. For example, there are 72 X-X pairs that are 0.55λ apart, and 71 X-X pairs that are 1.1λ apart. The spacing interval between element pairs is N x 0.55λ, where N = 1,2,3, etc.. Figure 5.1-12 shows the number of element pairs for each spacing interval. Since each interval reflects a single value in the frequency domain, multiple values of a particular interval could be added together, and a single value downlinked to the ground. A data downlink rate of 50-80% of the current estimate may be possible using this approach. Techniques to reduce the data downlink rate from the L-band radiometer by on-board processing are suggested for future analysis and evaluation. A 12 bit word per correlation was used in the sizing of the spacecraft data system resulting in the overall mass and power discussed in other sections.

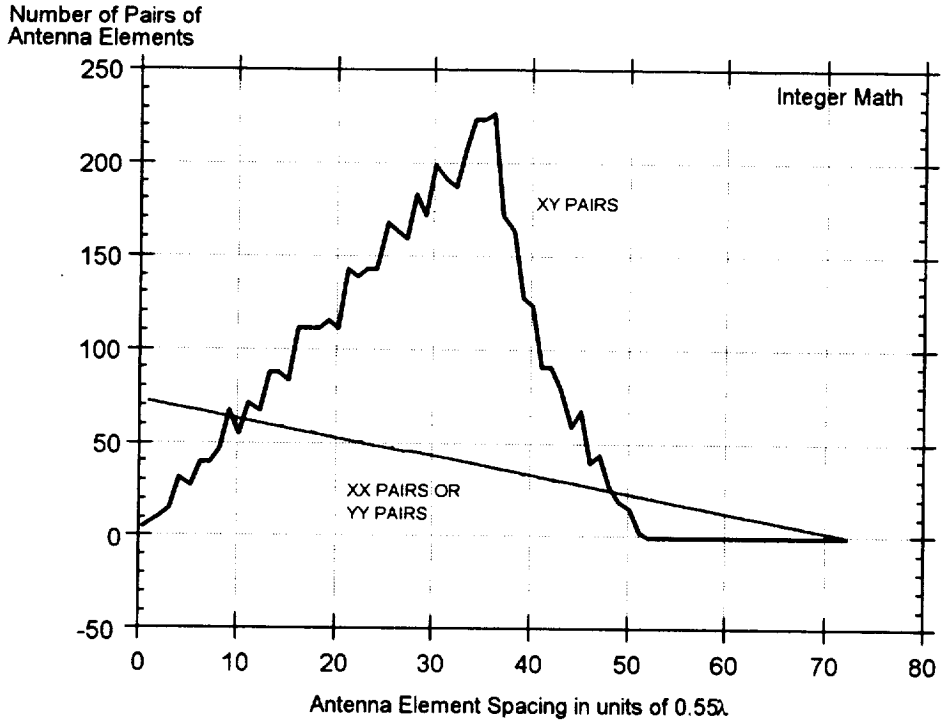

Figure 5.1-12. Number of Correlation Pairs for 145 Elements

5.1.5. L-band Radiometer Mass and Power Summary

The estimated mass of the L-band radiometer is 166 kg including the antennas, the structure, and the electronics. The power dissipation of the instrument is 209 watts. Table 5.1-4 provides a summary of the mass and power for the L-band radiometer. A more detailed breakdown of the mass and power is provided in Appendix C.

Item	Quantity	Mass * (kg)	Mass %	Power ** (w)	Power %
Antenna Structure	1	39.65	23.9%	-	-
Antenna Elements	145	16.59	10.0%	-	-
Motors/Mechanisms	1	35.61	21.5%	-	-
Other Structure	1	19.08	11.5%	-	-
Launch Restraints	1	5.9	3.6%	-	-
Front End Module	145	17.34	10.5%	101.50	48.6%
ILPLL	33	6.37	3.8%	31.50	15.1%
Local Oscillator	5	0.61	0.4%	3.50	1.7%
Cables: RF, Digital, Power	~180	16.36	9.9%	-	-
Data Receive Module	4	2.34	1.4%	8.40	4.0%
Master Oscillator	1	0.32	0.2%	3.85	1.8%
CPU	1	3.9	2.4%	19.66	9.4%
Power Supply	1	1.56	0.9%	40.60	19.4%
L-band Total		**165.63**	**100%**	**209.01**	**100%**

* including 30% margin ** including 40% margin

Table 5.1-4. L-band Radiometer Mass and Power Summary

5.2. Infrared Scanning Radiometer

The sea surface temperature measurement is provided by an IR scanning radiometer using two spectral bands in the 8 to 12 micron region. The IR approach was selected for its small size, low mass (8.9 kg), and low power consumption (14 watts). It has both day and night observation capabilities, although its performance is limited in the presence of cloud cover. An alternate approach, using another radar band (C or X band) to measure the sea surface temperature, is desirable to overcome the cloud obscuration, but has disadvantages in increased volume, mass and power.

This two band IR instrument is a line scanning imager with 10 km spatial, and ±1 K temperature resolution. The accuracy of a single wavelength IR instrument for sea surface temperature measurement is adversely affected by the atmospheric water vapor encountered along the line of sight of the instrument. The use of a second spectral band provides the capability to estimate the water vapor content, and apply the necessary correction to the sea surface temperature measurement. The IR instrument also provides a capability for identification and registration of ground targets seen by the overlapping fields of view of the IR and L-band instruments. By viewing the same scene in both IR and radar signatures, the interpretation of the target is easier and allows registration of selected targets by either human or machine methods. A more detailed description of the instrument is provided in Appendix A.

5.3 Visible Video Camera

The main objectives of the mission can be achieved by the L-band and IR instruments discussed previously. However, a video camera is included in the conceptual system due to its high spatial resolution capability (<1 km), low mass (0.5 kg), and low power consumption (4 watts). Similar to the IR scanner, the video camera overlaps the L-band field of view, and assists in the spatial registration of radiometer data with various land and coastal features.

The design selected is a black and white slow scan camera sensitive to wavelengths in the 0.45 to 1.1 micron region. The exact spectral band should be the subject of further analysis to optimize the design relative to the scientific goals of the mission. The range selected is likely to include the near IR up to 1.1 microns to minimize haze effects. The camera operates in a burst mode with five frames in each burst. The video concept uses a frame grabber on board the satellite. This device averages the five video frames acquired in each burst, and the result is sent to the ground at the rate of one averaged frame every 60-90 seconds. The slow scan approach was adopted to minimize the downlink data rate required for the video signal. Alternate video camera concepts were identified and are shown in Appendix B.

6. SPACECRAFT BUS

Several spacecraft designs were briefly reviewed to obtain data on which to base the concept for the ESTAR platform. No attempt was made to select the preferred bus or vendor. This approach allowed an assessment of the technical feasibility of an ESTAR mission using spacecraft parameters compatible with current offerings from manufacturers. Most of the data presented for the spacecraft design is derived from the Pegastar spacecraft from Orbital Sciences Corporation (OSC). This is because more detailed data was available on this bus at the time of the study. An advantage of this bus, for applications that use OSC launch vehicles, is the use of an integrated avionics for the launch vehicle and spacecraft control functions. The integrated approach permits the use of the spacecraft data processing components to control the launch vehicle during orbit insertion. The reduction achieved in mass to orbit is particularly advantageous for missions using the smaller Pegasus vehicle. This is discussed further in section 4.0, Launch Vehicles. All the buses identified offer numerous options and configurations. Therefore, the recommendation or selection of the bus for the ESTAR mission will be the subject of future analyses and comprehensive trade studies.

6.1. Derived Spacecraft Bus Requirements

The spacecraft bus requirements are derived from the ESTAR mission and instrument requirements, and the launch vehicle interface requirements. The major accommodation requirements for the ESTAR payload are summarized in table 6.1-1.

Payload Mass	178 kg
Payload Power	248 watts
Payload Data per Orbit	2.5 Gbits
Orbital Altitude	402 km
Orbital Inclination	Sun Synchronous
Pointing Control	±0.30 deg
Lifetime	3 years

Table 6.1-1. ESTAR Payload Requirements

The constraints imposed by the launch vehicle are the total mass to be transported to the desired orbit, the available volume inside the shroud, and environmental factors. These parameters are discussed in the following sections.

The payload power requirement of 248 watts continuous, in conjunction with a small satellite class bus mandates full sun-tracking solar-arrays augmented by batteries for

power during the shadow portion of the orbit. A low earth orbital altitude of 402 km in conjunction with what will probably be a small ballistic coefficient will produce a large fuel requirement for orbital altitude maintenance. The fine pointing requirement of the payload dictates the need for a star tracker and/or a rate integrating gyro to determine attitude, along with a GPS system for position determination. Lastly, to achieve a low cost design the systems do not include redundant hardware except in a few critical areas such as parts of the communications, data processing, and propulsion systems.

6.2. Bus Description

The basic spacecraft bus configuration can be seen in figure 6.2-1. The core structure of the bus is a hexagonal aluminum framework measuring 0.97 m across and 1.30 m high. The external faces are fabricated with an aluminum honeycomb sandwiched between aluminum face sheets. The bus portion of the spacecraft accommodates equipment mounted both internally and externally. Payload equipment is mounted in the section above the bus.

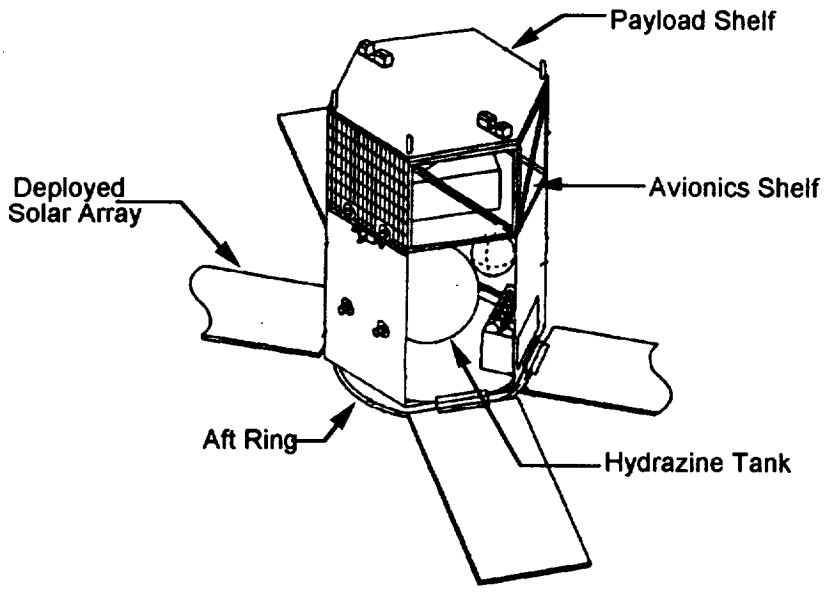

Figure 6.2-1. Spacecraft Bus Configuration

The configuration of the spacecraft integrated with the ESTAR instrument is shown in figure 6.2-2 in various stages of deployment.

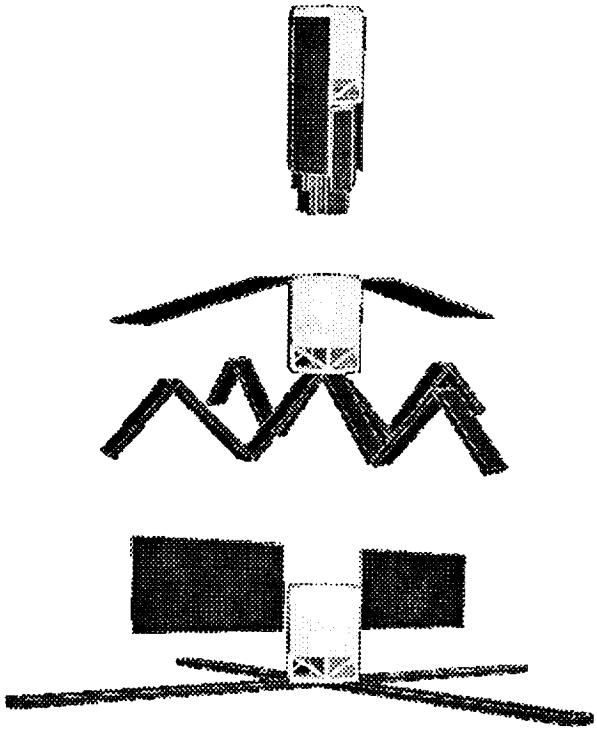

a) Launch configuration: solar arrays folded around antenna

b) Partially deployed: arrays driven by beta joints

c) Fully deployed: operational configuration

Figure 6.2-2. Deployment Stages of the Integrated Satellite

6.2.1. Power System

Gallium arsenide solar cells (similar to those used in the Earth Observing System (EOS) AM baseline) are used because of their relatively high beginning-of-life (BOL) efficiency of 18.5 percent. They are mounted on core panels (0.56 m x 2.06 m) that are fabricated using an epoxy-carbon-fiber honeycomb construction. There are two solar arrays each made up of two such panels. The arrays are folded around the bus during launch, and are deployed on-orbit. Once deployed they are fully sun-tracking with two-degrees of freedom (figure 6.2-2c). The battery system used for energy storage is composed of four nickel-hydrogen battery packs. Each of these 28 volt packs uses a common pressure vessel type of construction, and is rated at six ampere hours. The batteries operate at 80 percent efficiency and a maximum depth of discharge of 45 percent. The Battery Charge Regulator (BCR) provides charge regulation between the solar arrays and the batteries. It also controls the battery discharge and maintains the bus voltage to the power distribution at 28V $\pm$4V.

6.2.1.1. Power Allocation and Generation

The total power required for all the instruments is 177 W, but due to uncertainties, a 40% margin is added giving a total payload power of 248 W. Power requirements for the spacecraft components are based on industry figures, modified to account for anticipated design variations. The margin on the spacecraft components is limited to 10%, reflecting the maturity of the component designs. The orbit-averaged power requirement for the satellite is 473 W. Assumptions, as stated in table 6.2-1 were used to determine the design parameters for the power system.

Regulator Efficiency	87 %
Battery Efficiency (charge/discharge)	80 %
Battery Maximum Depth of Discharge	51 %
Time in Sunlight	0.94 hr
Time in Shadow	0.60 hr
Solar Cell Packing Factor (% of area)	90 %
Solar Cell Efficiency at EOL	0.1694

Table 6.2-1. Assumptions Used in Power System Design

The total energy required from the solar arrays during the sunlit portion of the orbit is the sum of the energy required to operate the integrated spacecraft, and the energy required to charge the batteries. The total energy required during each orbit is 868 whr. The energy generation capability was calculated for fully articulating gallium arsenide arrays. The maximum advertised array size for the bus used in this concept is 4.66 m^2. This size and the end-of-life (EOL) efficiency are used to determine the operating margin. This results in a total energy generation capability of 904 whr, and an EOL margin of 4.2% for the arrays selected.

The required energy storage is 284 whr, and requires a minimum battery capacity of 19.7 Ahr. The batteries used each have a capacity of 6 Ahr. Therefore, four batteries are required giving a total storage capacity of 672 whr resulting in a 42% depth of discharge.

6.2.2. Command and Data Handling

The Command and Data Handling (C&DH) system includes the components for spacecraft control processing, health and status monitoring, and storage of both spacecraft and science data. The spacecraft is controlled by a single 68000 based central processing unit (CPU). The main memory has a capacity of eight megabytes (MB). It is housed in the same enclosure as the CPU, and is used for spacecraft data processing and for the storage of health and status data. The Spacecraft Maintenance Unit (SMU) provides the

interface between the CPU and the various subsystems and components that control and monitor the spacecraft functions. The two SMUs accommodated in the bus are connected to provide a redundant backup capability.

The science data from the instruments is stored in the payload memory. This memory is also located in the C&DH area, and interfaces to the L-band electronics compartment as well as to the communications system. The following assumptions were used to determine the worst case memory capacity requirement for the spacecraft data system:

- Twenty-four hour operation of science instruments
- Enough mass memory for the data acquired during two orbits
- Fifteen percent overhead to include ID, time tagging, etc.
- Utilization of only twelve (12) bits per correlation from a possible 32 bit double-word

It was determined that a storage capacity of five gigabits is required. This is discussed in more detail in the communications analysis section (section 7.4). In that section, table 7.4-1 shows the data rates for the TV camera, IR scanner, L-band radiometer and spacecraft telemetry, and indicates the aggregate volume of data collected for two orbits. The data system is capable of recording at an aggregate data rate of 450 Kbps.

A comparison, summarized in table 6.2-2, was made between solid state memory and magnetic tape recording technologies. Solid state dynamic random access memory (DRAM) was selected to take advantage of the lower mass and power associated with this technology. The memory accepts 16 bit wide data words, and is accommodated on ten 0.5 GB plug-in boards. The enclosure is similar to that used for the data processor. Future studies should include a more comprehensive analysis to optimize the scheme for data storage, formatting and retrieval.

	Solid State Memory	**Magnetic Tape Recorder**
Implementation	10 modules, 0.5 Gbits each	Three recorders, 1.7-1.8 Gbits each
Size (cm)	Plug in boards	23 x 35 x 18 (per unit)
Mass (kg)	15.1 (10 @ 1.51 each)	31.2 (3 @ 10.4 each)
Power (watts)	60 (10 @ 6.0 each)	69-126 (3 @ 23-42)

Table 6.2-2. Mass Memory Comparison

6.2.3. Communication

The communication system provides an S-band data link to many of the ground stations controlled by NASA and others. The on-board dual-function system is capable of communicating with the Standard Tracking and Data Network (STDN), and with the U. S. Air Force's Space to Ground Link Subsystem (SGLS). There are two S-band omnidirectional antennas on the nadir side of the spacecraft that are deployed on orbit. Mounted on the interior of the spacecraft are the S-band transfer switch, S-band coupler, and a pair of dual redundant STDN/SGLS transponders used for both uplink and downlink. These transponders, which may require some development for the dual function concept, interface to the Command and Data Handling System (C&DHS), and receive uplinked command and control data, as well as providing a downlink for science data and spacecraft telemetry. Table 6.2-3 lists the components that comprise the communication system.

Item	Quantity	Mass (kg)	Power (watts)
RF Harness	1	3.64	0.00
S-Band Omni Antenna	2	0.45	0.00
S-Band Transfer Switch	1	0.07	0.25
S-Band Coupler	1	0.05	0.00
STDN Transponder	2	8.20	36.00

Table 6.2-3. Communication system components

This system was selected over an alternative concept using the Tracking and Data Relay Satellite System (TDRSS). The analysis selection process used is described in section 7.4. The STDN/SGLS has lower mass and lower power consumption, and was determined to be feasible for this conceptual design, although the data rate margin is small.

6.2.4. Attitude Control and Determination

The spacecraft is controlled by the attitude control and determination system, which utilizes the data system CPU to process the control algorithms. Orbital position is determined by means of a six-channel GPS receiver with dual redundant antennas. Attitude is controlled by a momentum wheel, three magnetic torquers, and a hydrazine reaction control system. Attitude determination utilizes a combination of several sensors including scanning horizon sensors, two-axis sun sensors, a three-axis magnetometer, and a star tracker. This system provides a pointing accuracy of 0.1 deg, and pointing knowledge of 0.02 deg.

6.2.5. Propulsion

The propulsion system is a monopropellant hydrazine system. A titanium tank with a separate helium pressurant tank has a 102.45 kg capacity. The propulsion system provides a specific impulse (Isp) of 220 seconds and has an efficiency of 90 percent.

6.2.6. Thermal

The spacecraft thermal design is primarily passive with active heating provided only for the batteries. The payload platform is mounted on struts that thermally separate the payload from the spacecraft bus (figure 6.2.1). A warm cavity design is used for the spacecraft bus with the electronic systems providing heat to the interior, while multi-layer insulation and thermal coatings provide control of external heat exchange.

6.2.7. Mass and Power Summary

The mass and power summary for the spacecraft is shown in table 6.2-4. The mass of the spacecraft systems and the associated mass margins are based on manufacturer's data, which was provided in great detail. The given data included various mass margins depending on the maturity of the design for each component (e.g., previously built, prototyped, or breadboarded). Using these criteria, estimates were also made for each spacecraft component requiring changes from the published reference configuration. In the table the margins for each system are given, and these are included in the mass estimates provided. The power estimates are presented in a similar manner and include a ten percent margin for the spacecraft systems, also based on manufacturer's data. Most of the power data is unchanged from the published configuration. Systems that were changed for this concept retain the same ten percent margins since most of the changes are to the quantities of components (e.g., DRAM) rather than new designs.

The mass and power for the ESTAR experiment, including all three instruments, are also presented in table 6.2-4. The mass margin is 30 percent, and the power margin is 40 percent. These relatively high margins are used because of the preliminary state of the ESTAR design. The detailed mass and power breakdown is located in appendix A. The dry mass fractions of the instruments in the Pegasus and Taurus cases are 0.43 and 0.41 respectively.

	Mass Margin (%)	Mass (kg)	Power Margin (%)	Power (watts)
ESTAR Experiment	30	178.43	40	248.21
Spacecraft				
Data Management	10	33.76	10	106.59
Orbit Determination	8	2.41	10	4.18
Structure	8	51.87	10	0.00
Ordnance	1	9.29	10	0.00
Thermal	10	6.01	10	16.50
Communication	10	13.65	10	39.88
Hydrazine Propulsion	7	17.43	10	3.99
Electrical Power	10	99.67	10	28.70
Attitude Control	8	20.20	10	25.15
Expendables	10	102.45	10	0.00
Totals		535.16		473.19

Table 6.2-3. ESTAR Spacecraft Mass and Power Breakdown by System

7. SYSTEMS ANALYSES

7.1. Launch Loads Analysis

A structural launch loads analysis of the 2-D ESTAR instrument was performed to establish a basis for mass estimation. The structural design was verified using launch loads since these are typically the highest loads that a spacecraft encounters. In addition to determining the most appropriate mass, the analysis determined the areas in the design that require additional stiffening. The analysis considered only periods of maximum acceleration loading rather than a comprehensive analysis of the entire launch sequence. The maximum loads used are described as quasi-static accelerations, and were obtained from the manufacturer's published data for the launch vehicles considered. Both the Pegasus and the Taurus launch vehicle cases were studied. The Pegasus has fixed wings and is dropped from an aircraft at launch. This results in a high transverse acceleration load on the payload. The Taurus, however, is launched on a vertically oriented first stage booster, and thus produces a high axial load. The analysis was performed using the study baseline instrument with each launch vehicle.

7.1.1. Design Constraints and Assumptions

The L-band instrument was the subject of this analysis. The spacecraft was not modeled due to a lack of structural definition of the bus and its mechanical interfaces. The instrument configuration is defined by the number of antenna patches, their spacing, and the instrument performance requirements. The primary design drivers are the length of each arm, the width of the structure, and the layout of the antenna arms in the form of a cross. The rectangular, tubular cross section described in section 5.1.2 was selected leaving the wall thickness as the main design variable for optimization.

It was assumed, in the finite element analysis, that the structure had no bulkheads or stiffeners. Such supporting structure was not included since the analysis was limited to assessing the feasibility of a conceptual design. Another assumption used in the finite element model was that the spacecraft bus would not affect the overall response of the system. Supporting boundary conditions at the interface were added.

The factor of safety, and the knockdown factor used are 2.0, and 0.85 respectively (ref. 9). The factor of safety was applied to the maximum expected operating load to provide a conservative design. Knockdown factors are strength reduction factors, and were used to account for uncertainties in the composite materials.

7.1.2. Materials

To ensure a high strength to weight ratio, a graphite-epoxy laminate was selected for the structure. Graphite-epoxy is light-weight and has a very low thermal conductivity. This is important for thermal considerations and is discussed in more detail in 7.2.

The thickness of each lamina (or ply) is 0.127 mm (0.005"). The material properties for a single lamina are shown in table 7.1-1. These properties for the combined laminate are determined by the orientation and stacking sequence of each ply, and may be optimized for specific performance characteristics. In the analysis, the composite ply orientation was determined by the need to keep the thermal coefficients of expansion as low as possible while maintaining relatively high moduli. The three cases presented have different laminate configurations and thicknesses. Table 7.1-2 lists the corresponding properties.

Property	SI Units	English Units
E_1	13.4 GPa	19.45 Mpsi
E_2	11.7 GPa	1.70 Mpsi
G_{12}	6.89 GPa	1.0 Mpsi
ν_{12}	0.31	0.31
α_1	-1.167×10^{-7} m/m/°C	-0.21×10^{-6} in/in/°F
α_2	8.89×10^{-6} m/m/°C	16.0×10^{-6} in/in/°F
ρ	0.001606 kg/cm^3	0.058 lb/in^3

Table 7.1-1. Graphite-Epoxy Single Ply Properties

Property	10 Ply	20 Ply	40 Ply
Orientation	$(0,\pm30,0,90)_s$	$(0_2,\pm30,90_2,\pm30,0_2)_s$	$(\pm30,0_2,\pm30,0_2,\pm30,$ $90_2,\pm30,0_2,\pm30,0_2)_s$
t	0.05 in	0.10 in	0.20 in
E_1	12.5 Mpsi	12.5 Mpsi	13.06 Mpsi
E_2	5.63 Mpsi	5.63 Mpsi	3.92 Mpsi
G_{12}	2.22 Mpsi	2.22 Mpsi	2 Mpsi
ν_{12}	0.299	0.299	0.3
α_1	0.413×10^{-6} in/in/°F	0.413×10^{-6} in/in/°F	-0.06×10^{-6} in/in/°F
α_2	3.36×10^{-6} in/in/°F	3.36×10^{-6} in/in/°F	5.30×10^{-6} in/in/°F

Table 7.1-2. Laminate Properties

7.1.3. Finite Element Model of Stowed Configuration

Analysis of the finite element model was completed using MSC/NASTRAN and pre-processing and post-processing were performed using the I-DEAS software from Structural Dynamics Research Corporation (SDRC). The finite element model has 1220 thin shell elements. This includes 552 linear triangle, 660 linear quadrilateral, and 8 parabolic quadrilateral elements.

The stowed configuration of the finite element model is shown in figure 7.1-1. The four arms are folded into the launch position. The square central base has fixed, clamped supports to model the boundary condition of the bus interface. The hinges are assumed to be in a locked position. Detailed analysis of the hinges has not been performed due to a lack of hardware definition. All electronics, antenna elements, motors, and hinges are modeled as non-structural mass. The antenna elements are bonded to two-centimeter thick honeycomb substrate segments that are attached along the length of the structure, and are assumed to have no structural stiffness. Rigid straps, not shown in the figure, connect the corners of adjacent arms, and support the structure by preventing the arms from folding out.

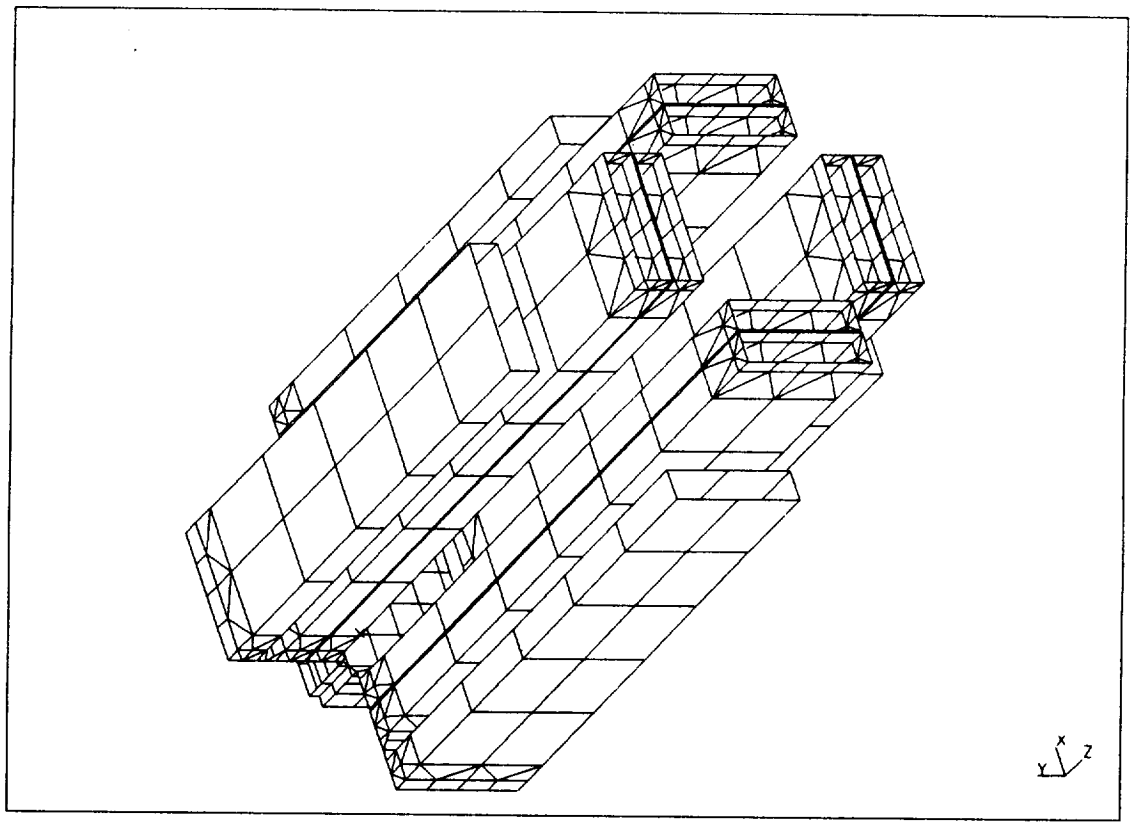

Figure 7.1-1. Finite Element Model of 2-D ESTAR in a Stowed Configuration

7.1.4. Launch Load Results

Initial analysis was performed considering a Pegasus launch vehicle. A second case using a Taurus launch vehicle was studied after it was found that the Pegasus capability was insufficient to achieve the desired orbit. The quasi-static launch load results for both cases are presented. The finite element model of the stowed configuration is the same in both cases; the only difference is the magnitude of the loads.

7.1.4.1. Pegasus Launch Vehicle

A schematic created by Orbital Sciences Corporation (ref. 4), which outlines the Pegasus launch profile, is shown in figure 7.1-2. The Pegasus is a winged, three-stage booster that is released from an aircraft. The maximum quasi-static loads occur just after the start of the first stage ignition as the vehicle begins to lift following its release from the aircraft (ref. 4). During this period, large transverse and axial loads are present. The published loads are listed in table 7.1-3. A factor of safety of 2.0 was applied to these loads for the analysis, but is not included in the figures in the table.

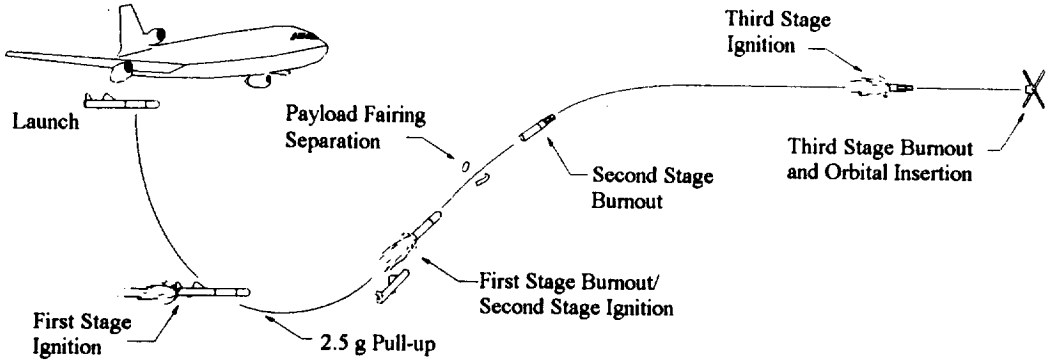

Figure 7.1-2. Standard Pegasus Mission Profile (ref. 4)

Direction	Acceleration	Load
Transverse	A_x	0.5 g
Transverse	Ay	2.5 g
Axial	A_z	-3.65 g

Table 7.1-3. Pegasus Launch Loads

Since the configuration of the stowed satellite is primarily cantilevered, the transverse load caused high stress concentrations at the base and at the hinge locations. This resulted in large deformations at the base and the top of the first and second arm folds. The results in table 7.1-4 list the deflections, failure indices, and margins of safety for three different wall thicknesses. The failure index and margin of safety are measures of the possibility of failure and the stress concentration.

The Hoffman failure index, which is used, was specifically developed as a criterion for failure of composites. It takes into account the allowable stresses of the fiber and the matrix in tension and compression, and the allowable shear stress. The knockdown factor of 0.85 is applied to the allowable stress values to take into account variations and discrepancies in the composite materials. This factor is included in the Hoffman failure index, and is a non-dimensional value that represents a probability of failure. If the failure index value is greater than one then failure may occur and conversely if the value is less than one then the design is assumed to be safe.

The results at three critical regions of a single, typical arm are given in table 7.1-4. The three different laminates of 10, 20, and 40 plies were studied to determine the resulting trends. For the 20 and 40 ply cases, the margins of safety are relatively high and yield a safe design based on the imposed loads. In the 10 ply case large deflections and some negative margins of safety exist. However, these high stresses occur only in the areas that are listed. The structure along the length of the arms, which constitutes the majority of the mass, has a positive stress margin. It should be reiterated that bulkheads and stiffeners are not included in the analysis. Substantial support for the structure in the critical regions for the 10 ply case is necessary to properly optimize the mass and should be included in future analyses.

Laminate thickness	Location	Deflection (cm)	Hoffman Failure Index	Margin of Safety
10 Plies	Base of 1st Fold	0.55	1.12	-0.06
	Top of 2nd Fold	1.57	1.55	-0.20
	Base of 2nd Fold	2.07	0.95	0.03
20 Plies	Base of 1st Fold	0.10	0.17	1.42
	Top of 2nd Fold	0.34	0.19	1.30
	Base of 2nd Fold	0.37	0.13	1.79
40 Plies	Base of 1st Fold	0.04	0.10	2.17
	Top of 2nd Fold	0.14	0.05	3.43
	Base of 2nd Fold	0.14	0.06	3.08

Table 7.1-4. Results for 2-D ESTAR on Pegasus Launch Vehicle

7.1.4.2. Taurus Launch Vehicle

The Taurus launch vehicle is an in-line booster that has a higher mass-to-orbit capability than the Pegasus. The magnitude of the transverse loads is less in this case; however, the maximum axial load is much greater. The maximum quasi-static load for each axis, which occurs during first and second stage burns, is listed in table 7.1-5. A factor of safety of 2.0 was applied to these loads for the analysis, but is not included in the figures in the table.

Direction	Acceleration	Load
Transverse	A_x	0.5 g
Transverse	Ay	0.5 g
Axial	A_z	-11.5 g

Table 7.1-5. Taurus Launch Loads

A displacement plot of the structure with a 400% deformation scale is shown in figure 7.1-3. The 10 ply case presented has a wall thickness of 1.27 mm (0.05"). The deflections at the most critical areas, along with their corresponding failure indices and margins of safety, are tabulated in table 7.1-6. It can be seen from the failure index that allowable stress levels have been met providing acceptable margins of safety. The deformation and stresses of the arms are small and acceptable. However, the deformation in the middle of the center motor housing is relatively high (0.98 cm.), and is shown separately in figure 7.1-4. This is probably unacceptable for the antenna patches and electronics that are mounted on the plate, and requires additional stiffeners to reduce the deflections.

Location	Deflection (cm)	Failure Index	Margin of Safety
Center Motor Housing	0.98	0.18	1.36
Top of 2nd Fold	0.37	0.43	0.52
Base of 2nd Fold	0.38	0.22	1.13

Table 7.1-6. Results for 2-D ESTAR on Taurus Launch Vehicle

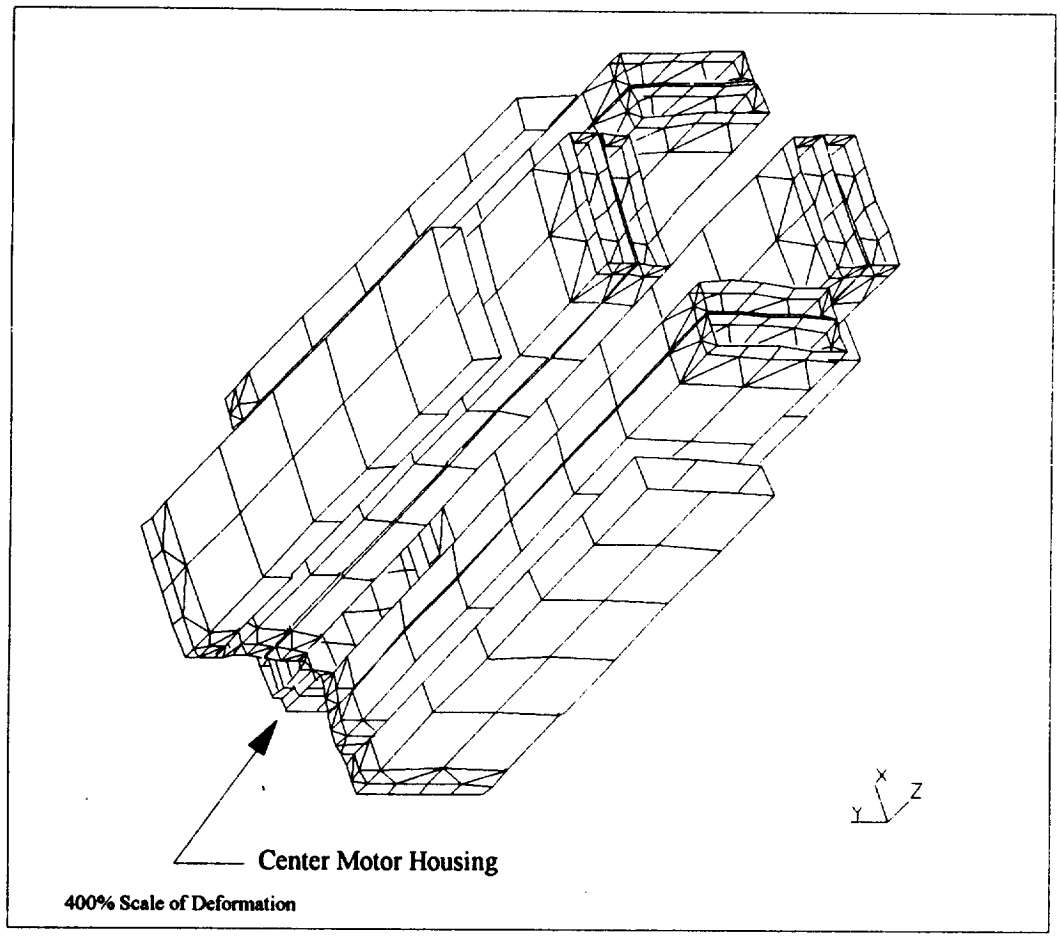

Figure 7.1-3. Deformation of 2-D ESTAR due to Taurus Launch Loads

7.1.5. Summary

The launch loads analysis was performed to support the mass estimates. The wall thickness of the graphite-epoxy structure was the main parameter studied. The intent was not to perform a complete launch analysis that covers every load scenario, rather a preliminary analysis was made to determine the areas in which the conceptual design would need additional support structure. The maximum quasi-static loads imposed on the instrument were defined by the Pegasus and Taurus launch vehicle environments. In both instances a minimum wall thickness of 1.27 mm (10 composite plies) is needed along with bulkheads and stiffeners in critical sections.

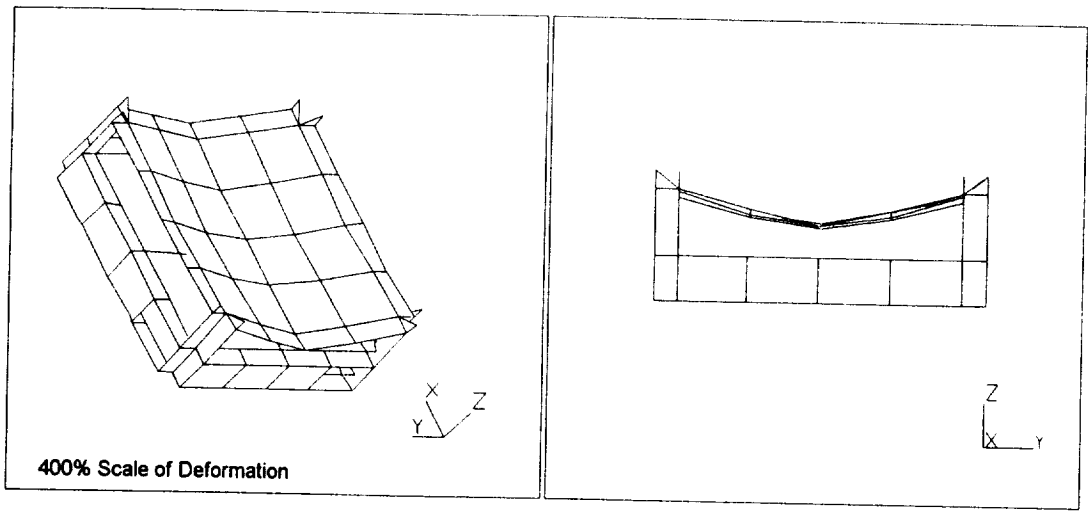

Figure 7.1-4. Isometric and Side View of the Center Motor Housing Deformations

7.2. Thermal Analysis

A preliminary thermal analysis was completed to determine whether the instrument would meet the flatness requirement during the thermal cycling experienced in earth orbit. A goal for the flatness requirement is $\lambda/40$ where λ is the wavelength (21.26 cm.) of the 1.41 GHz input signal. A large relative displacement in the nadir direction between any two antenna patches would result in erroneous phase shifts between the signals received at the antennas. This would result in errors in the correlation products derived from these inputs, and degrade the overall measurement.

The Thermal Model Generator (TMG) module of the I-DEAS software was used to convert the structural finite element model to a finite difference model, to simulate the thermal characteristics and orbital fluxes, and to calculate the temperatures throughout the structure. A structural-thermal distortion analysis was then performed on the original finite element model using MSC/NASTRAN. Results were studied utilizing the post-processing capabilities of I-DEAS.

7.2.1. Design Constraints and Assumptions

In the structural-thermal finite element analysis, only the graphite-epoxy structure is modeled. All electrical components, motors, hardware, and antenna patches are defined as non-structural mass. As in the launch loads analysis, the bus is not considered. However, boundary conditions at the spacecraft bus interface set the X, Y, and Z displacements to zero at the center of the instrument.

For temperature determination the bus is assumed to be thermally de-coupled from the instrument. However, the effects of shadowing of the instrument by the spacecraft bus are

modeled. The structural-thermal distortion analysis assumes the structure to be composed of composite materials. However, since TMG cannot model composite materials the thermal properties are assumed to be isotropic. The following section describes the properties in more detail.

The orbital parameters under consideration at the start of this analysis were for an orbit at a 400 km altitude, and a 60° inclination. All temperatures determined here are for this orbit. Analyses were not performed for sun synchronous orbits since no appreciable difference in the temperature extremes is anticipated.

7.2.2. Materials

For the thermal analysis of the antenna structure there are two sets of material properties to consider: the graphite-epoxy of the antenna structure, and the fiberglass-epoxy honeycomb used for the antenna base or substrate. The design properties of the structural graphite-epoxy laminate are described in section 7.1.2. The wall thickness chosen for this analysis is 1.27 mm (10 composite plies). The fiberglass-epoxy material selected for the antenna base is Hexcel HRH-10 honeycomb. This provides a stiff material to support the antenna patches. It has a high dielectric constant, and a mass density of 80 kg/m^3. The thermal properties for both materials used in the thermal analysis are given in table 7.2-1. Each is assumed to be isotropic for use in TMG.

Thermal coatings are to be used on the graphite-epoxy and honeycomb. Specific coatings were not selected, but the solar absorptivities and thermal emissivities shown in table 7.2-1 are assumed for the analysis. Optimization of the coatings has not been performed, and is left for future consideration.

Property	Graphite-Epoxy	Honeycomb
Thermal Conductivity	2.42 W/m K	0.06 W/m K
Specific Heat	850 J/kg K	850 J/kg K
Solar Absorptivity	0.2	0.2
Thermal Emmisivity	0.9	0.9

Table 7.2-1. Thermal Properties of Graphite-Epoxy Structure

7.2.3. Temperature Analysis

The finite difference model of the antenna, the structure, and the bus is shown in figure 7.2-1 in an exploded view. The antenna sensor elements include the honeycomb dielectric and antenna patches. They are attached to the nadir side of the structure, and the bus is attached to the zenith side. From the orbital and internal heat fluxes, and the thermal characteristics of the entire spacecraft TMG determines the thermal loads to which the satellite is exposed. Temperatures at each of twelve time steps were determined for the duration of one orbit.

The most extreme thermal loads occur at solar noon. At this time the highest temperature gradients exist. A thermal contour plot displaying the nadir and zenith side of the instrument is shown in figure 7.2-2. The effects of shadowing are clearly distinguishable on the structure. Incident solar radiation is blocked by the bus, keeping one arm of the instrument at a significantly lower temperature than the others. Also visible in the figure is a "hot spot" at the center of the structure. This exists because of the inability of the heat to be radiated into deep space due to blockage by the bus. Since the details of the bus and interface structures have not been defined, it is assumed that the bus and the instrument are thermally de-coupled. Therefore, conduction from the bus to the instrument is not modeled.

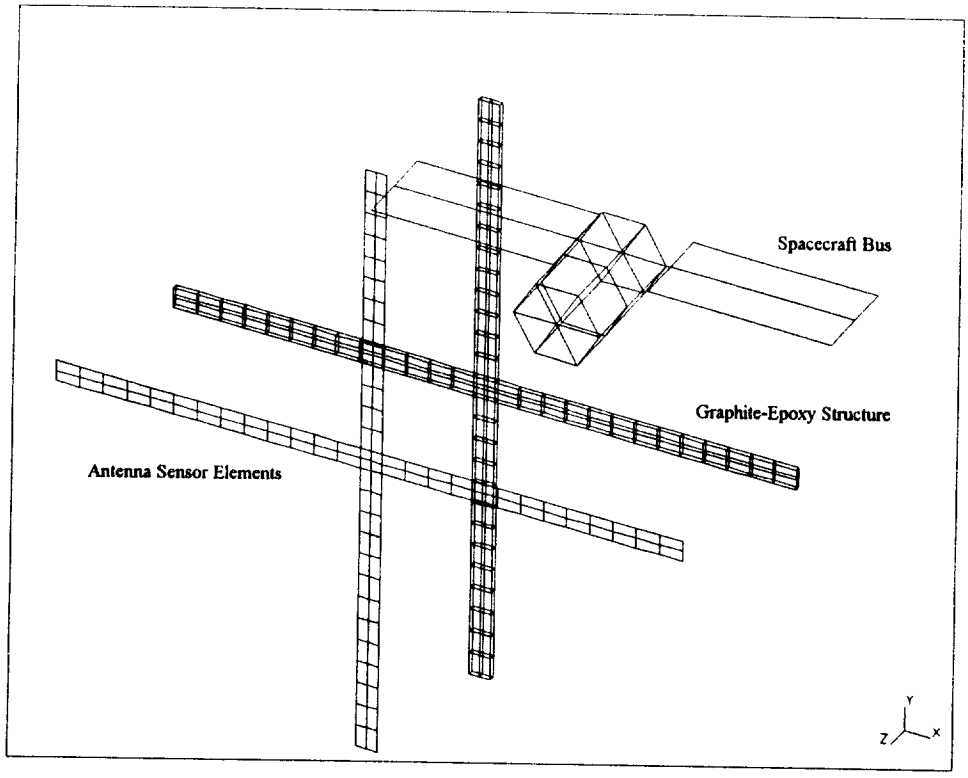

Figure 7.2-1. Exploded View of 2-D ESTAR Finite Difference Model

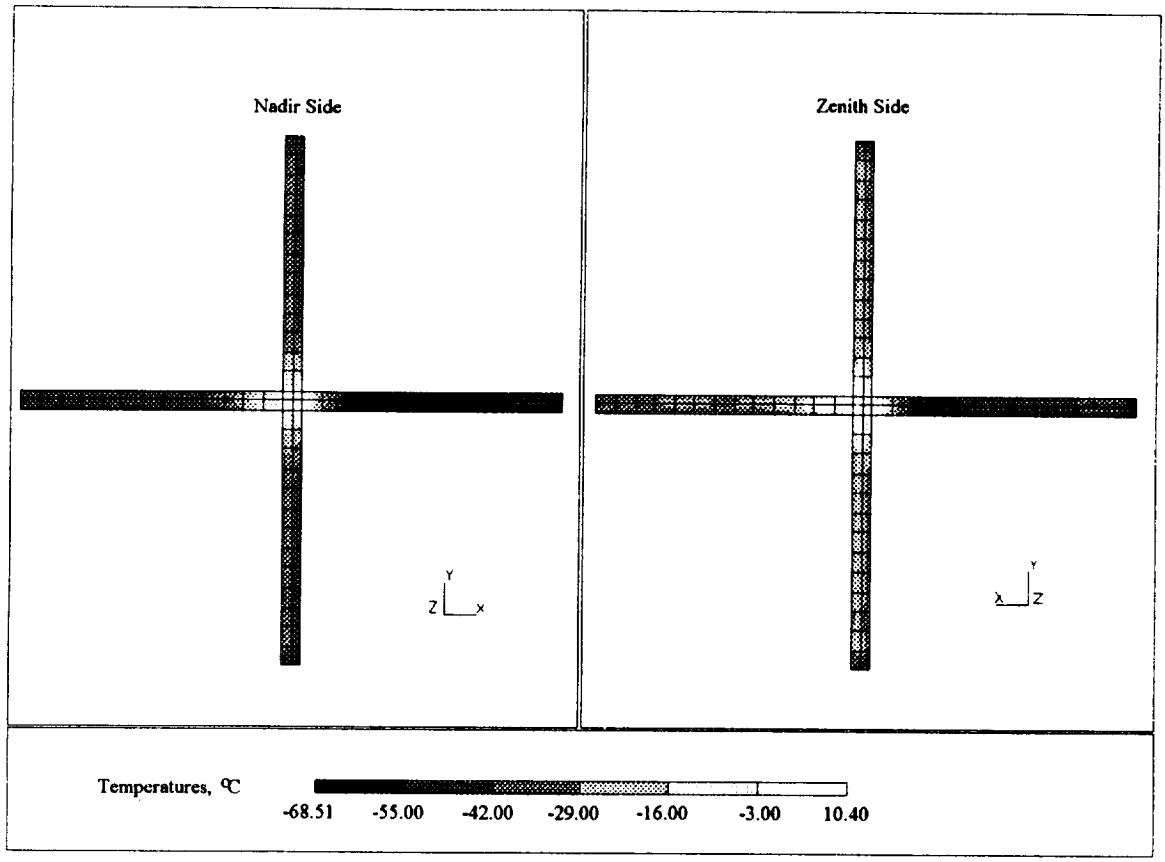

Figure 7.2-2. Applied Temperatures on 2-D ESTAR

7.2.4. Thermal Results

Thermal loads on the satellite were determined for multiple time steps with the worst case occurring at solar noon. The displacement plot of the instrument at solar noon is given in figure 7.2-3. There is a nearly symmetric downward displacement at the ends of the arms resulting in a concave shape in the nadir direction. This occurs because the temperatures are relatively higher on the zenith side than on the nadir side of the structure. The angle of twist along the length of the arms is 0.0132 degrees. The maximum displacement, which occurs at the tip, is 0.053 cm. This is below the $\lambda/40$ (0.531 cm) flatness goal by a factor of ten. In addition, the minimum margin of safety encountered at any point of the structure is 2.0. Therefore, from these preliminary results it can be seen that the effect of temperature is not detrimental to the structure, or to the flatness of the antenna.

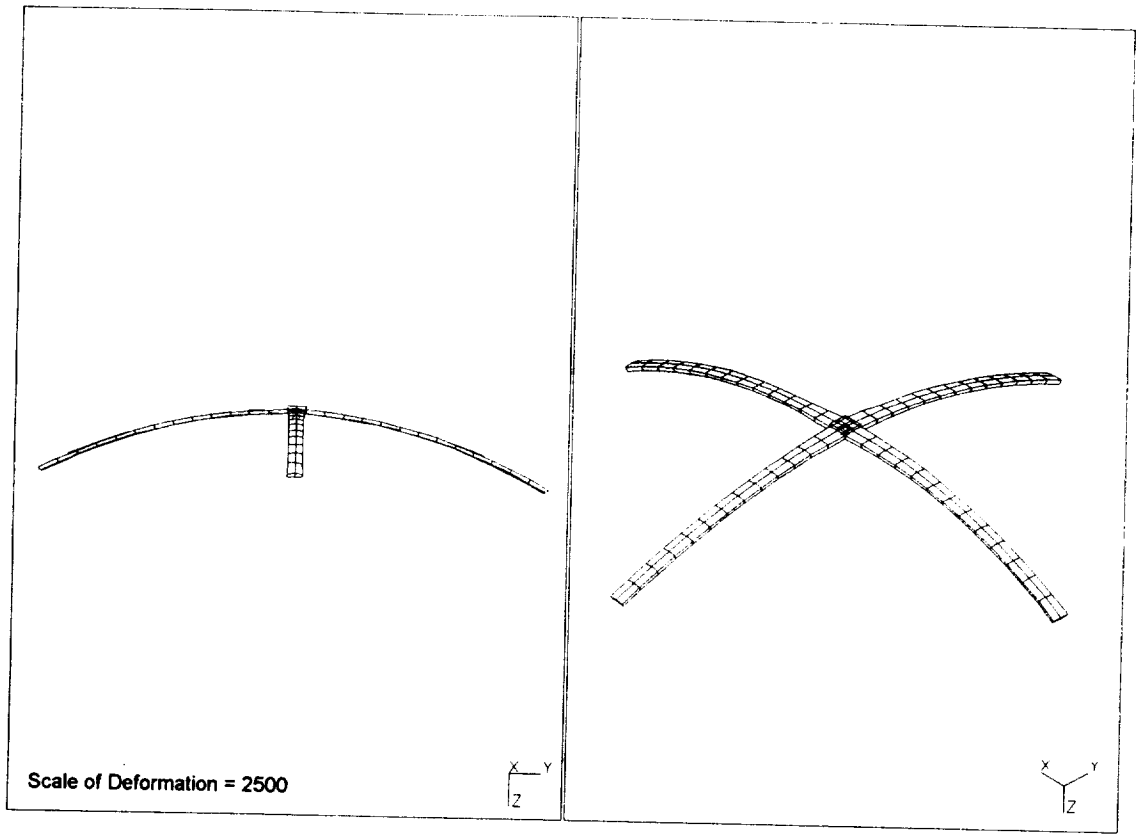

Figure 7.2-3. Side and Isometric View of 2-D ESTAR Thermal Deflection

7.3. Orbit Analysis and Propulsion Requirements

7.3.1. Orbit Lifetime

Orbit lifetime analysis of the initial GSFC concept indicated that the ESTAR satellite would not remain in orbit for its full 3 year lifetime. Subsequent analyses of detailed LaRC models with one degree-of-freedom sun-tracking arrays predicted that a mission to a 402 km circular orbit would remain in orbit 495 days during the solar minimum, and 107 days during the solar maximum. The analyses were performed using the Orbit Lifetime module of the LaRC ASCD IDEAS^2 program, with a two-sigma (97.7% probability) Jacchia 70 atmospheric model.

A reboost strategy was formulated to meet the 3 year requirement. The instrument performance and the fuel consumption were considered as selection criteria in developing this strategy. Allowing the altitude of the spacecraft to degrade to less 402 km improves the instrument resolution, but reduces the swath width of the radiometer. Moreover, the spacecraft experiences greater drag as it encounters increasing atmospheric density at lower altitudes. Conversely, increasing the altitude beyond 402 km reduces the instrument resolution, increases swath width, and results in reduced atmospheric drag. The effect of

drag on the fuel consumption was considered to be the more significant criterion. In cooperation with the Principal Investigator a 10% reduction in resolution and a corresponding increase in swath width were determined to be acceptable. This limits the reboost altitude to 442 km. Allowing the spacecraft altitude to decay from 442 km to 402 km on each cycle provides the highest average altitude and consequently minimizes fuel use. However, as the atmospheric density varies with changes in the solar cycle the reboost intervals must also vary to achieve this flight pattern. For operational simplicity, a constant time strategy with one month centers was chosen. In this scenario the reboost altitude is varied such that the orbit decays to 402 km in one month as illustrated in figure 7.3-1. During periods of maximum solar activity the reboost altitudes exceed 439 km.

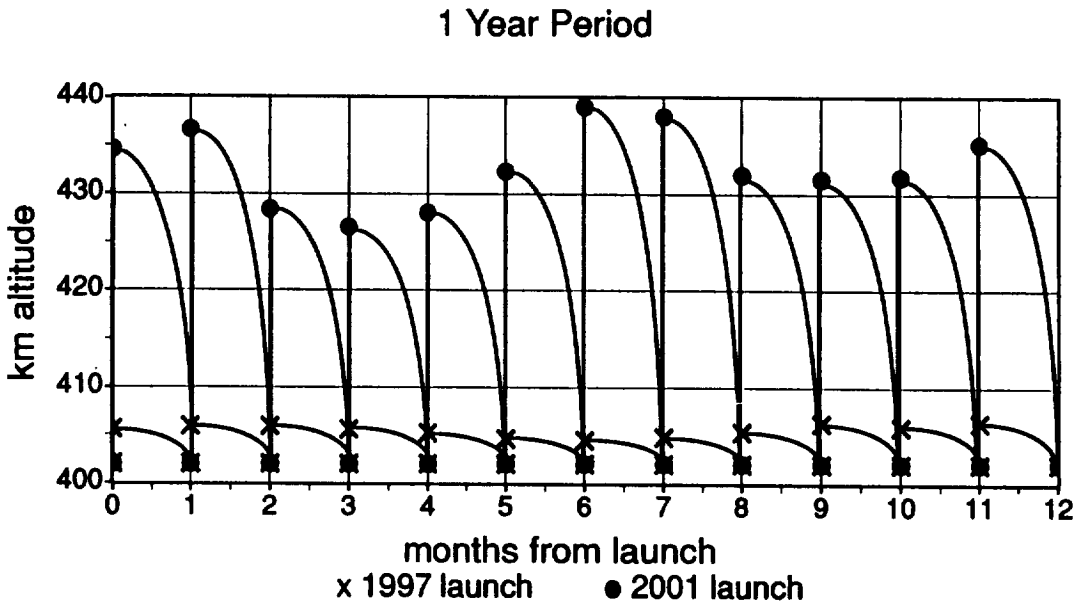

2 sigma atmospheric model
solar cycle minimum (1/97) and maximum (4/01)
single degree of freedom sun tracking and feathering
35.4 kg/m^2 ballistic coefficient using 394.7 kg initial mass

Figure 7.3-1. Pegasus Launched ESTAR Reboost Strategy

The amount of fuel provided is a compromise between the orbit lifetime, the fuel tank capacity, and the mass-to-orbit capability of the launch vehicle. It is also significantly affected by the time within the solar cycle that is chosen for the launch date. The reboost fuel requirements were determined assuming an I_{sp} of 220 seconds. The worst case for the constant time strategy is with a launch in April 2000 (approaching the peak of the solar cycle), and an initial orbit insertion altitude of 402 km. In this case, maintaining a three year life would require 102.4 kg of reboost fuel. Adding 10% for attitude control and allowing for a 10% margin the total fuel load would be 124 kg, which exceeds the 102.1 kg baseline Pegastar fuel tank capacity. A larger fuel tank was not considered since this would also affect the structure of the spacecraft bus. An April 2000 launch date

would result in a lifetime of two years and five months. Using the excess Taurus capability to launch to 432 km instead 402 km would only increase the lifetime to two years and seven months. Therefore, the spacecraft must be launched before January 1999, or after June 2001 to ensure a three year lifetime.

The alternate mission described in section 8 uses a Pegasus launch vehicle, and the mission lifetime requirement is reduced from 3 years to 1 year. The worst case reboost fuel requirement for a 1 year mission occurs when the launch is in April 2001. Assuming an I_{sp} of 220 seconds, this mission requires 36.6 kg of fuel for reboost plus 10% for attitude control, and another 10% for margin. Although the worst case condition was used for the design of the spacecraft, it should be noted that the best case reboost fuel load was only 4.3 kg.

7.3.2. Global Coverage

The orbit inclinations chosen for this study were sun synchronous, and 60 degrees. These were chosen by GSFC to meet a science requirement for 90% global coverage in 3 days. Qualitative verification of this coverage was performed using the Satellite Tool Kit software from Analytical Graphics. A plot showing an overlay of 3 days of ground tracks on an earth projection was produced for each orbit inclination (figures 7.3-2 and 7.3-3). Both cases appeared to provide the 90% coverage. A more precise pixel-based numeric calculation was considered. However, during a review of the plotted results it was considered that this type of coverage analysis did not fully address the needs of the science community. The pixel-based calculation was therefore not pursued in favor of the fixed site coverage analysis described in the following section.

7.3.3. Fixed Site Coverage

The most useful soil moisture measurements made by radiometric means are obtainable when the local time in the region being monitored is approximately 11:00 a.m.. This time is long enough after sunrise to allow the morning dew to evaporate. At earlier times the surface dew contributes to the radiometric measurement, and later in the day the surface is dried by the sun. These effects detract from the ability of the radiometer to detect emissions that accurately correspond to the moisture content of the soil.

A coverage analysis was completed using Orbital Workbench software from Cygnus Engineering. Oklahoma City was selected for coverage analysis because the GSFC aircraft experiments have previously acquired data at this location, and it is therefore a candidate for future calibration tests. The ground site used in the analysis is a single point in that area. A window was defined as a one hour period centered about 11:00 a.m. local time at the test site. The analysis determined the number of times during a one month period that the site would be within the instrument's swath during the specified one hour window. Each such occurrence is referred to herein as a contact.

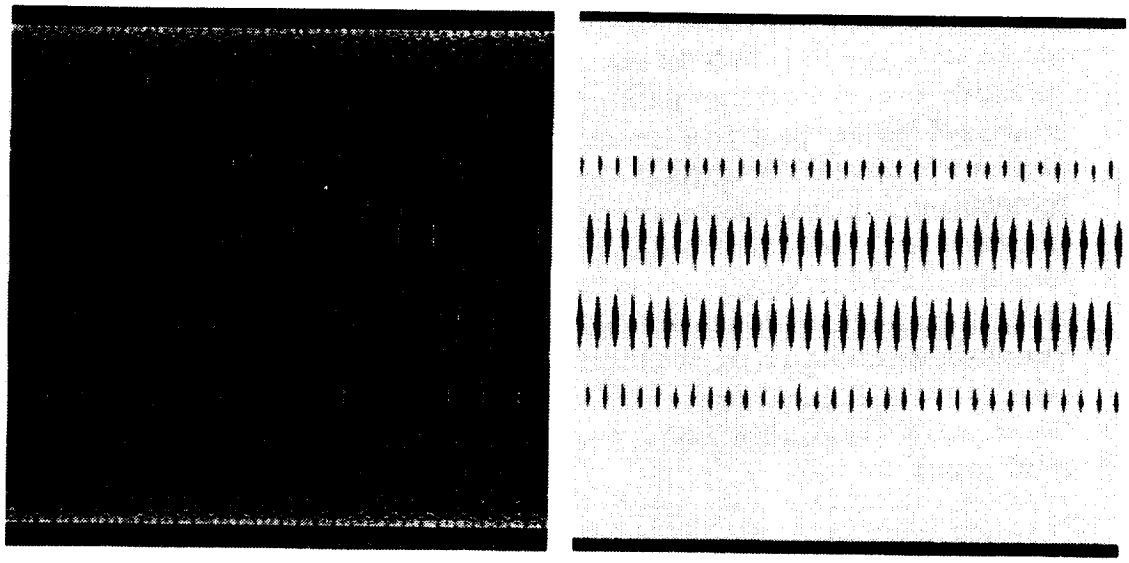

45 Orbit Ground Track

Ground Coverage

45° half-cone field of view

Figure 7.3-2. ESTAR Coverage Analysis--Sun Synchronous Orbit

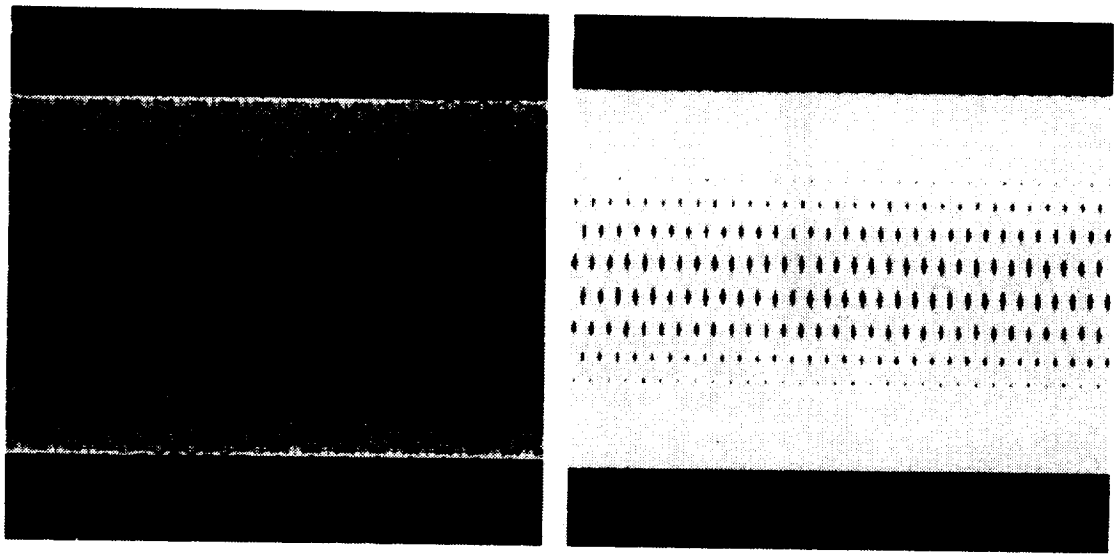

45 Orbit Ground Track

Ground Coverage

45° half-cone field of view

Figure 7.3-3. ESTAR Coverage Analysis--60° Inclination Orbit

A histogram of the results is shown in figure 7.3-4. This indicates that a sun synchronous orbit with an initial nodal ascension of 11:00 a.m. provides approximately 20 contacts between 10:30 a.m. and 11:30 a.m. during the following 31 day period. There are a number of factors that affect the orbit over long periods, and these could not be modeled accurately enough to extrapolate over the life of the mission. Consequently it is anticipated that an operational scenario involving station-keeping maneuvers would be necessary to maintain these repeat contacts over an extended period. Some of the factors contributing to orbit variations are altitude changes due to reboost, atmospheric density variations, and gravitational variations that were not modeled. A 60 degree orbit with the same initial nodal crossing provides 18 contacts as shown in figure 7.3-5. However, the nodal crossing of a 60 degree orbit changes progressively with each succeeding orbit. Therefore, depending on the initial nodal crossing for the particular one month period being considered, the 60 degree histogram may be shifted to the left or to the right. Consequently, the possibility exists that there will sometimes be no contacts at all for an entire month.

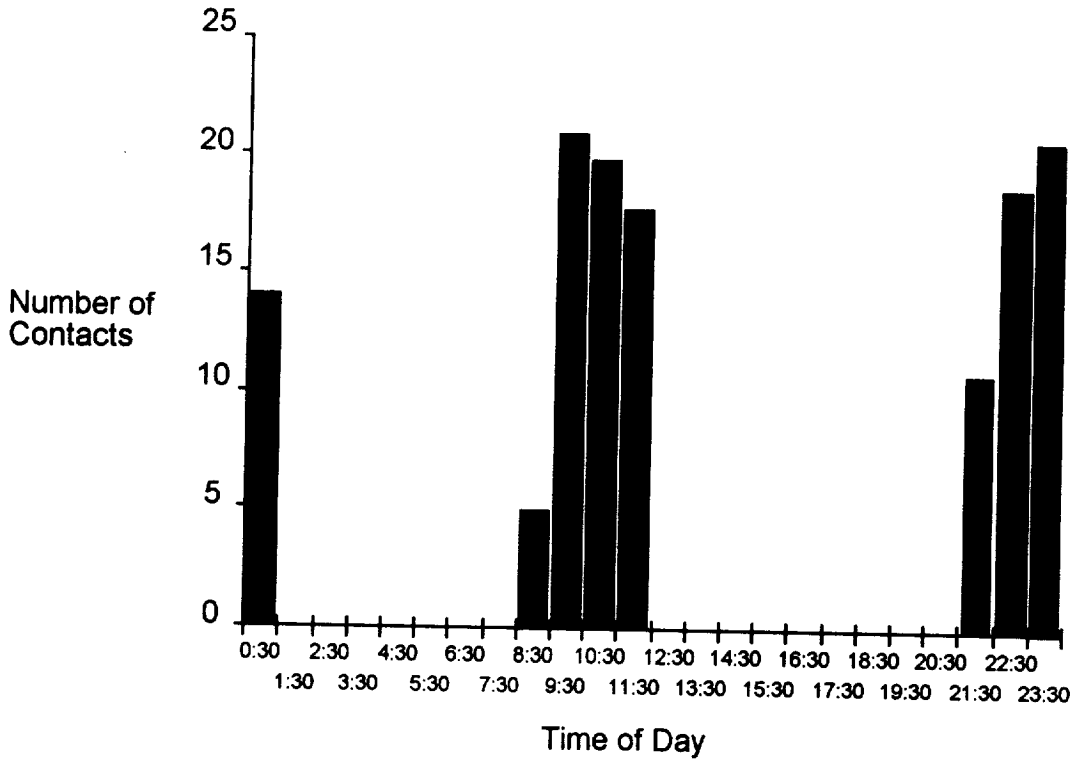

Figure 7.3-4. Contacts with a Fixed Ground Site--Sun Synchronous Orbit

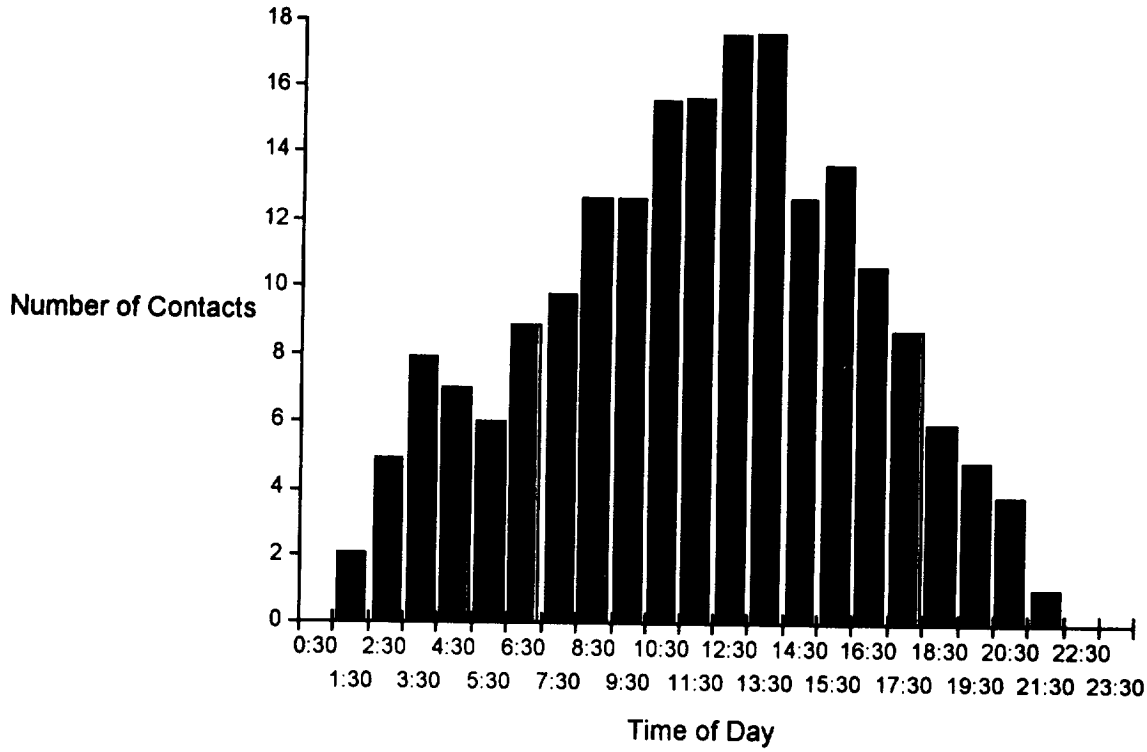

Figure 7.3-5. Contacts with a Fixed Ground Site--60° Inclination Orbit

7.4. Communications

The ESTAR conceptual design includes a communication system to receive command and control data from the ground control centers at scheduled intervals, and to transfer science and spacecraft data to the ground in near real-time (downlink to next available ground station). A comparison was made between the network services available, and a performance assessment was made for the design concept selected.

7.4.1. Assumptions

The following assumptions were used in defining the spacecraft bus communications system:

- Use of a Pegasus launch vehicle (implied mass constraint)
- A sun synchronous circular orbit at a 402 km altitude, and an inclination of 97 degrees
- Data from each orbit is downlinked on the next orbit after acquisition

7.4.2. Data Volume

The ESTAR concept involves the processing, storing and ground site retrieval of large quantities of data. In determining the total data volume to be downlinked it is assumed

that all instruments operate continuously. The effective data rate per instrument plus the data rate for spacecraft health and telemetry are shown in table 7.4-1. A 15 percent overhead is added to the estimated data generation rate to include IDs, time tagging, synchronization and error correction. Data framing and formatting in accordance with the Consultative Committee for Space Data Systems (CCSDS) standards are assumed in deriving this percentage. The 15 percent figure is based on the S-Band downlink used for the Space Station Freedom communications system. This is expected to be a conservative estimate for the ESTAR application, and the actual percentage overhead may be lower. Using this rationale the overall data rate for the ESTAR downlink is approximately 2.5 Gbits per orbit.

Item	Average Data Rate (kbps)	Data Storage (Mbits) **
Infrared	12	132
B/W Television Camera	24	267
L-band Radiometer	412	4572
Spacecraft	2	25
TOTAL	**450 ***	**4996**

* includes 15% overhead for each instrument ** Two orbit period of 185.1 minutes

Table 7.4-1. Data Rates and Storage

7.4.3. Communications Network Selection

A comparison was made between use of the NASA Space Tracking Data Network (STDN) in combination with the U. S. Air Force's Space to Ground Link Subsystem (SGLS), and the Tracking Data Relay Satellite System (TDRSS) S-band system. The STDN/SGLS system has a maximum downlink capability of three megabits per second using omnidirectional antennas. This is the maximum achievable bandwidth, and it should be noted that current applications achieve no more than approximately half that data rate. Use at three megabits per second may require some modification to the ground site recording capabilities. This system uses direct transmission to ground sites, and access time is consequently limited to the times when the spacecraft comes within the RF line of site of the ground stations. The TDRSS provides geostationary relay satellites that are in view of the satellite most of the time, and is capable of increased bandwidth up to six megabits per second. To achieve this performance a directional antenna with active antenna pointing and tracking must be utilized. The STDN/SGLS flight hardware has lower power consumption and mass than a comparable TDRSS system. These distinctions are shown in table 7.4-2, and are primarily due to the difference in antenna configurations.

The communications system concept for ESTAR was derived concurrently with other elements of the study, and since the use of a Pegasus launch vehicle was an initial assumption, the concept was developed to minimize both the power consumption and the mass. The system selected on this basis is compatible with STDN/SGLS. During the

study the other systems analyses for the ESTAR mission led to the selection of the Taurus vehicle for the baseline concept. Given the increased capability of this vehicle, and the mass margin achieved in the spacecraft concept, the TDRSS communications option should also be considered in future studies.

	STDN/SGLS	TDRSS
Antenna Type	omni-directional	directional horn (SSA) or omni (MA) that must be pointed at TDRSS
Mass (kg)	12.41	50.42
Power (watts)	36.21	41.25

Table 7.4-2. Communication System Mass and Power

7.4.4. Performance Assessment

Having selected the STDN/ SGLS network for the communications system on the basis of mass and power consumption, it was necessary to assess the performance of the system relative to the data volume to be downlinked. In this assessment candidate ground sites were identified, and the contact times were determined. These data together with the downlink bandwidth capabilities provide an estimate of the overall performance of the system. It was an initial goal that the data acquired during any given orbit would be downlinked to the ground during the next orbit. This strategy was used as part of the criteria for sizing the data storage device.

7.4.4.1. Ground Site Selection

It was assumed that any compatible NASA, NOAA, Air Force, or independent S-band ground site may be used. However, the non-NASA sites for which NASA will be able achieve agreements for this use were not known at the time of the study, and this assumption will require validation in future studies. A further assumption was that uplink of command and control data would not be necessary at every ground station, but could be scheduled to operate from a subset of the selected stations on an as needed basis. The seven candidate ground stations shown in figure 7.4-1 were identified, and used for the coverage analysis.

7.4.4.2. Ground Site Coverage Time

Given the maximum STDN/SGLS data rate of 3.0 Mbps, it takes nearly 13.9 minutes of ground site coverage time to successfully downlink the 2.5 Gbits of data acquired during a complete orbit. A coverage analysis was performed to determine the downlink time

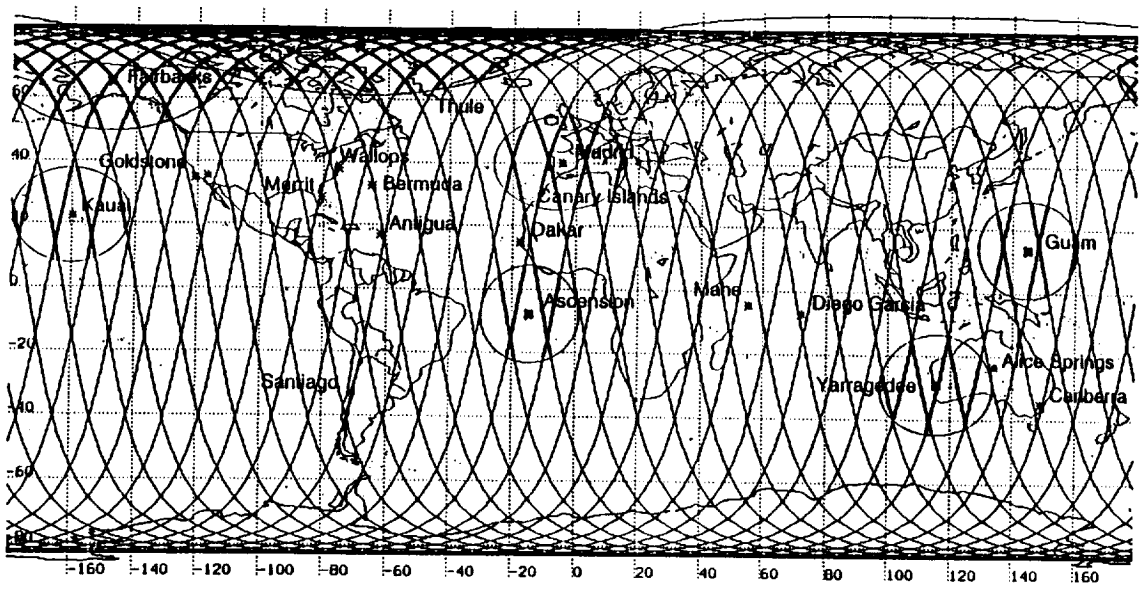

Figure 7.4-1. ESTAR Ground Track and Ground Station Locations

available using the STDN/SGLS system. The analysis consisted of an evaluation of the ground site contact opportunities, and was quantified using the Satellite Tool Kit software. All contact times were based on a sun-synchronous, 402 km, circular orbit.

A simplified approach to contact time analysis was made by considering line of site geometry only. The times for acquisition of signal at the beginning of each contact and loss of signal toward the end of each contact were not evaluated. It was found that the orbit pattern repeats (within 0.2 degrees) in a cycle of thirty-one orbits, and the analysis was performed to determine the contact times for each of these orbits. The contact times for 31 successive orbits are shown in figure 7.4-2. The total of all these contact times is sufficient to downlink the data acquired during the same period. The analysis shows that some orbits do not provide enough contact time to downlink all the data from the preceding orbit, while other orbits exceed the required time. To accommodate these variations the data storage capacity was increased to store the data from two orbits.

7.4.5. Communications Assessment Summary

With the seven ground sites selected it is only marginally feasible to downlink all the necessary data using this concept. The data from each orbit can be downlinked on the next orbit assuming average ground contact periods. However, the use of appropriately sized mass storage is necessary to cope with peak data volumes encountered during the downlink orbits having below average contact times. The assumption that certain non-NASA sites can be made available for the ESTAR mission is essential to the scenario described, and official confirmation has not been obtained for such use. The downlink data rate of 3 Mbps is rather optimistic since this is the maximum possible with this type of

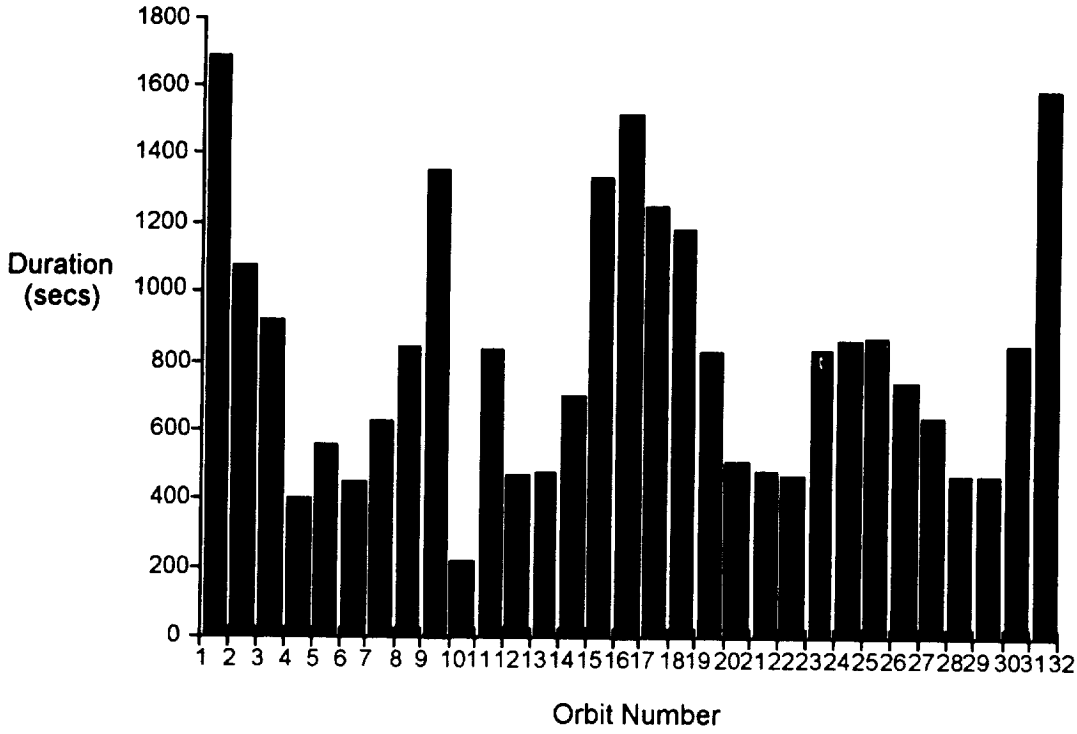

Figure 7.4-2. Ground Communication Periods over a Thirty One Day Period.

system. This analysis has shown the maximum capability that can be expected for a STDN type of system with the assumptions stated. Further optimization is desirable in view of the distinct mass advantage over TDRSS components.

An initial goal of future studies might be that of data rate reduction. The communications operating margin may be increased if a reduced duty cycle for instrument operation is considered. Continuous operation was assumed during this study, but turning off the data acquisition at times when soil moisture measurement conditions are less than optimum will reduce the data volume. This could lead to reduced ground contact periods, reduced bandwidth, and reduced mass storage capacity. The latter also results in a further saving in mass and power. Each of these possibilities would create increased operating margins for the overall system.

The latter part of the spacecraft and launch vehicle study showed that a Taurus class of launch vehicle is required to achieve the desired orbit. This launch vehicle also provides an increase in the overall mass margin for the mission. As a result, future studies should reconsider the use of the TDRSS to enhance the downlink capability.

PAGE _____ INTENTIONALLY BLANK

8. ALTERNATE CONFIGURATION FOR PEGASUS LAUNCH

The total mass to orbit requirement for the integrated spacecraft was found to be 535 kg to an altitude of 402 km. The table 8.0-1 shows that the Taurus vehicle will achieve the required sun-synchronous orbit with ample margin. The Pegasus falls short of meeting the sun-synchronous orbit by 212 kg, and even with the integrated avionics, a 60 degree inclination, and the use of a parking orbit during insertion, there is a negative margin of 158 kg.

Vehicle	Orbit [1] Inclination (deg)	Mass to Orbit Capability (kg)	Spacecraft Mass (kg)	Mass Margin (kg)
Primary mission with 10 km resolution radiometer				
Pegasus	97	286	535	-249
Pegasus [2]	97	340	571	-231
Pegasus [2,3]	97	359	571	-212
Pegasus [2,3]	60	413	571	-158
Taurus	**90**	**1044**	**535**	**509**
Alternate mission with 20 km resolution radiometer				
Pegasus [2]	97	340	375	-35
Pegasus [2,3]	60	359	375	-16
Pegasus [2,3]	**60**	**413**	**375**	**38**

Notes:
1. altitude = 402 km
2. with integrated avionics
3. using parking orbit during insertion

Table 8.0-1. Launch Vehicle Performance Margins

A trade was made between instrument performance and mass to determine the extent to which mission requirements can be met when a Pegasus vehicle is used.

Options were considered to optimize the mass to orbit capability of the Pegasus launch vehicle. In each case it was assumed that certain launch vehicle avionics functions are integrated with the spacecraft electronics. The first trade was made by considering a lower inclination orbit. A 60 degree orbit is sufficient for coverage of the Earth's oceans and land masses, but does not provide repeated passes over a target at the same time of day, as does the sun synchronous orbit. The mass to orbit capability of the Pegasus is 359 kg for a 60 degree inclination orbit, which is 19 kg more than to a polar orbit. A further option is for the launch vehicle to insert the satellite into an interim parking orbit,

and then use the spacecraft's orbit adjust system to transfer to the final orbit. This technique provides a further increase of 44 kg, and a mass to orbit of 413 kg.

Since most of the mass of the ESTAR instrument is in the antenna assembly, the highest potential payoff is obtained by making a compromise between antenna size and spatial resolution of the instrument. A smaller antenna requiring only one 90° hinge for each arm provides 20 km of spatial resolution, and reduces the instrument mass by 87 kg. This antenna assembly is made up of 73 receiving elements and is approximately 4.5 m long. The mass savings are derived by reducing the structural mass and by scaling the ESTAR subsystem designs described in section five. The antenna size is reduced by a factor of two, reducing the number of receiver circuits by a factor of two and consequently reducing the number of correlations by a factor of four. As a result the data rate is also reduced by a factor of four, and the data storage requirement by 60%. The net reduction in power for L-band radiometer is approximately 33%. The effect of these reductions on the L-band radiometer is summarized in table 8.0-2.

Instrument	Mass (kg)	Power (watts)	Data Rate (kbps)	Data Volume (Gbits)
L-band Radiometer	60	92	104*	1.6**
IR Scanner	9	14	12	0.1
Video Camera	1	14	24	0.3
Total	70	120	140	2.0

* 5256 Correlations, 12 bit resolution ** 2 Orbits

Table 8.0-2. Spacecraft Payload Accommodation Summary (without margins)

The reduced instrument power and data requirements in turn permit reductions in the spacecraft power, data, and communications systems. The effect of this scaling-down is quantified in table 8.0-3. Also shown in this table is the reduction in expendables (fuel), and the 30 kg add-back attributed to the launch vehicle components that are incorporated into the spacecraft bus as part of the integrated avionics mass budget (the net mass to orbit benefit is 18 kg--see section 4.1.2 for details).

	Full Capability (kg)	Reduced Capability (kg)	Delta (kg)
Integrated Spacecraft	535	375	-160
Elements Changed:			
ESTAR Experiment	178	91	-87
Electrical Power	100	75	-25
Data System	34	18	-16
Expendables	102	40	-62
Other	6	36	+30
Total Changes			-160

Note: A number of systems are affected by using the integrated avionics; the net effect is shown. Appendix C provides a detailed mass breakdown for each configuration.

Table 8.0-3. Spacecraft Mass Reduction (with margins as defined in section 6.2.7)

The reduction in atmospheric drag associated with the smaller solar arrays and antenna result in a some reduction in the reboost fuel required. However, a more significant saving is due to reducing the mission lifetime from three years to one year. The reduction in reboost fuel is dependent on the atmospheric density (see section 7.3). This varies considerably during the 11 year solar cycle, and therefore, also changes depending on the launch date selected. A worst case atmospheric density is assumed for this assessment, and the savings will not be as great if an alternate launch date is chosen. The three year mission requires 102 kg of fuel whereas a one year mission requires 40 kg of fuel. The potential remains for a longer mission life if a more favorable launch date is selected.

8.1. Summary

By changing from a sun-synchronous orbit to an orbit with a 60 degree inclination, reducing the resolution from 10 km to 20 km, and reducing the lifetime from three years to one year a reduction in spacecraft mass of 160 kg can be achieved. The result is a spacecraft mass estimate of 375 kg. The Pegasus capability to this orbit is 413 kg providing a positive mass margin of 38 kg. This suggests that, with the reduced performance outlined here, the use of a Pegasus class launch vehicle might be feasible.

9. COST ESTIMATES

A parametric cost estimate was made to determine the probable cost range for both ESTAR concepts. The primary design with 10 km resolution has long antenna arms each having three hinges. The alternate design with 20 km resolution has shorter arms, and only a single hinge in each. The two concepts are referred to in this section as the as the three-fold and single-fold designs respectively. The overall cost estimates include the supporting spacecraft bus, the infrared (IR) scanner, the black and white video camera, and the launch vehicle and services. The estimates include the prime contractor prices for design, development, fabrication and testing.

9.1. Cost Models

The costs were derived primarily using the Martin Marietta PRICE^{TM} family of parametric cost estimating models. Brassboard, prototype and flight hardware were estimated with the PRICE H^{TM} hardware model. The basic inputs to the model included component weights, complexity factors, amount of new design and design repeat, quantities, number of prototypes, volume, integration factors, specification level, year of technology, and schedule dates.

Software was estimated using the PRICE S^{TM} software model. The basic inputs to PRICE S^{TM} included language type, Source lines of code (SLOC), amount of new design and new code, and factors related to processor utilization, integration, complexity, and application difficulty.

Ground support equipment (GSE) was estimated using a cost estimating relationship (CER) from the Estimating Manual for Spacecraft and Scientific Instruments (ref. 10). The input to the GSE CER was the hardware development cost.

9.2. Methodology

The work breakdown structure (WBS) shown in table 9.2-1 was established for the system. Range estimating techniques were used to assess the cost variations attributable to uncertainties in model input parameters and algorithms. In addition, differences in contractor rates, experience, tools, processes, and facilities, etc., were taken into account to determine the probable cost distribution for the program. Low, mean, and high costs were estimated for each element based on assumptions for the engineering and manufacturing processes. The low cost is an estimated best case that could only be achieved by 5% of the contractors. The high cost is the estimated cost that 95% of the contractors could meet. The mean of the cost distribution is the average cost for a number of different contractors.

WORK BREAKDOWN STRUCTURE	Engineering Complexity	Integration to Next Assembly	
		Electrical	Structural
L-BAND RADIOMETER:			
Brassboard			
Prototype/Flight Hardware:			
Antenna Elements	N	D	
Front End Modules	D	D	R
Injection Lock Phase Lock Loop	N	D	R
Master Oscillator	N	D	R
Master Oscillator Distribution Interface	N	D	R
Data Receive Modules	N	D	R
Correlator	D	DD	R
Power Supply	MOTS	d	R
Cables	MOTS	R	
Arms	N	D	
Center Structure	N	D	
Motors/Drives	OTS	R	
Hinges	N	D	
Launch Restraint	OTS	R	
Instrument Integration and Test			
Ground Support Equipment			
Software			
IR SCANNER	N		
VIDEO CAMERA	N		
SPACECRAFT BUS:			
Flight Hardware:			
Data Management	OTS	R	
Orbit Determination	OTS	R	
Structure	MOTS	R	
Thermal	OTS	R	
Communications	MOTS	R	
Propulsion	MOTS	R	
Electric Power	MOTS	R	
Attitude Control	OTS	R	
Ordnance	OTS	R	
Spacecraft Integration and Test			
Ground Support Equipment			
Software			
SYSTEM INTEGRATION & TEST	D		
LAUNCH VEHICLE			

Legend: N = Normal, R = Routine, d = Moderately Difficult, D = Difficult, DD = Very Difficult
OTS = Off The Shelf, MOTS = Modified Off The Shelf

Table 9.2-1. Work Breakdown Structure and Complexity Assumptions

9.3. General Engineering Assumptions

A number of assumptions have been made in preparing the cost estimates. For the L-band radiometer, it is assumed that a brassboard, a full size prototype, and a flight unit will be built, and for the IR scanner and video camera it is assumed that a prototype and a flight unit will be built. For the spacecraft bus, it is assumed that existing flight hardware will be procured and only minor modifications will be necessary. The flight electronic components are assumed to be rated class B in accordance with MIL-Handbook 217E. The development start date used is October 1993 with a launch date in October 1996. A typical prime contractor fee of 10% is applied. Individual considerations at each WBS element determine the amount of new design required, the amount of design repetition, the engineering complexity, the manufacturing complexity, and the integration difficulty.

9.4. Specific Assumptions

The cost estimates were made using the following assumptions about the design, the complexity, and the processes involved in the development, manufacturing, integration and test of the instruments and the spacecraft. Assumptions about engineering complexity and integration difficulty for some specific elements are listed in table 9.2-1. For the instrument, a 30% weight margin is included in the high or worst case estimate.

9.4.1. L-band Radiometer

9.4.1.1. Brassboard

The brassboard hardware includes ten Front End Modules, two Injection Lock Phase Lock Loop Modules, a Master Oscillator, a Master Oscillator Distribution Interface, a Data Receive Module, and a Correlator.

9.4.1.2. Prototype and Flight Hardware

Hybrid Microwave Integrated Circuits. The preceding engineering study assumed the use of MMIC microcircuits for several of the modules due the lower mass and power associated with this technology. During the cost analysis a trade study was conducted to estimate the cost of MMIC technology versus hybrid microwave integrated circuit (HMIC) technology. Figure 9.4-1 shows the comparative costs for various production quantities. The MMIC devices are estimated to be three to four times the cost of HMIC devices, and it was concluded that the break even point is beyond 100,000 units. Consequently, for the cost analysis it was assumed that only the HMIC technology would be used.

The Front End Modules (FEM) are custom designed HMIC with packaged dimensions of 5 x 11 x 1 centimeters. Individual microcircuits or devices performing each of the electronic functions are mounted on an alumina substrate. Manufacturing processes are assumed to include

many manual operations required for a new product line within an existing facility. The Master Oscillator, the Injection Lock Phase Lock Loop (ILPLL) modules, and the Master Oscillator Distribution Interfaces (MODIF) are custom designed HMICs with similar dimensions.

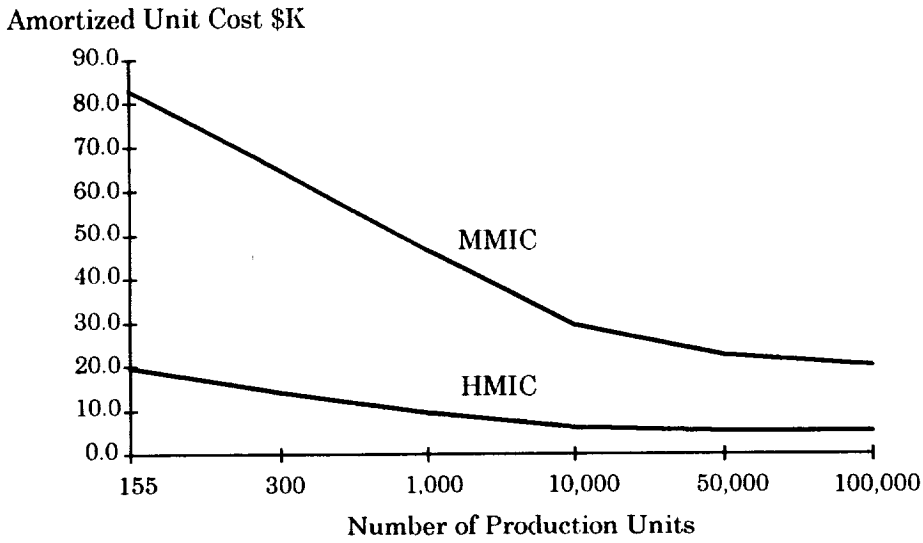

Figure 9.4-1. MMIC Versus HMIC Front End Module Cost Comparison

Data Receive Modules. The data receive modules are a new Very Large Scale Integrated (VLSI) circuit design with a normal engineering complexity.

Correlator. The correlator is a custom digital VHSIC microcircuit capable of 1600 correlation functions. The microcircuit is made up of 120,000 digital gates, and utilizes Complimentary Metal Oxide Semiconductor (CMOS) substrate technology. It is enclosed in a 20 x 20 mm pin grid array package having 211 pins. The complete custom microcircuit supports a maximum output data rate of 20 MHz. The correlator module is a printed circuit board (PCB) assembly incorporating seven identical correlator microcircuits, one off-the-shelf Central Processing Unit (CPU), and associated support devices. The packaged microcircuits are mounted on one side of a five-layer (33 x 33 cm) epoxy glass PCB. The module has a standard pin connector interface to the next higher assembly.

Antenna Elements. The antenna elements are an existing microstrip honeycomb design requiring some modification to meet the specific instrument requirements.

Structural Components. The arms, the center structure, and the hinges are all new designs. The hinges are made of fiberglass with ceramic bearings, and some unique tool design is anticipated. The launch restraints and pyrotechnic release hardware are purchased items.

Power Supply and Cables. The power supply is a purchased item requiring about 25% modification. The cables are purchased items with custom interface connectors.

Instrument Integration and Test: The integration includes the assembly of the antenna elements, arms, motors, harmonic drives, hinges, and centerpiece into a complete antenna structure with integral RF electronics. The testing includes the generation of acceptance test procedures, performance of the final acceptance test, and verification of overall specification compliance. It is assumed that the instrument prime contractor has experience in systems integration but has never integrated this specific type of system.

9.4.1.3. Spares

Spares are estimated on a case by case basis. For the antenna elements and front end modules, ten additional units are included, and for the ILPLLs two additional units are included. Ten percent of the other electronics hardware is for spares.

9.4.1.4. GSE Hardware

GSE is estimated as a function of the hardware development costs.

9.4.1.5. Software

Both the flight and ground software are entirely new designs. In each case complexity and environmental inputs for Price S^{TM} were estimated. Moderate values and uncertainties are assumed for an ADA development environment and an unmanned space operating environment. For the flight software, the range estimate of SLOC for the L-Band radiometer was derived from a moderately detailed functional analysis and from a function point count. Conservative SLOC estimates were made for the video camera and IR sensor. For the ground software, function point counts were used to estimate a SLOC range for ground simulation, mission operations, and minimal data reduction.

9.4.2. IR Scanner

The IR scanner is assumed to be a new design using existing technology.

9.4.3. Video Camera

The video camera design is based on an existing product with approximately 20 to 35 percent electronic redesign. The cost estimate also includes the purchase and qualification of a video framegrabber board.

9.4.4. Spacecraft Bus

9.4.4.1. Flight Hardware

Systems. All components in the data management, orbit determination, attitude control, ordnance and thermal systems are assumed to be off-the-shelf purchased items requiring no modification. Similarly, the components in the communications system except for the transponders are assumed to be off-the-shelf purchased items. Minor modification to the existing STDN transponder is required to accommodate alternate data and tracking systems.

The electrical power system is composed of off-the-shelf components except for the solar panel assembly. The solar arrays are specially configured to meet the requirements of the ESTAR mission.

The propulsion system is assumed to be a modification of an existing system to meet mission requirements. A new external pressurant tank along with the associated lines, fittings and mounting hardware are included for the 3-fold bus.

The structure is fabricated from aluminum with several design modifications required for this specific mission. The specific modifications include a new payload truss, a new avionics shelf, and associated brackets. These items are a new design with a normal engineering complexity

Spacecraft Bus Integration and Test. It is assumed that the spacecraft prime contractor has experience in systems integration and has integrated this type of system before. Existing or slightly modified drawings, plans and procedures will be used.

9.4.4.2. GSE Hardware

It is assumed that no GSE hardware development would be required.

9.4.4.3. Flight Software

A range estimate of SLOC was made from a moderately detailed functional analysis and from a function point count. A composite new design fraction of 53% was used. Complexity and environmental inputs for Price S^{TM} were estimated, assuming moderate values and uncertainties for an ADA development environment and an unmanned space operating environment.

9.4.5. System Integration and Test

This includes the integration of the L-band radiometer, IR scanner, video camera, and spacecraft bus into a total system. The testing includes the verification of specification compliance for the entire system. It is assumed the prime contractor has experience in systems integration but has never integrated this type of system. Existing drawings, plans and procedures cannot be used. The engineering complexity is assumed to be difficult.

9.4.6. Launch Vehicle

The Taurus and Pegasus launch vehicle prices are based on vendor quotes. The prices include the launch vehicle hardware, the launch operations, and the integration and test of the payload to the launch vehicle. The Taurus launch vehicle is used for the 3-fold instrument mission. The Pegasus launch vehicle is used for the 1-fold instrument mission.

9.5. Cost Estimates

9.5.1. L-band Radiometer

Low, mean and high price estimates for the two L-band radiometer concepts are presented in tables 9.5-1 and 9.5-2.

Instrument	Low	Mean	High
Brassboard	2,393	3,606	4,995
Prototype/Flight Hardware			
Antenna Elements	576	982	1,522
Front End Modules	4,912	6,972	8,870
ILPLL Modules	1,031	1,640	2,442
Master Oscillator	483	775	1,137
MODIF	445	685	971
Data Receive Module	1,196	1,936	2,841
Correlator	3,075	7,339	11,985
Power Supply	162	380	685
Cables	121	182	257
Arms	1,032	1,531	2,146
Centerpiece	873	1,246	1,695
Motors/Mechanisms	177	272	386
Hinge Mechanism	602	914	1,304
Launch Restraints	28	61	106
Integration and Test	10,507	14,360	20,214
Flight Spares	174	230	277
GSE	1,532	3,211	5,671
Flight Software	1,445	5,001	10,137
GSE Software	480	1,601	3,208
3-Fold L-band Total	**$31,244**	**$52,924**	**$80,849**

Table 9.5-1. L-band Radiometer Price (3-fold) (FY93 $K)

The results indicate that the major components driving cost are the correlator and the front end modules, which are both new development items. The estimated mean cost of the correlator, which includes chip development and fabrication, is about $7.3 million. Chip development and fabrication account for about 70% of the correlator cost. The remainder is primarily attributed to board development and fabrication. Development of the correlator is a critical item in the instrument development schedule.

Integration and testing (I&T) also contribute significantly to the cost of the L-band radiometer. I&T includes the cost to assemble the components into the end item and to test and calibrate the entire system. Integration and testing accounts for more than 25% of the cost of the 3-fold concept, and more than 20% of the cost of the 1-fold concept.

Flight and GSE software development accounted for about 12% of the 3-fold concept and 15% of the 1-fold concept total costs.

Instrument	Low	Mean	High
Brassboard	2,393	3,606	4,995
Prototype/Flight Hardware			
Antenna Elements	354	612	960
Front End Modules	3,288	4,929	6,468
ILPLL Modules	850	1,364	2,036
Master Oscillator	483	775	1,137
MODIF	432	667	947
Data Receive Module	1,107	1,808	2,668
Correlator	3,075	7,339	11,985
Power Supply	162	380	685
Cables	80	126	182
Arms	774	1,162	1,638
Centerpiece	873	1,246	1,695
Motors/Mechanisms	78	120	171
Hinge Mechanism	404	644	945
Launch Restraints	16	37	64
Integration and Test	6,546	9,899	13,870
Flight Spares	174	230	277
GSE	1,687	3,193	5,072
Flight Software	1,445	5,001	10,137
GSE Software	480	1,601	3,208
1-Fold L-band Total	**$24,703**	**$44,738**	**$69,139**

Table 9.5-2. L-band Radiometer Price (1-fold) (FY93 $K)

9.5.2. IR Scanner

Low, mean, and high prime contractor price estimates for the IR scanner are $2.1M, $4.3M, and $7.3M respectively. Software development accounts for about 26% of the total IR scanner cost. This is due to the large amount of engineering effort required compared with the hardware, which consists primarily of off-the-shelf items requiring no modifications or development. The major hardware cost driver is the detector assembly, which is assumed to be purchased from a subcontractor, and accounts for about 25% of the IR scanner cost.

9.5.3. Video Camera

Low, mean, and high prime contractor price estimates for the video camera are $0.6M, $1.6M, and $2.9M respectively. The major cost driver is software development, which accounts for over half of the camera cost. This is due to the large amount of engineering effort required compared with the hardware, which is a modified off-the-shelf item.

9.5.4. Spacecraft Bus

Low, mean and high prime contractor price estimates for the two spacecraft bus concepts are presented in tables 9.5-3 and 9.5-4. The major hardware cost drivers are the data management and electric power systems. The estimate for the data management system includes modifications to an existing system to meet mission requirements. The electrical power system requires some engineering to increase the output capability using GaAs solar arrays. The power system is a critical item in the development schedule. Other subsystems are low cost since they consist primarily of off-the-shelf hardware requiring no modification or development.

Spacecraft Bus	Low	Mean	High
Attitude Control	825	1,801	4,048
Communications	1,531	2,819	4,817
Data Management	2,269	4,176	8,103
Electric Power	2,539	4,672	8,839
Orbit Determination	130	298	693
Propulsion	598	1,098	2,058
Thermal	40	57	94
Structure	491	751	1,154
Ordnance	15	19	23
Bus I&T	978	1,654	2,683
Software	966	3,318	6,803
Spacecraft Total	**$10,382**	**$20,663**	**$39,315**

Table 9.5-3. Spacecraft Price (for 3-fold Instrument) (FY93 $K)

Spacecraft Bus	Low	Mean	High
Attitude Control	825	1,801	4,048
Communications	1,531	2,819	4,817
Data Management	1,350	2,824	6,049
Electric Power	2,061	3,850	7,396
Orbit Determination	130	298	693
Propulsion	207	411	864
Thermal	40	57	94
Structure	491	751	1,154
Ordnance	15	19	23
Bus Integration and Test	779	1,308	2,148
Software	966	3,318	6,803
Spacecraft Total	**$8,395**	**$17,455**	**$34,087**

Table 9.5-4. Spacecraft Price (for 1-fold Instrument) (FY93 $K)

9.5.5. System Integration and Test

The estimate for the integration and test of the complete system includes all costs to assemble the L-band radiometer with the satellite bus and test the total system. The estimate also includes the costs to integrate the IR scanner and video camera into the total system

9.5.6. Launch

The prices of the Taurus and Pegasus vehicles, based on vendor quotes that include services, are $20.9M and $9.9M respectively.

9.5.7. Total Program Cost

The total prime contractor prices for the 3-fold and 1-fold programs are depicted in tables 9.5-5 and 9.5-6. Comparing the mean cost of each program, the 1-fold program can be completed for about 25% less than the 3-fold program. Over 40% of this difference is due to the difference in launch vehicle costs.

System	Low	Mean	High
L-Band Radiometer	$31.2	$52.9	$80.8
IR Scanner	$2.1	$4.3	$7.3
Video Camera	$.6	$1.6	$2.9
Spacecraft Bus	$10.4	$20.7	$39.3
System Integration & Test	$5.3	$8.5	$12.4
Launch Vehicle/I&T/Ops	$20.9	$20.9	$20.9
Total	**$70.5**	**$108.9**	**$163.6**

Table 9.5-5. 3-Fold Program Summary (FY93 $M)

System	Low	Mean	High
L-Band Radiometer	$24.7	$44.7	$69.1
IR Scanner	$2.1	$4.3	$7.3
Video Camera	$0.6	$1.6	$2.9
Spacecraft Bus	$8.4	$17.5	$34.1
System Integration & Test	$3.8	$6.6	$9.9
Launch Vehicle/I&T/Ops	$9.9	$9.9	$9.9
Total	**$49.5**	**$84.6**	**$133.2**

Table 9.5-6. 1-Fold Program Summary (FY93 $M)

9.6. Higher Risk Approach

A higher risk development approach was also estimated for the L-band radiometers. In this case only a partial prototype, which uses brassboard electronics, and a flight unit are built and tested. The results are summarized in tables 9.7-1 and 9.7-2. Using this approach the L-band radiometer can be completed for about 20% less than it would cost if a brassboard, a full prototype, and a flight unit were produced. The savings realized would reduce the overall program cost by about 9 to 10 percent.

System	Low	Mean	High
L-Band Radiometer	$25.1	$42.3	$64.1
IR Scanner	$2.1	$4.3	$7.3
Video Camera	$0.6	$1.6	$2.9
Spacecraft Bus	$10.4	$20.7	$39.3
System Integration & Test	$5.3	$8.5	$12.4
Launch Vehicle/I&T/Ops	$20.9	$20.9	$20.9
Total	**$64.4**	**$98.3**	**$146.9**

Table 9.7-1. Higher Risk 3-fold Program Summary (FY93 $M)

System	Low	Mean	High
L-Band Radiometer	$20.5	$36.1	$56.3
IR Scanner	$2.1	$4.3	$7.3
Video Camera	$0.6	$1.6	$2.9
Spacecraft Bus	$8.4	$17.5	$34.1
System Integration & Test	$3.8	$6.6	$9.9
Launch Vehicle/I&T/Ops	$9.9	$9.9	$9.9
Total	**$45.3**	**$76.0**	**$120.4**

Table 9.7-2. Higher Risk 1-Fold Program Summary (FY93 $M)

PAGE _____ INTENTIONALLY BLANK

10. CONCLUSIONS AND RECOMMENDATIONS

The spacecraft and instrument configurations for a 2-D ESTAR mission were defined, and the capabilities of several launch vehicles were examined. It was determined that a 2-D ESTAR mission that fully meets the mission requirements is feasible using a Taurus class launch vehicle. Further study is needed to provide a more complete definition of the L-band radiometer. Some primary areas requiring development are:

- internal calibration methods (amplititude and phase)
- relative phase stability between measuremants
- thermal design, and analysis for the optimization of mechanical effects and RF electronic design parameters
- correlator design
- data and communications system alternatives including the use of data compression

A 2-D ESTAR mission that meets a reduced set of measurement requirements may be feasible using a Pegasus launch vehicle. The alternate concept developed in this study has a resolution approximately equal to one half that of the baseline 2-D ESTAR concept. Further study is required to optimize the capabilities of such a mission.

11. ACKNOWLEDGMENTS

The authors wish to acknowledge the contributions of the following people who provided engineering analysis, cost analysis, and technical support during the course of the study and the preparation of this report.

J. Kirk Ayers, Lockheed Engineering and Sciences Company
Frances Brice, Lockheed Engineering and Sciences Company
Dave Butler, NASA Langley Research Center, Systems Engineering Division.
Robert Fairbairn, Lockheed Engineering and Sciences Company
James W.Johnson, NASA Langley Research Center, Advanced Space Concepts Division
Phillip Mintz, Lockheed Engineering and Sciences Company

12. REFERENCES

1 Ruf, C. S.; Tanner, A. B.; and Le Vine, D. M.: "The Electronically Steered Thinned Array Radiometer," October 1987.

2 Le Vine, D.M.; Hilliard, L.; et al: "Electronically Scanned Thinned Array Radiometer (ESTAR) Earth Probe Concept: An Engineering Feasibility Analysis," NASA Goddard Space Flight Center, 1992.

3 Garrett, B.; Rowell, L. F.; Butterfield, A. J.; and King, C. B.: "Concept for Spacecraft Supporting the L-S-C ESTAR Passive Microwave Radiometer," NASA Langley Research Center, 1990.

4 Orbital Sciences Corporation: "Pegasus Payload User's Guide, release 2.0," Orbital Sciences Corporation, May 1991.

5 Orbital Sciences Corporation: "Commercial Taurus Launch System Payload User's Guide, release 1.0," Orbital Sciences Corporation, August 1992.

6 EER Systems Corporation: "Connestoga ELV Payload User's Guide," EER Systems Corporation, August 1992.

7 Le Vine, D.M.: "Small Spacecraft Mission to Measure Soil Moisture and Ocean Salinity: ESTAR on Pegasus," informal presentation, David LeVine, 1992.

8 University of Idaho: "CMOS Digital Correlator, Preliminary Product Specification, NASA SERC for VLSI Systems Design," University of Idaho, Moscow, Idaho, March 92.

9 "MSC/NASTRAN User's Manual, MSC/NASTRAN Version 67," ISSN 0741-8019, August 1991, p. 1.13-2.

10 PRC Systems Services Company: "Estimating Manual for Spacecraft and Scientific Instruments," PRC Systems Services Company, NAS1-15109, Huntsville, AL, 1980.

11 Infrared Associates Inc: "Infrared Detectors and Accessories Catalog," Infrared Associates Inc, 1992.

PAGE ____ INTENTIONALLY BLANK

APPENDICES

A. INFRARED SCANNING RADIOMETER

To determine ocean salinity, the L-band radiometer must be combined with sea surface temperature data. The IR scanner provides the sea surface temperature measurement. The IR scanner has the advantage that it provides this capability in a compact, light-weight instrument having a reasonable data rate. The IR instrument is an imager, and provides a collocated IR image that may also be used to correlate the soil moisture and salinity data with geophysical features. The IR approach also allows a day and night capability that extends the earth coverage time available for science measurements. The major limitation of this approach is loss of data due to cloud obscuration.

This instrument was initially defined as a medium resolution instrument with a scanned field of view (FOV) equal to that of the L-band radiometer. The initial requirements and capabilities for the instrument are described in section 5.0, and are shown in table 5.0-1. A quick analysis was done to define the number of spectral bands, and their limits for the IR scanner. Given an accuracy of 1K for the L-band radiometer, the desired salinity measurement implies that an IR accuracy of 3 K or less is required for the sea surface temperature measurement (see section 5.1, and figure 5.1-2). This accuracy requirement should be the subject of more rigorous analysis during follow-on studies for this mission. The concept developed is a two-color IR instrument that provides the capability to correct for atmospheric water vapor, and achieve an accuracy of approximately 1-3 K.

A.1. General Description

The concept is similar to the Visible Infrared Radiometer (VIRR) that flew on the Seasat satellite. The VIRR did not use a window, hence the rotating mirror bearing was exposed to free space. In this concept a window is used and the instrument is enclosed in a nitrogen filled structure to enhance the reliability of the moving parts. This instrument is a line scanner using a rotating mirror to achieve a cross track scan relative to the satellite flight vector. The main features of the instrument are as follows:

- Flying spot scanning radiometer
- Two detectors, 2 colors in the 8-12 μ band
- Uncooled detectors
- Calibration by on-board blackbody source in FOV
- Water vapor correction by ratio of 10μ to 8 μ bands
- Window is polycrystalline zinc selenide (Raytran ZnSe)
- A 50 mm diameter aperture

The optics consist of an IR window, a rotating 45 degree mirror, and an IR lens which images onto the detectors. The detectors are behind a beam-splitter to allow separate measurements of the two wavelengths of interest as shown in figure A-1.

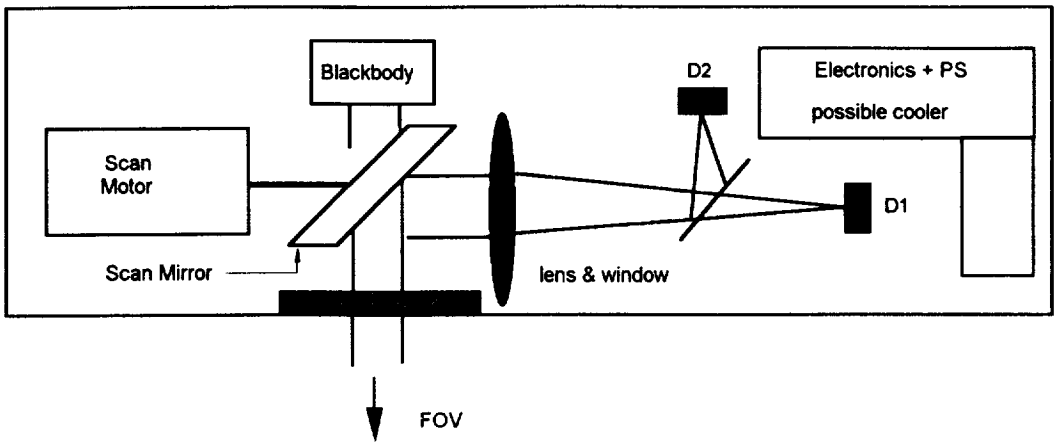

Figure A-1. Schematic Layout of the IR Radiometer

As the mirror rotates, the detectors view an internal black-body source that is used to calibrate the instrument during each scan. The overall performance and accommodation parameters are shown in table A-1.

Coverage	800 km swath
Resolution	10 km
Dynamic Range	275-315 K
Data Rate	10.3 kbps (data + mirror, 8 bit)
Size	24 x 15 x 10 cm
Mass	8.9 kg (incl. 20% contingency)
Power	14 watts

Table A-1. IR Radiometer Performance & Accommodation

The window material is Raytran zinc-selenide (ZnSe), which has an optical transmission of 70% from 0.5 to 12.5 microns. This material allows both the 10-12 μ and the 8-9 μ regions to be used. With this window a 3-5 μ band can also be added if future studies indicate that a benefit could be obtained from the data. The lens is a simple meniscus that is adequate to obtain the required on axis spot image.

The pyroelectric detector is uncooled (ref. 11). The frequency and sensitivity response of pyroelectric detectors appear to be adequate, but other uncooled choices, such as bolometer detectors, are also viable candidates. Detector selection should be optimized in future analysis. If this analysis indicates the need for higher sensitivity, thermoelectric cooling together with the use of Mercury Cadmium Telluride (HCT) detectors can be used

to increase the sensitivity. The increase in mass and power that would be incurred by changing to cooled detectors is estimated at <0.5 kg and approximately five watts for cooling to 170K.

The sensitivity for the IR radiometer used during this study was 1 K. This is adequate to determine the sea surface temperature to within +/- 1.5 K. Using the 10-12 μ band, for example, a Δt of 1 K requires a radiance detection of 2.7E-5 w/cm2/steradian at a source temperature of 275 K. Using an electronic bandwidth of 62 Hz and F/4 optics, the detector D* requirement is 4.5E7. Typically, pyroelectric and bolometer type detectors can achieve a D* of 1E8 or better, depending on the active surface size. It should be noted that F/4 optics are conservative and F/2 or greater is easily achievable. The design is conservative, and has adequate performance margin to allow for performance trades without increased mass, size or power. The estimated mass of the instrument is shown in table A-2.

Component	Mass (kg)
Case (0.1 AL)	2.4
IR Window (4 x 12 x 1 cm)	0.7
Scan motor	0.6
Black Body Assembly	0.4
IR Lens Assembly	0.4
(2) FPA and structure	1.0
Electronics - Signal Conditioning	)
- Detector Signal Processing	) 0.5
- Motor/BB Power Supply	)
Connectors, wire and supports	1.4
Component Total	7.4
20% contingency	1.5
Design Total	8.9

Table A-2. IR Radiometer Mass Estimate

There are no stringent pointing requirements for the IR radiometer. Hence, it is a strap-down system attached rigidly to the spacecraft. The spacecraft is stabilized to within a sub-pixel of the large L-band radiometer. This is satisfactory for the IR scanner and no special accommodation for line of sight stabilization is required.

A.2. Water Vapor Correction

To measure sea surface temperature with the required accuracy, the measurement of the IR radiation received at the aperture must be corrected to account for the emissivity of sea water, and for atmospheric attenuation effects. In this study, the emissivity of sea water is considered known, and is accounted for during the post flight data analysis. The atmospheric attenuation is the more variable of the two effects, and cannot be estimated in this manner with sufficient accuracy. The variability of the atmospheric attenuation was studied to establish the need for detection of two spectral bands versus one. The result of the analysis is that the uncorrected Δt is $\pm$ 10 K using one band. By using two spectral bands, a correction to within about $\pm$ 1 K is achievable. The latter meets the sea surface temperature measurement accuracy of three degrees that is required.

Atmospheric transmission in the 5 to 25 μ waveband varies considerably across regions of the Earth. It also varies with changing weather conditions. Figure A-2 shows typical examples for tropical, mid-latitude and sub-arctic regions during both summer and winter. The major variation, as shown in figure A-3, is due to changes in water vapor content.

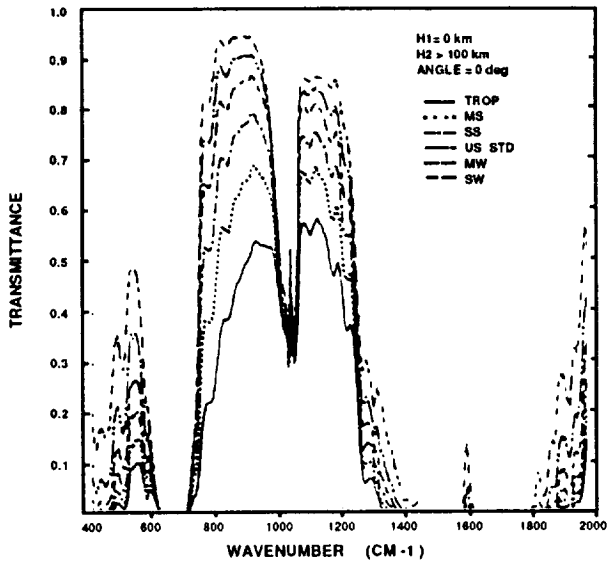

Figure A-2. IR Atmospheric Transmission

Two spectral bands were chosen for the instrument: 10-12 μ as the primary temperature measurement band, and 8.3-9.3 μ as the water vapor correction band. The ratio of the radiation in these bands, measured at the aperture while viewing the same source, has values from 0.963 (sub-arctic winter) to 1.18 (tropical) as shown in figure A-4. From this ratio the water vapor can be accounted for in post flight processing.

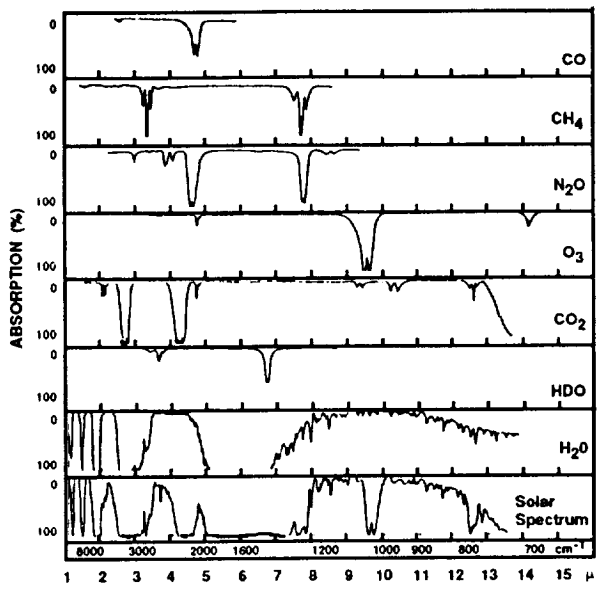

Figure A-3. Atmospheric Absorption by Species

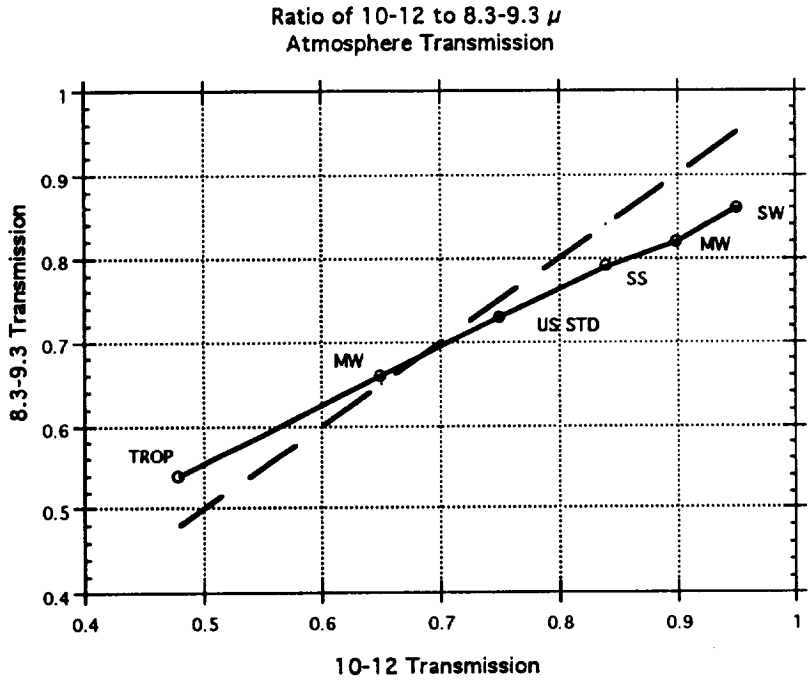

Figure A-4. Ratio of 8 to 12 μ Wavebands for Different Atmospheres

The analysis was done to determine the spectral performance of the IR scanner concept and to estimate its size and mass. Further analysis will be required to optimize the instrument design. This may include evaluation of a third spectral band to improve the accuracy of the sea water emissivity correction factor. This option would cause some

increase in the mass and power of the instrument, and would increase the downlink data rate. Alternatively, the use of the L-band radiometer data could be incorporated in the data set as a third channel providing this type of correction without increasing the overall downlink data rate. The above wavebands are not optimized, and follow-on studies may result in the use of somewhat different spectral ranges.

A.3. IR Radiometer Options and Recommendations

This study was to identify potential use for the IR imaging radiometer as an auxiliary to the L-band radiometer's ocean salinity measurement. This evaluation indicates good utility but other approaches are also viable. These include C-band and S-band microwave radiometers if mass and power are available. To further evaluate the IR instrument, it is recommended that the IR scanner be included in future studies of the 2-D ESTAR. It is suggested that more detailed analysis be conducted in the following areas:

- Cooled detector option (TE & HCT, 5 watts, 1 kg)
- Optimum water vapor correction (3-5 μ band, other)
- Multi-band IR + L-band potential science
- Mechanical and reliability
- Data compression algorithms

B. VIDEO CAMERA

The utility of a video camera was investigated during the study. The extent of the science role for this camera is not yet fully defined, but some uses have been determined. As discussed in section 5.0, two applications were identified. These were high resolution collocation of images and visible scene interpretation or cueing. Clearly it is of value to reduce uncertainty in scene interpretation, particularly if this can be achieved with only a minimal increase in mass and power. One is that both human and computer searches of the rather extensive data produced by the microwave radiometer could be conducted in a reference frame that is human compatible. For example, the presence of vegetation, its type, and its possible effect on L-band soil moisture measurements could be assessed using well-developed Landsat type algorithms. Other useful visible cues include snow presence, sun position, lakes smaller than the L-band resolution. The initial requirements for the video camera were defined as follows:

- Nadir Pointing
- ± 50 degree FOV
- 1 frame/minute

B.1. General Description

The video camera concept is driven by the need to minimize the mass, power, and data resource requirements placed on the spacecraft. A color camera would be superior to a black and white video camera (for cues). A major constraint in the overall systems analysis was to minimize spacecraft data resources. It was primarily for this reason that a black and white camera was chosen. However, both the black and white concept and the color video concept were addressed, and are described in the following sections. A ground resolution of one to two kilometers was selected as a compromise between the desired high resolution and an excessive data rate.

One major limitation of the video concepts presented is that they are daylight systems only. Other concepts are possible to extend the capability into the night side of the orbit but since some night capability exists with the IR scanning radiometer, these alternatives were not pursued. Such night vision devices as low light level TV, microchannel, and image intensified tube systems are options, but science benefits for these were not identified. In addition, such systems generally have reduced resolution and spectral limits compared to more orthodox video systems. Other devices, such as microchannel systems could be considered. The utility of video cameras is further limited by clouds and haze. Clouds obscure the scene for the video camera, and this is accepted as a limitation in this concept. Haze mitigation is discussed below.

B.1.1. Black and White Video Camera

A minimal black and white video camera was identified based on commercially available designs. Several vendors (e.g., Loral, Texas Instruments) make small half-inch CCD cameras for military uses on aircraft and for space applications. A generic concept based on the configuration of these products is shown in table B-1.

Camera	
Sensor Type	CCD, Black & White TV
Array Size	510 x 493 pixels
Resolution	380 x 350 pixels
Automatic Light Control Range	2000:1
Size	13 cm x 3 cm dia. without lens
	18 cm x 4 cm dia with lens
Mass	0.5 kg
Power	4 watts
Minimum Observation Rate (0 overlap)	96.6 sec.
Maximum Integration 'look' time	0.27 sec.
Output	5 frame burst, 1/30 sec per frame, 1 burst every 60-90 sec
Heritage	Loral Fairchild visible camera (full mil-spec.)
Data System Requirements	
Data Rate (8 bits/pixel)	20.8 kbit/sec contin. average (at 1 frame/96 sec)
Data Storage required	112 Mbit/orbit (w/o compression or night blank)
Asynchronous Frame-grabber	with 5 frame averaging

Table B-1. Black & White Video Camera Definition and Associated Data System Requirements

The concept has adequate ground resolution of 2 km at a 90 degree field of view as shown in figure B-1. The very light weight of 0.5 kg includes the required optical lens, but not a mechanical iris since the camera is equipped with a focal plane automatic light control (ALC) system with 2000:1 capability. Higher resolution (1 km) and a 90 degree FOV is achievable using a different CCD focal plane but would result in a higher data rate. Configurations with either standard analog or digital video outputs are available with each version having the same mass and volume.

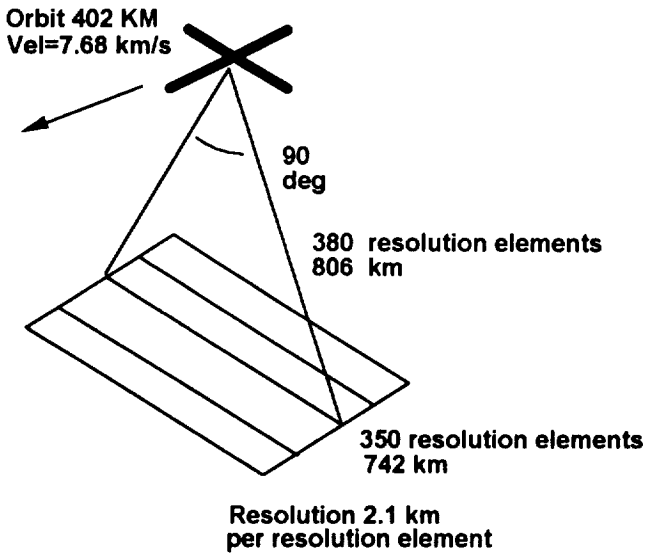

Figure B-1. Field of View & Resolution of the Black & White Video Concept

A spectral response from 0.45 to 1.1 microns, or any portion of this, is available with a sensitivity in the 0.5 lux range. The exposure time is the standard 1/30 second, but this can be extended to a maximum of about 1/4 second to recover sensitivity if required.

The initial guidelines indicated an exposure rate of 1 frame per second. However, based on the orbital velocity and ground resolution, the exposure time must be less than 0.27 seconds, therefore a video frame-grabber (or memory) is part of the concept. By using a 1/30 second exposure time, and digitally averaging a burst of 5 frames of data, an improved signal-to-noise ratio is achieved while keeping power consumption to a minimum. The burst is repeated at the desired observation rate of one burst every 60-90 seconds, and the averaged frame of data is stored at this rate before transmission to the ground.

These small, very light video cameras are rugged military components. Discussions with the vendors indicated that they would be suitable for space applications with only one minor change, changing the electrolytic capacitors to space qualified ones. This would not result in any alterations to the configurations described here.

As mentioned earlier, the spectral response of the CCD focal plane extends from 0.45 to 1.1 microns. The recommended waveband for the black and white concept is from about 0.7 to 1.0 microns but requires more detailed analysis. The longer wavelength is desirable for its ability to penetrate haze and light smog. Another benefit is that the chlorophyll reflective band is included which allows vegetation to be readily discriminated from bare soil, water, and other surfaces. The restriction to longer wavelengths also enables correlations to be made with data from Landsat 6, which operates in the 0.7 to 0.8 micron region.

B.1.2. Color Video Camera

A concept for a color video camera was prepared at the beginning of the study. This camera provides fuller spectral information and better cues, and is therefore more desirable than a black and white camera. However, the resources required for color are greater than for black and white, and the latter was finally selected for the 2-D ESTAR concept.

Sensor Type	CCD Color TV (daylight)
Field of View	86 x 55 deg. (100 x 64 deg. available)
Size: Camera Head	16 x 11 x 13 cm with lens
Electronics box	26 x 28 x 13 cm
Mass: Camera Head	3.3 kg
Electronics box	6.2 kg
Power	22 watts
Frame Rate	1 frame per 20 sec (1 frame per min. available)
Data Rate	341 kbps (1 frame per 20 sec, average)
Data Storage	800 Mbit (for 40 minutes)

Table B-2. Color Video Camera Definition

The color video camera described in table B-2, is based a space qualified video camera defined by Loral for use on the Space Station Freedom. This is a broadcast quality camera using three separate CCD focal plane arrays (figure B-2). This design operates at an observation frame rate of 1 frame per 20 seconds giving generous scene overlap, and a resolution of 1 km.

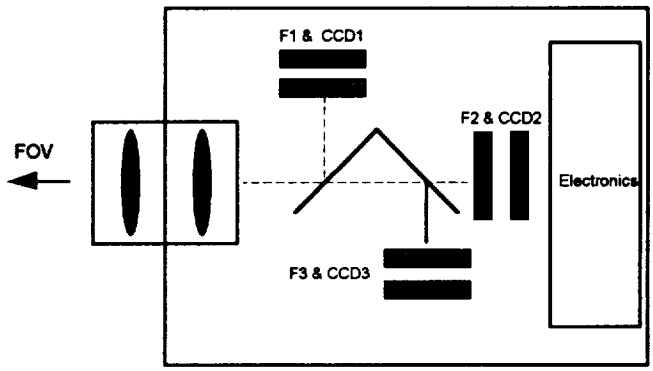

Figure B-2. Schematic Layout of Three CCD Color Video Camera

The higher performance resulted in a higher data rate that was deemed unacceptable for a minimum system during the study. This concept also uses a frame-grabber circuit board similar to the black and white concept discussed above.

Color video is highly desirable. The ability to interpret vegetation, water depth and turbidity, coast lines with sandbars and deltas and much more is valuable. The spectral wavelengths will depend on future analysis and science consensus, but several bands are already defined for other programs. These include 0.44, 0.52, 0.55 and 0.67 micron bands, plus the 0.75 micron vegetation band discussed above.

B.1.3. Three Camera Concept

A third concept that was considered uses three separate monochrome cameras, each with a selected spectral band filter mounted in front of the CCD focal plane. A full color image could be reconstructed from the outputs of the three cameras during ground data processing. One advantage of this concept is added reliability with little penalty. If one camera head fails, the others would still allow high resolution collocated images to be acquired, and the monochrome cameras have low mass and low power requirements. In the case of such a failure the cueing capability would be degraded, but may be recoverable to some extent by correlation with Landsat type data. Other video circuits such as frame-grabbers and data storage devices could either be separate for redundancy or time-shared to minimize mass and power. This concept was not used in this configuration of the integrated 2-D ESTAR, since the black and white camera has lower resource requirements. The three camera technique can result a robust design having considerable flexibility, and is worthy of further examination in future trade studies.

B.2. Options & Recommendations

The video camera provides high resolution (~ 2 km) and spectral cueing, which is of value in data interpretation. Although it is not all weather and does not provide a day and night capability, it is considered to be of value for this mission. The demand on spacecraft resources is not great. Future trades on the video concepts should be made, and the following items are considered to be worthy of further analysis:

- A color video camera is desirable, but its higher data rate, mass and power must be accommodated.
- The three monochrome camera concept provides higher reliability, and a similar capability to a color camera. The performance of this concept needs further evaluation (signal-to-noise ratio, waveband selection, etc.).
- A night capability may have science benefits, but this may compromise resolution, and add to system complexity.

C. DETAILED MASS AND POWER TABLES

The following tables provide a detailed breakdown of the mass and power for the component parts of the spacecraft and instrument.

C.1. Primary Mission

This section applies to the primary mission with the 10 km resolution L-band radiometer. The spacecraft does not require the integrated avionics feature because it is launched on a Taurus vehicle for this mission.

Item	Mass (kg)	Mass Margin	Power (W)	Power Margin	With Margins Mass (kg)	With Margins Power (W)
ESTAR Experiment	137.26	0.30	177.29	0.40	178.43	248.21
Data Management (DMS)	30.69	0.10	96.90	0.10	33.76	106.59
Orbit Determination (ODS)	2.22	0.08	3.80	0.10	2.41	4.18
Structure	47.82	0.08	0.00	0.10	51.87	0.00
Ordance	9.20	0.01	0.00	0.10	9.29	0.00
Thermal	5.46	0.10	15.00	0.10	6.01	16.50
Communications (COMM)	12.41	0.10	36.25	0.10	13.65	39.88
Hydrazine Propulsion (HPS)	16.32	0.07	3.63	0.10	17.43	3.99
Electrical Power (EPS)	90.76	0.10	26.09	0.10	99.67	28.70
Attitude Control (ACS)	18.64	0.08	22.86	0.10	20.20	25.15
Expendibles	93.13	0.10	0.00	0.10	102.45	0.00
Totals	**463.91**		**381.82**		**535.16**	**473.19**

3 Year Lifetime
12 Bit L-Band Resolution
10 % Power Margin on S/C
40 % Power Margin on Instruments
30 % Mass Margin on Instrumens
145 Elements
102.1 kg of Hydrazine Fuel, Maximum Internal Fuel Load (after 10% margin)
4 kg for External Pressurant Tank - included in Hydrazine Propulsion System (HPS)
0.36 Helium Pressurant (after 10% margin)--included in HPS
4 Batteries
Extended Solar Arrays

ESTAR Spacecraft Mass and Power Summary
Full Capability (10km Resolution)

ESTAR Experiment Item	Quantity	Unit Mass (kg)	Mass Margin	Unit Power (W)	Power Margin	Mass (kg)	Power (W)	With Margins Mass (kg)	With Margins Power (W)
Antenna Structure (Carbon)	1	30.500	0.30	0.00	0.40	30.50	0.00	39.65	0.00
Radiating Elements	145	0.088	0.30	0.00	0.40	12.76	0.00	16.59	0.00
Motors/Mechanisms	1	27.390	0.30	0.00	0.40	27.39	0.00	35.61	0.00
Other Structure	1	14.680	0.30	0.00	0.40	14.68	0.00	19.08	0.00
Launch Restraints	1	4.540	0.30	0.00	0.40	4.54	0.00	5.90	0.00
Total Antenna						89.87	0.00	116.83	0.00
Front End Module (FEM)	145	0.092	0.30	0.50	0.40	13.34	72.50	17.34	101.50
Injection Locked...(ILPLL)	33	0.149	0.30	0.68	0.40	4.90	22.50	6.37	31.50
Local Oscillator (MODIF)	5	0.094	0.30	0.50	0.40	0.47	2.50	0.61	3.50
Cables, RF	183	0.023	0.30	0.00	0.40	4.29	0.00	5.58	0.00
Cables, Digital	177	0.023	0.30	0.00	0.40	4.03	0.00	5.24	0.00
Cables, Power	187	0.023	0.30	0.00	0.40	4.26	0.00	5.54	0.00
Data Receiver Module	4	0.450	0.30	1.50	0.40	1.80	6.00	2.34	8.40
Master Oscillator (M/OS)	1	0.245	0.30	2.75	0.40	0.25	2.75	0.32	3.85
Central Procesor (CPU)	1	3.000	0.30	14.04	0.40	3.00	14.04	3.90	19.66
Internal Power Supply (IPS)	1	1.200	0.30	29.00	0.40	1.20	29.00	1.56	40.60
Total L-Band Electronics						37.54	149.29	48.80	209.01
IR Camera	1	8.900	0.30	14.00	0.40	8.90	14.00	11.57	19.60
Video Camera	1	0.450	0.30	4.00	0.40	0.45	4.00	0.59	5.60
Video Framegrabber Board	1	0.500	0.30	10.00	0.40	0.50	10.00	0.65	14.00
Totals						137.26	177.29	178.43	248.21

Data Management (DMS) Item	Quantity	Unit Mass (kg)	Mass Margin	Unit Power (W)	Power Margin	Mass (kg)	Power (W)	With Margins Mass (kg)	With Margins Power (W)
Spacecraft Memory Board	1	0.910	0.10	1.00	0.10	0.91	1.00	1.00	1.10
Spacecraft Maint. Unit (SMU	2	1.365	0.10	3.50	0.10	2.73	7.00	3.00	7.70
Spacecraft Computer	2	4.090	0.10	10.20	0.10	8.18	20.40	9.00	22.44
Mass Memory (3.0 GBit)	10	1.510	0.10	6.00	0.10	15.10	60.00	16.61	66.00
Payload User I/F Unit	1	1.500	0.10	3.50	0.10	1.50	3.50	1.65	3.85
Temporary Buffer	1	2.270	0.10	5.00	0.10	2.27	5.00	2.50	5.50
Totals						30.69	96.90	33.76	106.59

Orbit Determination (ODS) Item	Quantity	Unit Mass (kg)	Mass Margin	Unit Power (W)	Power Margin	Mass (kg)	Power (W)	With Margins Mass (kg)	With Margins Power (W)
GPS Antenna	2	0.175	0.05	0.00	0.10	0.35	0.00	0.37	0.00
GPS Preamp	2	0.160	0.05	0.00	0.10	0.32	0.00	0.34	0.00
GPS Receiver (6 ch)	1	1.550	0.10	3.80	0.10	1.55	3.80	1.71	4.18
Totals						2.22	3.80	2.41	4.18

Structure

Item	Quantity	Unit Mass (kg)	Mass Margin	Unit Power (W)	Power Margin	With Margins Mass (kg)	With Margins Power (W)	With Margins Mass (kg)	With Margins Power (W)
Aft Ring	1	4.430	0.05	0.00	0.10	4.43	0.00	4.65	0.00
Aft Shelf	1	2.050	0.10	0.00	0.10	2.05	0.00	2.26	0.00
Avionics Shelf	1	3.180	0.10	0.00	0.10	3.18	0.00	3.50	0.00
Bracket, +Y Umbilical	1	0.230	0.10	0.00	0.10	0.23	0.00	0.25	0.00
Bracket, -Y Umbilical	1	0.230	0.10	0.00	0.10	0.23	0.00	0.25	0.00
Bracket, Aft Shelf Interface	6	0.073	0.05	0.00	0.10	0.44	0.00	0.46	0.00
Bracket, Avionics Shelf Cone	2	0.045	0.10	0.00	0.10	0.09	0.00	0.10	0.00
Bracket, Avionics Shelf Interf	8	0.128	0.05	0.00	0.10	1.02	0.00	1.07	0.00
Bracket, Bus Panel Connect	1	0.050	0.10	0.00	0.10	0.05	0.00	0.06	0.00
Bracket, IMU Support	2	0.225	0.10	0.00	0.10	0.45	0.00	0.50	0.00
Bracket, PPE S-Band & S/C	2	0.210	0.05	0.00	0.10	0.42	0.00	0.44	0.00
Bracket, PPE Connector	1	0.050	0.10	0.00	0.10	0.05	0.00	0.06	0.00
Bracket, PPE GPS	1	0.110	0.10	0.00	0.10	0.11	0.00	0.12	0.00
Bracket, S/C GPS	1	0.230	0.10	0.00	0.10	0.23	0.00	0.25	0.00
Bracketry, Miscellaneous	1	2.270	0.10	0.00	0.10	2.27	0.00	2.50	0.00
Bus Panels, +Z	2	2.500	0.10	0.00	0.10	5.00	0.00	5.50	0.00
Bus Panels, -Z	2	2.500	0.10	0.00	0.10	5.00	0.00	5.50	0.00
Bus Panels, +Y	1	2.540	0.05	0.00	0.10	2.54	0.00	2.67	0.00
Bus Panels, -Y	1	2.500	0.10	0.00	0.10	2.50	0.00	2.75	0.00
Hydrazine Tank Supports	1	0.730	0.10	0.00	0.10	0.73	0.00	0.80	0.00
Hydrazine Thruster Supports	4	0.285	0.10	0.00	0.10	1.14	0.00	1.25	0.00
Misc. Attach Hardware	1	2.270	0.10	0.00	0.10	2.27	0.00	2.50	0.00
Payload Shelf	1	4.550	0.10	0.00	0.10	4.55	0.00	5.01	0.00
Payload Truss, Bracket, 3-ta	6	0.068	0.10	0.00	0.10	0.41	0.00	0.45	0.00
Payload Truss, Bracket, 1-ta	6	0.032	0.10	0.00	0.10	0.19	0.00	0.21	0.00
Payload Truss, End Fitting	24	0.055	0.05	0.00	0.10	1.31	0.00	1.38	0.00
Payload Truss, Frame	1	1.600	0.10	0.00	0.10	1.60	0.00	1.76	0.00
Payload Truss, Tube, Diagon	6	0.158	0.10	0.00	0.10	0.95	0.00	1.04	0.00
Payload Truss, Tube, Vertica	6	0.137	0.10	0.00	0.10	0.82	0.00	0.90	0.00
RCS Line Supports/Tiedown	1	0.090	0.10	0.00	0.10	0.09	0.00	0.10	0.00
RCS Tank Support Brackets	2	0.250	0.10	0.00	0.10	0.50	0.00	0.55	0.00
S/C Battery Support Structur	1	0.450	0.10	0.00	0.10	0.45	0.00	0.50	0.00
Separation Ring	1	2.520	0.01	0.00	0.10	2.52	0.00	2.55	0.00
Totals						47.82	0.00	51.87	0.00

Ordance

Item	Quantity	Unit Mass (kg)	Mass Margin	Unit Power (W)	Power Margin	Mass (kg)	Power (W)	With Margins Mass (kg)	With Margins Power (W)
Bolt Cutter / Cartridges	2	0.150	0.01	0.00	0.10	0.30	0.00	0.30	0.00
Clamp Band Assebly	1	6.220	0.01	0.00	0.10	6.22	0.00	6.28	0.00
Pyro Driver Unit	1	1.090	0.01	0.00	0.10	1.09	0.00	1.10	0.00
Spring Assemblies	4	0.398	0.01	0.00	0.10	1.59	0.00	1.61	0.00
Totals						9.20	0.00	9.29	0.00

Thermal

Item	Quantity	Unit Mass (kg)	Mass Margin	Unit Power (W)	Power Margin	Mass (kg)	Power (W)	With Margins Mass (kg)	With Margins Power (W)
Heaters/Thermostats etc.	1	0.910	0.10	15.00	0.10	0.91	15.00	1.00	16.50
MLI Blankets	1	4.550	0.10	0.00	0.10	4.55	0.00	5.01	0.00
Totals						5.46	15.00	6.01	16.50

Communication (COMM)

Item	Quantity	Unit Mass (kg)	Mass Margin	Unit Power (W)	Power Margin	Mass (kg)	Power (W)	With Margins Mass (kg)	With Margins Power (W)
RF Harness	1	3.640	0.10	0.00	0.10	3.64	0.00	4.00	0.00
S-Band Antenna (OMNI)	2	0.225	0.10	0.00	0.10	0.45	0.00	0.50	0.00
S-Band Transfer Switch	1	0.070	0.05	0.25	0.10	0.07	0.25	0.07	0.28
S-Band Coupler	1	0.050	0.05	0.00	0.10	0.05	0.00	0.05	0.00
STDN Transponder	2	4.100	0.10	18.00	0.10	8.20	36.00	9.02	39.60
Totals						12.41	36.25	13.65	39.88

Hydrazine Propulsion System

Item	Quantity	Unit Mass (kg)	Mass Margin	Unit Power (W)	Power Margin	Mass (kg)	Power (W)	With Margins Mass (kg)	With Margins Power (W)
Blankets/Shielding	1	0.570	0.10	0.00	0.10	0.57	0.00	0.63	0.00
Heaters/Temp Sensors	1	0.140	0.10	3.63	0.10	0.14	3.63	0.15	3.99
Hydrazine Filter	1	0.170	0.01	0.00	0.10	0.17	0.00	0.17	0.00
Hydrazine Tank	1	8.100	0.05	0.00	0.10	8.10	0.00	8.51	0.00
Hydrazine Thrusters	4	0.310	0.05	0.00	0.10	1.24	0.00	1.30	0.00
Lines & Fittings	1	0.910	0.10	0.00	0.10	0.91	0.00	1.00	0.00
External Pressurant Tank	1	4.000	0.10	0.00	0.10	4.00	0.00	4.40	0.00
Mounting Hardware	1	0.450	0.10	0.00	0.10	0.45	0.00	0.50	0.00
Pressure Transducer	2	0.035	0.01	0.00	0.10	0.07	0.00	0.07	0.00
Pyrovalve	1	0.140	0.05	0.00	0.10	0.14	0.00	0.15	0.00
Service Valves	3	0.177	0.05	0.00	0.10	0.53	0.00	0.56	0.00
Totals						16.32	3.63	17.43	3.99

Expendables								With Margins	
Item	Quantity	Unit Mass (kg)	Mass Margin	Unit Power (W)	Power Margin	Mass (kg)	Power (W)	Mass (kg)	Power (W)
Gas He Pressurant	1	0.327	0.10	0.00	0.10	0.33	0.00	0.36	0.00
Hydrazine Propellant	1	92.806	0.10	0.00	0.10	92.81	0.00	102.09	0.00
Totals						93.13	0.00	102.45	0.00

Electrical Power Subsystem								With Margins	
Item	Quantity	Unit Mass (kg)	Mass Margin	Unit Power (W)	Power Margin	Mass (kg)	Power (W)	Mass (kg)	Power (W)
Battery Charge Regulator(BC	1	4.500	0.10	26.09	0.10	4.50	26.09	4.95	28.70
Bus Harness	1	8.500	0.10	0.00	0.10	8.50	0.00	9.35	0.00
HPS Harness	1	1.140	0.10	0.00	0.10	1.14	0.00	1.25	0.00
Power Harness	1	3.500	0.10	0.00	0.10	3.50	0.00	3.85	0.00
Power Transfer Switch Assy	1	1.860	0.01	0.00	0.10	1.86	0.00	1.88	0.00
PPE Harness	1	6.820	0.10	0.00	0.10	6.82	0.00	7.50	0.00
S/A Deployment Hinge Assy	4	0.380	0.10	0.00	0.10	1.52	0.00	1.67	0.00
S/A Launch Lock (HOP) Ass	4	0.150	0.10	0.00	0.10	0.60	0.00	0.66	0.00
S/A Shear Cone Assy	16	0.085	0.10	0.00	0.10	1.36	0.00	1.50	0.00
S/A Tracking Mechanism (2-	2	1.820	0.10	0.00	0.10	3.64	0.00	4.00	0.00
S/A Yoke Assy	2	0.680	0.10	0.00	0.10	1.36	0.00	1.50	0.00
S/C Battery Assy	4	7.955	0.10	0.00	0.10	31.82	0.00	35.00	0.00
Solar Panel Assembly									
cells, wiring, adhesives	4	2.536	0.10	0.00	0.10	10.14	0.00	11.16	0.00
substrates, adhesives, ins	4	3.500	0.10	0.00	0.10	14.00	0.00	15.40	0.00
Totals						90.76	26.09	99.67	28.70

Attitude Control Subsystem (ACS)								With Margins	
Item	Quantity	Unit Mass (kg)	Mass Margin	Unit Power (W)	Power Margin	Mass (kg)	Power (W)	Mass (kg)	Power (W)
ACS Electronics Unit (ACE)	1	4.550	0.10	22.86	0.10	4.55	22.86	5.01	25.15
ACS Harness	1	0.450	0.10	0.00	0.10	0.45	0.00	0.50	0.00
Horizon Sensor	1	0.860	0.10	0.00	0.10	0.86	0.00	0.95	0.00
Magnetic Torque Rods	3	2.000	0.05	0.00	0.10	6.00	0.00	6.30	0.00
Magnetometer, 3-axis	1	0.120	0.05	0.00	0.10	0.12	0.00	0.13	0.00
Momentum Wheel	1	3.300	0.10	0.00	0.10	3.30	0.00	3.63	0.00
Sun Sensor	2	0.545	0.10	0.00	0.10	1.09	0.00	1.20	0.00
Star Tracker (Ball Aero CT-6	1	2.270	0.10	0.00	0.10	2.27	0.00	2.50	0.00
Totals						18.64	22.86	20.20	25.15

C.2. Alternate Mission

This section applies to the alternate, reduced-capability, mission with the 20 km resolution L-band radiometer. The spacecraft includes the integrated avionics feature for launch on a Pegasus vehicle.

Item	Mass (kg)	Mass Margin	Power (W)	Power Margin	With Margins Mass (kg)	With Margins Power (W)
ESTAR Experiment	70.08	0.30	119.75	0.40	91.11	167.65
Data Management (DM	16.03	0.10	44.70	0.10	17.63	49.17
Orbit Determination (O	2.22	0.08	3.80	0.10	2.41	4.18
Structure	47.82	0.08	0.00	0.00	51.87	0.00
Ordance	8.11	0.01	0.00	0.10	8.19	0.00
Thermal	5.46	0.10	15.00	0.10	6.01	16.50
Communications (COM	12.41	0.10	36.25	0.10	13.65	39.88
Hydrazine Propulsion (	12.32	0.06	3.63	0.10	13.03	3.99
Electrical Power (EPS)	68.25	0.10	26.09	0.10	75.08	28.70
Attitude Control (ACS)	18.64	0.08	22.86	0.10	20.20	25.15
Pegasus Provided	34.96	0.04	0.00	0.10	36.22	0.00
Expendibles	36.49	0.09	0.00	0.10	39.61	0.00
Totals	**332.80**		**272.08**		**375.00**	**335.22**

1 Year Lifetime
12 Bit L-Band Resolution
10 % Power Margin on S/C
40 % Power Margin on ESTAR Instruments
30 % Mass Margin on Instruments
73 Elements
1.024 Gbits Storage in 3 @ 0.5 Gbit Boards
33.67 kg of Hydrazine fuel (with 10% margin) for 60 deg, Dec 2000 Launch
3 Batteries
No Solar Array Extensions

ESTAR Spacecraft Mass and Power Summary
Reduced Capability (20 km Resolution)

ESTAR Experiment Item	Quantit	Unit Mass (kg)	Mass Margin	Unit Power (W)	Power Margins	Mass (kg)	Power (W)	With Margins Mass (kg)	With Margins Power (W)
Antenna Structure (Carbon)	1	15.560	0.30	0.00	0.00	15.56	0.00	20.23	0.00
Receiving Elements	73	0.088	0.30	0.00	0.00	6.42	0.00	8.35	0.00
Motors/Mechanisms	1	7.980	0.30	0.00	0.00	7.98	0.00	10.37	0.00
Other Structure	1	6.380	0.30	0.00	0.00	6.38	0.00	8.29	0.00
Launch Restraints	1	2.270	0.30	0.00	0.00	2.27	0.00	2.95	0.00
Total Antenna						38.61	0.00	50.20	0.00
Front End Module (FEM)	73	0.092	0.30	0.50	0.40	6.72	36.50	8.73	51.10
Injection Locked...(ILPLL)	18	0.149	0.30	0.68	0.40	2.67	12.27	3.47	17.18
Local Oscillator (MODIF)	4	0.094	0.30	0.50	0.40	0.38	2.00	0.49	2.80
Cables, RF	95	0.023	0.30	0.00	0.40	2.23	0.00	2.90	0.00
Cables, Digital	91	0.023	0.30	0.00	0.40	2.07	0.00	2.69	0.00
Cables, Power	97	0.023	0.30	0.00	0.40	2.21	0.00	2.87	0.00
Data Receiver Module	2	0.450	0.30	1.50	0.40	0.90	3.00	1.17	4.20
Master Oscillator (M/OS)	1	0.245	0.30	2.75	0.40	0.25	2.75	0.32	3.85
Central Procesor (CPU)	1	3.000	0.30	6.23	0.40	3.00	6.23	3.90	8.72
Internal Power Supply (IPS)	1	1.200	0.30	29.00	0.40	1.20	29.00	1.56	40.60
Total L-Band Electronics						21.62	91.75	28.10	128.45
IR Camera	1	8.900	0.30	14.00	0.40	8.90	14.00	11.57	19.60
Video Camera	1	0.450	0.30	4.00	0.40	0.45	4.00	0.59	5.60
Video Framegrabber Board	1	0.500	0.30	10.00	0.40	0.50	10.00	0.65	14.00
Totals						70.08	119.75	91.11	167.65

Data Management (DMS) Item	Quantit	Unit Mass (kg)	Mass Margin	Unit Power (W)	Power Margins	Mass (kg)	Power (W)	With Margins Mass (kg)	With Margins Power (W)
Spacecraft Memory Board	1	0.910	0.10	1.00	0.10	0.91	1.00	1.00	1.10
Spacecraft Maint. Unit (SMU	2	1.365	0.10	3.50	0.10	2.73	7.00	3.00	7.70
Spacecraft Computer	1	4.090	0.10	10.20	0.10	4.09	10.20	4.50	11.22
Mass Memory (1.5 GBit)	3	1.510	0.10	6.00	0.10	4.53	18.00	4.98	19.80
Payload User I/F Unit	1	1.500	0.10	3.50	0.10	1.50	3.50	1.65	3.85
Temporary Buffer	1	2.270	0.10	5.00	0.10	2.27	5.00	2.50	5.50
Totals						16.03	44.70	17.63	49.17

Orbit Determination (ODS) Item	Quantit	Unit Mass (kg)	Mass Margin	Unit Power (W)	Power Margins	Mass (kg)	Power (W)	With Margins Mass (kg)	With Margins Power (W)
GPS Antenna	2	0.175	0.05	0.00	0.10	0.35	0.00	0.37	0.00
GPS Preamp	2	0.160	0.05	0.00	0.10	0.32	0.00	0.34	0.00
GPS Receiver (6 ch)	1	1.550	0.10	3.80	0.10	1.55	3.80	1.71	4.18
Totals						2.22	3.80	2.41	4.18

Structure Item	Quantit	Unit Mass (kg)	Mass Margin	Unit Power (W)	Power Margins	Mass (kg)	Power (W)	With Margins Mass (kg)	With Margins Power (W)
Aft Ring	1	4.430	0.05	0.00	0.00	4.43	0.00	4.65	0.00
Aft Shelf	1	2.050	0.10	0.00	0.00	2.05	0.00	2.26	0.00
Avionics Shelf	1	3.180	0.10	0.00	0.00	3.18	0.00	3.50	0.00
Bracket, +Y Umbilical	1	0.230	0.10	0.00	0.00	0.23	0.00	0.25	0.00
Bracket, -Y Umbilical	1	0.230	0.10	0.00	0.00	0.23	0.00	0.25	0.00
Bracket, Aft Shelf Interface	6	0.073	0.05	0.00	0.00	0.44	0.00	0.46	0.00
Bracket, Avionics Shelf Cone	2	0.045	0.10	0.00	0.00	0.09	0.00	0.10	0.00
Bracket, Avionics Shelf Interf	8	0.128	0.05	0.00	0.00	1.02	0.00	1.07	0.00
Bracket, Bus Panel Connect	1	0.050	0.10	0.00	0.00	0.05	0.00	0.06	0.00
Bracket, IMU Support	2	0.225	0.10	0.00	0.00	0.45	0.00	0.50	0.00
Bracket, PPE S-Band & S/C	2	0.210	0.05	0.00	0.00	0.42	0.00	0.44	0.00
Bracket, PPE Connector	1	0.050	0.10	0.00	0.00	0.05	0.00	0.06	0.00
Bracket, PPE GPS	1	0.110	0.10	0.00	0.00	0.11	0.00	0.12	0.00
Bracket, S/C GPS	1	0.230	0.10	0.00	0.00	0.23	0.00	0.25	0.00
Bracketry, Miscellaneous	1	2.270	0.10	0.00	0.00	2.27	0.00	2.50	0.00
Bus Panels, +Z	2	2.500	0.10	0.00	0.00	5.00	0.00	5.50	0.00
Bus Panels, -Z	2	2.500	0.10	0.00	0.00	5.00	0.00	5.50	0.00
Bus Panels, +Y	1	2.540	0.05	0.00	0.00	2.54	0.00	2.67	0.00
Bus Panels, -Y	1	2.500	0.10	0.00	0.00	2.50	0.00	2.75	0.00
Hydrazine Tank Supports	1	0.730	0.10	0.00	0.00	0.73	0.00	0.80	0.00
Hydrazine Thruster Supports	4	0.285	0.10	0.00	0.00	1.14	0.00	1.25	0.00
Misc. Attach Hardware	1	2.270	0.10	0.00	0.00	2.27	0.00	2.50	0.00
Payload Shelf	1	4.550	0.10	0.00	0.00	4.55	0.00	5.01	0.00
Payload Truss, Bracket, 3-ta	6	0.068	0.10	0.00	0.00	0.41	0.00	0.45	0.00
Payload Truss, Bracket, 1-ta	6	0.032	0.10	0.00	0.00	0.19	0.00	0.21	0.00
Payload Truss, End Fitting	24	0.055	0.05	0.00	0.00	1.31	0.00	1.38	0.00
Payload Truss, Frame	1	1.600	0.10	0.00	0.00	1.60	0.00	1.76	0.00
Payload Truss, Tube, Diagon	6	0.158	0.10	0.00	0.00	0.95	0.00	1.04	0.00
Payload Truss, Tube, Vertica	6	0.137	0.10	0.00	0.00	0.82	0.00	0.90	0.00
RCS Line Supports/Tiedown	1	0.090	0.10	0.00	0.00	0.09	0.00	0.10	0.00
RCS Tank Support Brackets	2	0.250	0.10	0.00	0.00	0.50	0.00	0.55	0.00
S/C Battery Support Structur	1	0.450	0.10	0.00	0.00	0.45	0.00	0.50	0.00
Separation Ring	1	2.520	0.01	0.00	0.00	2.52	0.00	2.55	0.00
Totals						47.82	0.00	51.87	0.00

Ordance

Item	Quantit	Unit Mass (kg)	Mass Margin	Unit Power (W)	Power Margins	Mass (kg)	Power (W)	With Margins Mass (kg)	With Margins Power (W)
Bolt Cutter / Cartridges	2	0.150	0.01	0.00	0.10	0.30	0.00	0.30	0.00
Clamp Band Assebly	1	6.220	0.01	0.00	0.10	6.22	0.00	6.28	0.00
Spring Assemblies	4	0.398	0.01	0.00	0.10	1.59	0.00	1.61	0.00
Totals						8.11	0.00	8.19	0.00

Thermal

Item	Quantit	Unit Mass (kg)	Mass Margin	Unit Power (W)	Power Margins	Mass (kg)	Power (W)	With Margins Mass (kg)	With Margins Power (W)
Heaters/Thermostats etc.	1	0.910	0.10	15.00	0.10	0.91	15.00	1.00	16.50
MLI Blankets	1	4.550	0.10	0.00	0.10	4.55	0.00	5.01	0.00
Totals						5.46	15.00	6.01	16.50

Communication (COMM)

Item	Quantit	Unit Mass (kg)	Mass Margin	Unit Power (W)	Power Margins	Mass (kg)	Power (W)	With Margins Mass (kg)	With Margins Power (W)
RF Harness	1	3.640	0.10	0.00	0.10	3.64	0.00	4.00	0.00
S-Band Antenna (OMNI)	2	0.225	0.10	0.00	0.10	0.45	0.00	0.50	0.00
S-Band Transfer Switch	1	0.070	0.05	0.25	0.10	0.07	0.25	0.07	0.28
S-Band Coupler	1	0.050	0.05	0.00	0.10	0.05	0.00	0.05	0.00
STDN Transponder	2	4.100	0.10	18.00	0.10	8.20	36.00	9.02	39.60
Totals						12.41	36.25	13.65	39.88

Hydrazine Propulsion System

Item	Quantit	Unit Mass (kg)	Mass Margin	Unit Power (W)	Power Margins	Mass (kg)	Power (W)	With Margins Mass (kg)	With Margins Power (W)
Blankets/Shielding	1	0.570	0.10	0.00	0.10	0.57	0.00	0.63	0.00
Heaters/Temp Sensors	1	0.140	0.10	3.63	0.10	0.14	3.63	0.15	3.99
Hydrazine Filter	1	0.170	0.01	0.00	0.10	0.17	0.00	0.17	0.00
Hydrazine Tank	1	8.100	0.05	0.00	0.10	8.10	0.00	8.51	0.00
Hydrazine Thrusters	4	0.310	0.05	0.00	0.10	1.24	0.00	1.30	0.00
Lines & Fittings	1	0.910	0.10	0.00	0.10	0.91	0.00	1.00	0.00
Mounting Hardware	1	0.450	0.10	0.00	0.10	0.45	0.00	0.50	0.00
Pressure Transducer	2	0.035	0.01	0.00	0.10	0.07	0.00	0.07	0.00
Pyrovalve	1	0.140	0.05	0.00	0.10	0.14	0.00	0.15	0.00
Service Valves	3	0.177	0.05	0.00	0.10	0.53	0.00	0.56	0.00
Totals						12.32	3.63	13.03	3.99

Expendables

Item	Quantit	Unit Mass (kg)	Mass Margin	Unit Power (W)	Power Margins	Mass (kg)	Power (W)	With Margins Mass (kg)	With Margins Power (W)
Gas He Pressurant	1	0.200	0.01	0.00	0.10	0.20	0.00	0.20	0.00
Gas N2 Propellant	1	5.680	0.01	0.00	0.10	5.68	0.00	5.74	0.00
Hydrazine Propellant	1	30.610	0.10	0.00	0.10	30.61	0.00	33.67	0.00
Totals						36.49	0.00	39.61	0.00

Electrical Power Subsystem

Item	Quantit	Unit Mass (kg)	Mass Margin	Unit Power (W)	Power Margins	Mass (kg)	Power (W)	With Margins Mass (kg)	With Margins Power (W)
Battery Charge Regulator(BC	1	4.500	0.10	26.09	0.10	4.50	26.09	4.95	28.70
Bus Harness	1	8.500	0.10	0.00	0.10	8.50	0.00	9.35	0.00
HPS Harness	1	1.140	0.10	0.00	0.10	1.14	0.00	1.25	0.00
Power Harness	1	3.500	0.10	0.00	0.10	3.50	0.00	3.85	0.00
S/A Deployment Hinge Assy	4	0.380	0.10	0.00	0.10	1.52	0.00	1.67	0.00
S/A Launch Lock (HOP) Ass	4	0.150	0.10	0.00	0.10	0.60	0.00	0.66	0.00
S/A Shear Cone Assy	16	0.085	0.10	0.00	0.10	1.36	0.00	1.50	0.00
S/A Tracking Mechanism (2-	2	1.820	0.10	0.00	0.10	3.64	0.00	4.00	0.00
S/A Yoke Assy	2	0.680	0.10	0.00	0.10	1.36	0.00	1.50	0.00
S/C Battery Assy	3	7.955	0.10	0.00	0.10	23.87	0.00	26.25	0.00
Solar Panel Assembly									
cells, wiring, adhesives	4	1.919	0.10	0.00	0.10	7.68	0.00	8.44	0.00
substrates, adhesives, ins	4	2.648	0.10	0.00	0.10	10.59	0.00	11.65	0.00
Totals						68.25	26.09	75.08	28.70

Attitude Control Subsystem (ACS)

Item	Quantit	Unit Mass (kg)	Mass Margin	Unit Power (W)	Power Margins	Mass (kg)	Power (W)	With Margins Mass (kg)	With Margins Power (W)
ACS Electronics Unit (ACE)	1	4.550	0.10	22.86	0.10	4.55	22.86	5.01	25.15
ACS Harness	1	0.450	0.10	0.00	0.10	0.45	0.00	0.50	0.00
Horizon Sensor	1	0.860	0.10	0.00	0.10	0.86	0.00	0.95	0.00
Magnetic Torque Rods	3	2.000	0.05	0.00	0.10	6.00	0.00	6.30	0.00
Magnetometer, 3-axis	1	0.120	0.05	0.00	0.10	0.12	0.00	0.13	0.00
Momentum Wheel	1	3.300	0.10	0.00	0.10	3.30	0.00	3.63	0.00
Sun Sensor	2	0.545	0.10	0.00	0.10	1.09	0.00	1.20	0.00
Star Tracker (Ball Aero CT-6	1	2.270	0.10	0.00	0.10	2.27	0.00	2.50	0.00
Totals						18.64	22.86	20.20	25.15

Pegasus Provided Equipment Item	Quantit	Unit Mass (kg)	Mass Margin	Unit Power (W)	Power Margins	With Margins Mass (kg)	With Margins Power (W)	Mass (kg)	Power (W)
Flight Computer	1	3.090	0.01	0.00	0.10	3.09	0.00	3.12	0.00
GPS Antenna	1	0.410	0.10	0.00	0.10	0.41	0.00	0.45	0.00
GPS Receiver	1	1.550	0.10	0.00	0.10	1.55	0.00	1.71	0.00
IMU	1	5.770	0.01	0.00	0.10	5.77	0.00	5.83	0.00
Power Transfer Switch Assy	1	1.860	0.01	0.00	0.10	1.86	0.00	1.88	0.00
PPE Harness	1	6.820	0.10	0.00	0.10	6.82	0.00	7.50	0.00
Pyro Driver Unit	1	1.090	0.01	0.00	0.10	1.09	0.00	1.10	0.00
RCS (GAS N2) Tank	1	6.590	0.01	0.00	0.10	6.59	0.00	6.66	0.00
RCS Filter Assembly	2	0.410	0.01	0.00	0.10	0.82	0.00	0.83	0.00
RCS Pressure Transducer	1	0.140	0.01	0.00	0.10	0.14	0.00	0.14	0.00
RCS Lines & Fittings	1	0.450	0.10	0.00	0.10	0.45	0.00	0.50	0.00
RCS Disconnect Coupling	1	0.050	0.10	0.00	0.10	0.05	0.00	0.06	0.00
RCS Thruster Driver Unit	2	0.410	0.05	0.00	0.10	0.82	0.00	0.86	0.00
RCS Thruster Assembly	2	0.570	0.05	0.00	0.10	1.14	0.00	1.20	0.00
S-Band Antenna	2	0.340	0.01	0.00	0.10	0.68	0.00	0.69	0.00
S-Band Transmitter	1	0.500	0.01	0.00	0.10	0.50	0.00	0.51	0.00
S3 Mux	1	1.360	0.01	0.00	0.10	1.36	0.00	1.37	0.00
Transient Battery Assy (NiCd	1	1.820	0.01	0.00	0.10	1.82	0.00	1.84	0.00
Totals						34.96	0.00	36.22	0.00

D. ACRONYMS

A/D	Analog to Digital
ALC	Automatic Light Control
ASCD	NASA LaRC Advanced Space Concepts Division
B/W	Black and White
BB	Black Body
BCR	Battery Charge Regulator
BOL	Beginning of life
C&DH	Command and Data Handling
C&DHS	Command and Data Handling System
C-band	Radio frequency band between 4 and 8 GHz
CCD	Charge Coupled Device
CCSDS	Consultative Committee for Space Data Systems
CER	Cost Estimating Relationship
CMOS	Complimentary Metal Oxide Semiconductor
CPU	Central Processing Unit
DARPA	Defense Advanced Research Projects Agency
DRAM	Dynamic Random Access Memory
EMC	Electromagnetic Compatibility
EOL	End of life
EOS	Earth Observing System
ESTAR	Electronically Scanned Thinned Array Radiometer
FEM	Front End Module
FOV	Field of view
FPA	Focal Plane Assembly
GPS	Global Positioning System
GSE	Ground Support Equipment
GSFC	Goddard Space Flight Center
HCT	Mercury Cadmium Telluride
HMIC	Hybrid Microwave Integrated Circuit
I&Q	In-phase and Quadrature
I&T	Integration and Test
IF	Intermediate Frequency
ILPLL	Injection Locked Phase Locked Loop
IR	Infrared
Isp	Specific Impulse
L-band	Radio frequency band between 1 and 2 GHz
LaRC	NASA Langley Research Center
LO	Local Oscillator
MA	Multiple Access
MMIC	Monolithic Microwave Integrated Circuit
MO	Master Oscillator
MODIF	Master Oscillator Distribution Interface
MOTS	Modified off the shelf

NASA	National Aeronautics and Space Agency
NIR	Near Infrared
NOAA	National Oceanographic and Atmospheric Agency
OSC	Orbital Sciences Corporation
OTS	Off the shelf,
PCB	Printed Circuit Board
RF	Radio Frequency
S-band	Radio frequency band between 2 and 4 GHz
SDRC	Structural Dynamics Research Corporation
SGLS	U. S. Air Force's Space to Ground Link Subsystem
SI	The International System of Units
SLOC	Source Lines of Code
SM	Soil Moisture
SMU	Spacecraft Maintenance Unit
SSA	S-band Single Access
SST	Sea Surface Temperature
STDN	Standard Tracking and Data Network
TBD	To be determined
TDRSS	Tracking and Data Relay Satellite System
TE	Thermal Electric
TIR	Thermal Infrared Radiometer
TMG	Thermal Model Generator
TV	Television
VHSIC	Very High Scale Integrated Circuit
VIRR	Visible Infrared Radiometer
VLSI	Very Large Scale Integration
WBS	Work Breakdown Structure
WV	Water Vapor

REPORT DOCUMENTATION PAGE

Form Approved
OMB No. 0704-0188

1. AGENCY USE ONLY (leave blank)	2. REPORT DATE	3. REPORT TYPE AND DATES COVERED
	November 1993	Technical Memorandum

4. TITLE AND SUBTITLE

A Conceptual Design Study for a Two-Dimensional, Electronically Scanned Thinned Array Radiometer

5. FUNDING NUMBERS

419-09-01

6. AUTHOR(S) Philip Mutton, Christopher C. Chromik, Patrick A. Cosgrove, Iain Dixon, Richard B. Statham, Frederic H. Stillwagen, Alfred E. Von Theumer, George G. Ganoe, Washito A. Sasamoto, Paul A. Garn

7. PERFORMING ORGANIZATION NAME(S) AND ADDRESS(ES)

National Aeronautics and Space Administration
Langley Research Center
Hampton, VA 23681-0001

8. PERFORMING ORGANIZATION REPORT NUMBER

9. SPONSORING / MONITORING AGENCY NAME(S) AND ADDRESS(ES)

National Aeronautics and Space Administration
Washington D. C. 20546-0001

10. SPONSORING / MONITORING AGENCY REPORT NUMBER

NASA TM-109051

11. SUPPLEMENTARY NOTES

Mutton, Chromik, Cosgrove, Dixon, Statham, Stillwagen, Von Theumer: Lockheed Engineering and Sciences Company, Hampton, VA. Ganoe and Sasamoto: Advanced Space Concepts Division, Langley Research Center, Hampton, VA. Garn: Science and Technology Corporation, Hampton, VA.

12a. DISTRIBUTION / AVAILABILITY STATEMENT

Unclassified - Unlimited
Subject Category 43

12b. DISTRIBUTION CODE

13. ABSTRACT (Maximum 200 words)

This report describes a conceptual design for the Two-Dimensional, Electronically Steered Thinned Array Radiometer (ESTAR). This instrument is a synthetic aperture microwave radiometer that operates in the L-band frequency range for the measurement of soil moisture and ocean salinity. Two auxiliary instruments, an 8-12 micron, scanning infrared radiometer and a 0.4-1.0 micron, CCD video camera, are included to provided data for sea surface temperature measurements and spatial registration of targets respectively. The science requirements were defined by Goddard Space Flight Center. Instrument and the spacecraft configurations are described for missions using the Pegasus and Taurus launch vehicles. The analyses and design trades described include: estimations of size, mass and power, instrument viewing coverage, mechanical design trades, structural and thermal analyses, data and communications performance assessments, and cost estimation.

14. SUBJECT TERMS

Synthetic aperture, electronically scanned thinned array antenna, soil moisture, ocean salinity, correlation, microwave radiometer, IR radiometer, ESTAR

15. NUMBER OF PAGES

114

16. PRICE CODE

A06

17. SECURITY CLASSIFICATION OF REPORT	18. SECURITY CLASSIFICATION OF THIS PAGE	19. SUCURITY CLASSIFICATION OF ABSTRACT	20. LIMITATION OF ABSTRACT
Unclassified	Unclassified	Unclassified	UL